UNIVERSITY OF TRENTO

Department of Mathematics

PhD in Mathematics

XXIX CYCLE

Dynamical models for diabetes: insights into insulin resistance and type 1 diabetes

Advisors:

Professor Corrado Priami

Doctor Ozan Kahramanoğulları

PhD student:

Federico Reali

Committee members:

Professor Riccardo Bonadonna (University of Parma, Italy)
Doctor Daniel Crowther (Sanofi-Aventis Deutschland, Germany)
Doctor Ozan Kahramanoğulları (University of Trento, Italy)

Department of Mathematics, University of Trento
24 March 2017

Abstract

Diabetes is a family of metabolic disorders that affects millions of people worldwide. This disease affects the glucose-insulin system and it is characterized by a chronic excessive amount of glucose in the blood. It leads to severe harm, including long-term damages, dysfunction and failure of various organs. It is usually diagnosed in two types called type 1 and type 2.

Mathematical and dynamical models have been shown to provide a useful framework for the development of mechanistic descriptions of many biological phenomena. The results in this dissertation exemplify how this may lead to valuable insights for biological phenomena related to diabetes.

This thesis is dedicated to mathematical models devoted to the study of diabetes type 1 and insulin resistance that are subject of study in Chapters 3 and 4.

Chapter 3 describes two dynamical models that characterize the glucose-insulin system in patients with diabetes type 1 that are on insulin pump therapy. We have built our models on a dataset with ten patients that have undergone a mixed meal test and a hyperinsulinemic euglycemic clamp (HEC) test. Their blood glucose and insulin level were collected, as well as their standard clinical parameters. For some of the patients, the mixed meal test was repeated with a same or doubled size meal. The models were used to reproduce the data and to infer unknown parameters. The parameter estimates for the HEC model have driven the inference of the unknown parameters for the mixed meal test model. The integration of the two experiments and their parameter estimates have provided a reliable and reproducible description of the glucose-insulin system in T1D patients on pump therapy.

Recently, many studies have elucidated the essential role of ceramides and sphingolipids in the glucose homeostasis and insulin signaling. However, the mechanistic interplay between various components of ceramide metabolism remains to be quantified. Chapter 4 describes an extended model of ceramide production through both the *de novo* synthesis and the salvage pathways. We verify our model with a combination of published models and independent experimental data. We performed in silico experiments of the behavior of ceramide and related bioactive lipids in accordance with the observed transcriptomic changes in obese murine macrophages at 5 and 16 weeks support the observation of insulin resistance at the later phase. Our analysis suggests the pivotal role of certain enzymes involved in the *de novo* synthesis and the salvage pathways in influencing insulin resistance versus its regulation.

The content of the chapters is presented as the published version, or the final typeset, of the correspondent articles.

Essentially, all models are wrong,
but some are useful.

— George E. P. Box

Acknowledgments

Contents

List of Figures

List of Tables

Chapter 1

Introduction

This thesis summarizes my work in systems biology as a PhD student at The Microsoft Research - University of Trento Centre for Computational and Systems Biology (COSBI) and at the University of Trento, department of Mathematics.

Systems biology is an interdisciplinary field that aims at integrating biology with computational and mathematical methods to gain a better understanding of biological phenomena [5, 6]. Among these methods, mathematical and dynamical modeling have driven the discovery of mechanistic insights from the static representations of phenomena, that is, data. As a result, mathematical and dynamical models have now become standard tools to support new discoveries in biology and in public health issues. For example, models assist governments in determining the policies to contain the spreading of the diseases and in decisions such as vaccine purchases [7]. Similarly, complex and accurate models of the cardio-vascular systems guide surgeons during many procedures on patients [8]. Furthermore, dynamical models of signaling cascades help researchers in identifying new potential drug targets and therapies for many diseases [9]. We used these modeling techniques to address biological questions related to diabetes and insulin resistance. Within this framework, this thesis contains two articles I contributed to, that focus on diabetes. These works are published in the journal of Nature Scientific Reports and are included in Chapters 3 and 4.

A significant contribution to the development of these models, and models in general, is given by optimization. Optimization is often used in modeling to determine certain unknown values or factors in a way that allow the model to optimally reproduce the experimental data. Moreover, the parameters of a model that correctly describe the undergoing dynamics may be used as diagnostic tools [10–13]. To this end, this thesis contains a methodological appendix that includes a review of optimization algorithms that has been submitted to the journal of Frontiers in Applied Mathematics and Statistics, special topic Optimization. The content of this article is reported in Appendix A.

1.1 Diabetes and insulin resistance

Diabetes mellitus, here referred as diabetes, is a family of metabolic disorders that affects millions of people worldwide. This disease affects the glucose-insulin system and it is characterized by chronic hyperglycemia, i.e., excessive amount of glucose in the blood. It leads to severe harm, including long-term damages, dysfunction and failure of various organs [14]. It is diagnosed usually in two types called type 1 and type 2 that are subject of study in Chapters 3 and 4, respectively. There are also other forms of diabetes, for example, gestational diabetes that affects pregnant women. However, such and other rare forms of diabetes are not part of this dissertation.

1.1.1 Diabetes type 1

Diabetes type 1 is also called *juvenile diabetes* since it is mostly diagnosed in early ages. In diabetes type 1, patient pancreas is not able to properly secrete insulin because its cells are impaired or destroyed. As a consequence, patients depend on injected insulin to regulate their glucose level in the blood. This disease may be controlled by evaluating the glucose concentration in the blood and consequently by injecting an adequate amount of insulin into the blood stream. However, this procedure is not only tedious, but it is also subject to a number of flaws. From errors in measurement, due to the bad timing for the injection or to measurement tools, to the amount of insulin actually injected. In the long run, this may lead to serious consequences for patients, from problems in managing their weight, to more serious problems such as kidney failure, heart disease and blindness [14].

This emphasizes the need for developing closed loop models that are able to reproduce the patient curves of insulin and glucose, at least in very controlled scenarios. This may help in the development of robust control algorithms that aim at delivering the right amount of insulin according to the registered amount of glucose. The full development of such a tool, commonly referred as *artificial pancreas*, could change the life of millions of people.

Recently a first step in this direction has been done. In September 2016, the food and drugs administration (FDA) approved the human trial of a similar device, produced by Medtronic, for 123 patients. This device mimics pancreas functionality, monitoring the level of glucose and insulin and adjusting the amount of insulin injected in patients' blood stream to control the glucose level. However, this device still needs the human intervention to regulate the proper amount of insulin after a meal. This highlights even more the need for algorithms and models that are able to control these devices in order to remove the human intervention.

I contributed in the development of one of these models in collaboration with MD Professor Riccardo Bonadonna and his research group at the University of Verona, School of Medicine. Our model identified the glucose-insulin system, providing a good fit of the experimental data and showing a good reproducibility of the model parameters in repeated studies. Our contribution to the topic lead

to a publication in the journal of Nature Scientific Reports in November 2016 [15]. Chapter 3 contains this article.

1.1.2 Diabetes type 2 and insulin resistance

Diabetes type 2 is the result of genetic predisposition and life style factors and it is usually developed in adult age. The development of this type of diabetes goes through different stages of impairment of the glucose-insulin system, and often through *insulin resistance*. Insulin resistance is the impairment of the regular crosstalk between insulin and the cells. The latter does not respond adequately to normal levels of insulin [16], requiring always more insulin to stimulate the glucose uptake. The more the cells are insulin resistant, the more severe are the consequences for the organism. In the long run, this leads to an unsustainable scenario, impairing the functionality of pancreatic cells and eventually leading to diabetes and the similar serious consequences as diabetes type 1.

This specific topic is gaining increasing attention in the research community and a lot of research effort is focused on how to revert insulin resistance. In contrast to diabetes type 1, where there is an organ failure that impairs the normal regulation of glucose and insulin, insulin resistance can be slowed down or, in some cases, reversed. This result can be achieved following healthier life-style habits or through the use of specific drugs that aim at restoring the normal cellular uptake of glucose in response to insulin. The crosstalk between insulin and the cells is a very complex mechanism, where many actors play different roles in the promotion or inhibition of the consequent glucose uptake.

Part of my PhD research was dedicated to investigating the role in this crosstalk of a specific family of lipids, called *sphingolipids*. Certain representatives of these sphingolipids have a role in promoting or inhibiting the signaling cascade that starts from the cell membrane, where insulin binds to the insulin receptors and arrives at the glucose transportase protein that promotes the glucose uptake from the blood to the cells [17].

Recently, there has been an increase on the investigations on these sphingolipids. Sphingolipids were originally known for their structural role, in composing the cellular membrane. However, thanks to new technologies, their important role in many other cellular regulation mechanisms has become clearer. Sphingolipids are involved in a variety of processes including cell survival, proliferation, apoptosis and inflammatory stress [18]. Thus, they become potential drug targets for several diseases.

To better understand the involvement of sphingolipids in the development of insulin resistance, we have developed a dynamical model of the sphingolipid metabolism. The integration of the dynamical model with lipidomic and gene expression data has suggested mechanistic explanations for the development of insulin resistance for a specific tissue in obese mice. This work has been done in collaboration with Daniel Crowther and his research group at Sanofi Deutschland, Frankfurt. Our results lead to a paper in the journal of Nature Scientific Reports, which is in press at the time of writing. The article is included in Chapter 4 of this thesis.

Chapter 2

The biological and modeling background

2.1 Digestion and glucose homeostasis

The process of digestion mechanically and chemically reduces complex molecules to simpler ones that can be assimilated. Among the different nutrients that are absorbed along this process, here we focus on glucose. The absorbed glucose is one of the fundamental contributors as an energy supplier and its concentration in the blood is subject to a number of control mechanisms. These mechanisms maintain its amount inside a specific physiological range [19]. This homeostasis is a very complex system with a variety of hormones and mechanisms involved that regulate the glucose uptake and release. For example, the insulin hormone reduces glucose concentration whereas other hormones, such as glucagon, stimulate the liver glucose release when its concentration is low. In addition, other hormones, such as incretins and leptin, are parts of this regulation process [20, 21].

In this dissertation, we consider the glucose-insulin interactions (Fig. 2.1). Insulin is a hormone produced by the pancreatic β-cells of the islet of Langerhans. It promotes the cellular glucose uptake and consequently reduces the glucose concentration in the blood. As a response to an increased glucose concentration in the blood, insulin is immediately released during the so-called *acute response*. In the successive minutes and hours, further releases are secreted with the aim of normalizing the glucose level in the blood [20]. Insulin also reduces the liver endogenous glucose production [22].

At a cellular level, insulin binds to the insulin receptor (IR) and triggers a signaling cascade that promotes the glucose uptake mediated by the glucose transport proteins (GLUT) [23]. Here we focus on the interaction of a specific family of lipids, called *sphingolipids*, that affect this signaling pathway. A growing body of literature has elucidated the role of the sphingolipids in the impairment of the insulin signaling cascade and in the development of insulin resistance [17, 24]. In fact, certain representatives of this family, i.e., ceramide
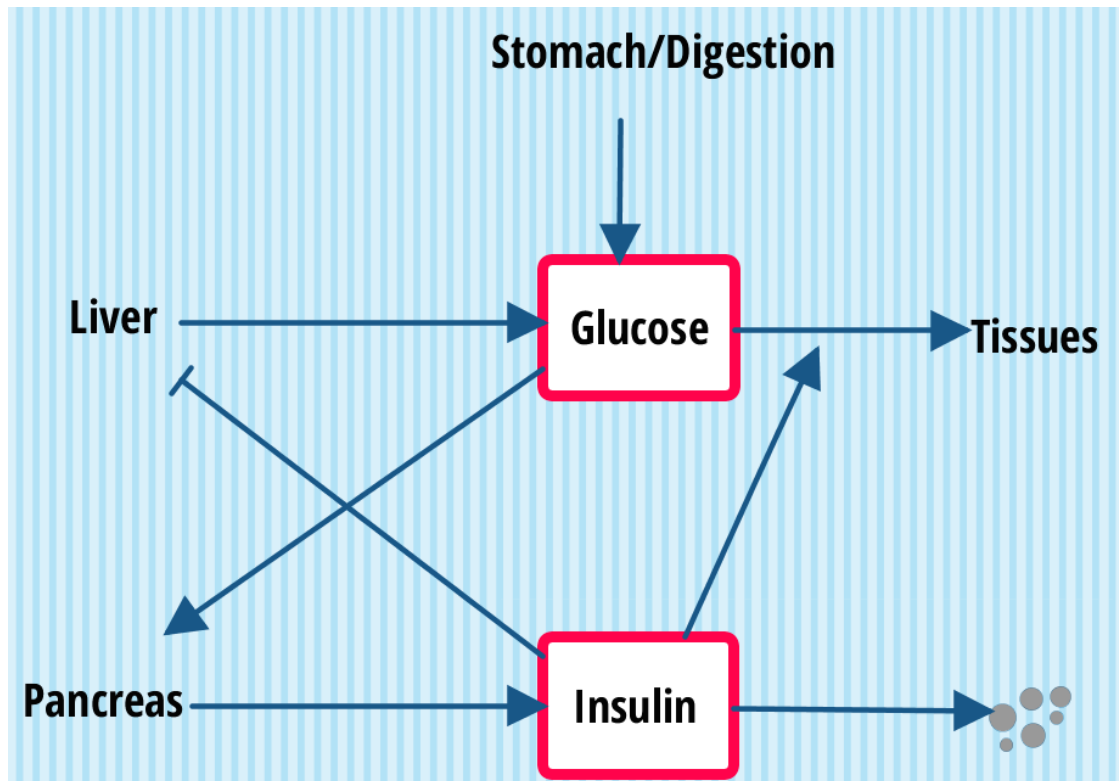
Figure 2.1: *A schematic representation of the glucose-insulin regulation.*

(Cer) and the ganglioside GM3, inhibit the glucose uptake, whereas others, such as sphingosine-1-phosphate (S1P), promote it [17, 25]. Figure 2.2 shows some of these interactions between the sphingolipids and the insulin signaling cascade.
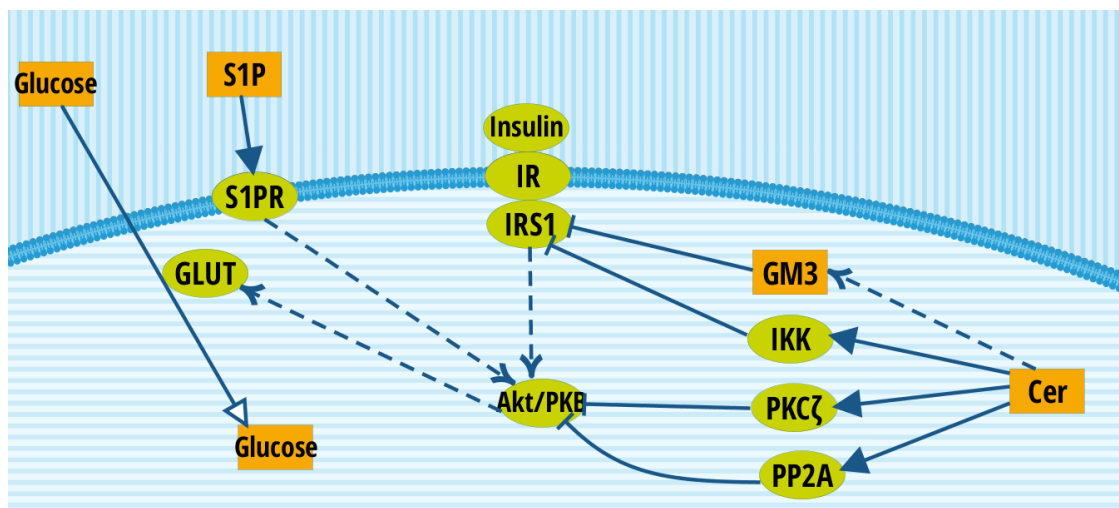
Figure 2.2: *A schematic and simplified representation of the insulin signaling cascade and the interactions with the sphingolipids. In this representation, the continuous arrows indicate direct regulations and dashed ones indicate indirect regulations.*

These mechanisms may be subject to different impairments and failures, both at

whole-body or cellular level [14]. Among these impairments, in this thesis, we consider diabetes. Type 1 diabetes patients rely on insulin injections to control their glucose level in the plasma because their pancreas is impaired and cannot secrete enough insulin. Patients depend on insulin analogs and these analogs are usually divided into two categories that is, fast and slow acting insulins. The former refers to those analogs, such as Lispo, Aspart, and Glulisine, that are meant to substitute the insulin bolus released after a meal. The latter refers to those, such as Detemir, Degludec, and Glargine, that are meant to substitute the basal level of insulin [26]. A mathematical model of the glucose-insulin system for type 1 diabetes patients is reported in Chapter 3. In the following sections, we provide an introduction to the long history of whole-body models for the glucose-insulin system.

Type 2 diabetes often undergoes a phase of insulin resistance. In insulin resistance, insulin is secreted but the glucose uptake is impaired. At a cellular level, a variety of descriptions has been proposed to elucidate the role of different molecules in the glucose-insulin homeostasis. Nevertheless, our model is the first dynamical representation that investigates the interplay between the sphingolipids and the development of insulin resistance in mice [27]. We refer to Chapter 4 for a complete description of the model.

2.2 The glucose metabolism and tolerance tests

Along the years, medical doctors and researchers have developed several tests to assess patient conditions with respect to their glucose metabolism. At the same time, these tests aim at unveiling the mechanisms behind the glucose homeostasis [14]. Some of these tests are focused on the glucose-insulin system and they are particularly suitable to be described through mathematical models [22]. We describe here some of the most important tests to determine patient conditions and we provide a short description of some of the associated mathematical models in Section 2.3.

The Intravenous Glucose Tolerance Test (IVGTT) [20] mostly analyzes the glucose metabolism in a short period of time. The test consists of the injection of a glucose bolus (0.33 g/kg) over a period of 30 or 60 seconds after an overnight fasting. The resultant plasma glucose and insulin concentrations are measured. The sampling schedule for a standard IVGTT usually requires three pretest samples taken at the time -15, -5, and 0. In addition, it requires up to 25 blood samples taken during the following 2 or 3 hours [28]. This test is particularly important to determine the acute response of the insulin secretion. However, since the test does not involve digestion, it is a very abstract representation of the nutrition process [29].

To overcome this limitation, the Oral Glucose Tolerance and Mixed Meal Tests (OGTT/MMT) were introduced [30]. The first involves the ingestion of a fixed amount of glucose, whereas the latter involves the consumption of a standardized meal. These tests trigger more complex processes, like the digestion and the physiological secretion of other glucose-regulating hormones, such as gastroin-

testinal incretins. As a consequence, they provide a more reliable abstraction. In addition, these tests are easier to perform because they require fewer blood samplings than the IVGTT [31].

In the OGTT, the patient drinks a 75 g dose of glucose after 8-12 hours fasting. Blood samples are taken before the test and after every 30 or 60 minutes for the following 2 or 3 hours [28]. The OGTT experiment permits to determine an important clinical measure, that is, the two-hours-glucose. This value is an auxiliary diagnostic tool [31], and it indicates the amount of glucose in the bloodstream recorded two hours after the ingestion of the glucose dose. Together with the recorded glucose level at fasting, it makes it possible to assess the patient glucose tolerance. The patients are considered *normal* if their fasting glucose concentration is below 6 mM and is below 7.8 mM after two hours from the test. They have an *impaired glucose tolerance* if these values are between 6 and 7 mM at fasting and between 7.9 and 11 mM after 2 hours. The patients are considered *diabetics* if their values are above these thresholds [32].

The IVGTT and OGTT were extended using radio-labeled glucose, often referred as *tracers*, to provide a more accurate description of the glucose in the bloodstream. The use of tracers has allowed researchers to better understand the glucose-insulin system [12, 22, 33]. However, the use of trackers increases the complexity of the experimental procedure [15].

The Mixed Meal Test (MMT) is similar to the OGTT; instead of the glucose dose, the patient eats a standardized meal [15]. Since it triggers all the mechanisms of digestion and glucose regulation, it is the most physiological test. The MMT is described in Chapter 3, where it is coupled with a mathematical description of its dynamics in diabetes type 1 patients [15].

2.3   The glucose-insulin system models

In this section, we present mathematical models that describe the glucose-insulin system. We discuss the minimal model for the intravenous glucose tolerance test, considered as one of the most influential models for describing the glucose-insulin system. In addition, we describe an extension of the minimal model that describes the oral glucose tolerance test. We provide references to some refinements and extensions of these models, as well. A complete description of a model for the mixed-meal test is reported in Chapter 3.

2.3.1   IVGTT and the minimal model

The efforts to describe the intravenous glucose tolerance test (IVGTT) through dynamical models have led to the development of several models for animals and humans [11, 34–39]. We describe here one of the better known of these models, that is, the minimal model [11].

This model rests on two fundamental assumptions. First, the system is composed of two separate parts, i.e., compartments, describing the dynamics of the glucose and the insulin as known inputs. Second, the insulin action takes place

in a remote and non-observable compartment. This compartment is different from plasma and it is nowadays known to be the interstitium [22]. This compartment was originally considered as a modeling assumption that described some empirical evidence that was not confirmed [22]. The minimal model is composed of three equations that describe, in terms of concentrations, the dynamics of the plasma glucose G, the plasma insulin I, and the remote and non-observable compartment X.

The glucose compartment   The physiological assumption behind the model and the compartments is that the glucose uptake does not depend directly on the plasma insulin concentration I [11]. It depends on the insulin concentration in a remote compartment, modeled through the auxiliary function X, whose dynamics depends on I. The following equations describe the dynamics of the glucose compartment.

$$\begin{cases} \frac{d}{dt}G(t) = -(p_1 + X(t))G(t) + p_1 G_b & , G(0) = G_b + \Delta_G \\ \frac{d}{dt}X(t) = -p_2 X(t) + p_3(I(t) - I_b) & , X(0) = 0 \end{cases} \qquad (2.1)$$

The glucose concentration exhibits a linear clearance and a degradation term that is proportional to the insulin action. The latter models the insulin mediated glucose uptake. In addition, the equation shows the self-promoting glucose release that is proportional to the basal level. The remote compartment X shows a linear clearance and a term that changes sign according to the insulin concentration I. This term regulates X according to the insulin oscillation compared to the basal level I_b [11]. Δ_G is the instantaneous change in glucose due to the glucose bolus injection. G_b and I_b are the glucose and insulin basal levels. In this compartment, the insulin concentration I appears as the linear interpolation of the experimental data. The glucose compartment dynamics includes four unknown parameters, namely, p_1, p_2, p_3, and Δ_G.

The insulin compartment   The dynamics of the insulin compartment is described by the following equation:

$$\frac{d}{dt}I(t) = -n(I(t) - I_b) + \gamma t[G(t) - h]^+, \qquad I(0) = I_b + \Delta_I \qquad (2.2)$$

The insulin dynamics exhibits a linear clearance rate n and an insulin secretion proportional to both the glucose level and the time elapsed since the bolus injection. The first phase insulin release is modeled by Δ_I that accounts for the acute insulin response that follows the bolus injection. The insulin secretion is proportional to the glucose concentration that exceeds h. The parameter h, also called target glycemia, models the threshold needed for stimulating the second phase pancreatic insulin production [11, 40]. The glucose concentration G appears in this compartment as the linear interpolation of the experimental data. The insulin compartment dynamics includes four unknown parameters, namely, n, γ, h, and Δ_I.

Parameter estimation   To obtain parameter identifiability, certain values, such as p_1, are fixed according to population studies [11]. In addition, the estimation procedure of the unknown parameters is divided into two phases, where either the glucose or the insulin compartment parameters are estimated separately. During such a procedure, the dynamic of the remaining compartment is obtained by considering the experimental data. On the one hand, this assumption permits to determine the model parameters with reduced uncertainty since the estimation is carried out for fewer parameters. On the other hand, considering the time series as a reference may affect the accuracy of the results by not accounting for the biological noise of the underlying processes. Nevertheless, a rigorous mathematical analysis of the minimal model has demonstrated that it is impossible to correctly identify the parameters of the two compartments simultaneously [40].

Insulin sensitivity index   It is possible to derive an important clinical measure from the kinetic parameters of the glucose compartment, that is, the *Insulin Sensitivity index S_I* [11]. This index reflects the quantitative influence of the basal insulin concentration to increase the glucose effectiveness at steady state, i.e.:

$$S_I = \frac{\partial}{\partial I_b} \left[-\frac{\partial}{\partial G} \frac{dG}{dt} \right]_{steadystate} = \frac{p_3}{p_2} \tag{2.3}$$

This index quantifies the efficacy at which the patient responses to a glucose stimulus. Consequently, if a model correctly describes the glucose-insulin system, S_I is expected to reflect patients' conditions. For example, the S_I of the minimal model for the IVGTT is a good estimator [10, 11]. Nevertheless, the gold standard to assess such an index is the hyperinsulinemic euglycemic clamp (HEC) [41], described in Chapter 3.

Beyond the IVGTT minimal model   The simple and elegant minimal model has inspired several representations of the glucose-insulin system [22]. However, this model shows some drawbacks. For example, the complex behavior of the glucose, after the bolus injection, may exceed the modeling power of a single glucose compartment. To circumvent this limitation, some tests and models have introduced the use of radio-labeled glucose tracers to distinguish the endogenous production from the injected glucose [42]. Nevertheless, the resulting test procedures are more complex than the standard IVGTT. Moreover, the models require more compartments and parameters than the minimal model [34].

Other important drawbacks are related to the parameter identification procedure. In fact, to properly infer the model parameters from the experimental data, the procedure requires to tune separately the two compartments and set certain parameters according to fixed population values [11, 40]. This permits the estimation of the remaining parameters, however, this may bias the procedure. With the aim of solving this problem, in [40] the authors have introduced a

model that correctly identifies the parameters simultaneously, using integro-differential equations. However, this modeling technique increases the model complexity, diverging from the idea of minimality.

Another important limitation of the IVGTT minimal model is that it does capture the β-cell function, taking mostly into account the acute insulin response (i.e., first 10 minutes of the insulin data). For example in [43–45], the authors have extended the minimal model by including in the insulin compartment the β-cell and C-peptide dynamics. This permits a more accurate description of the insulin dynamics, but on the other hand, it requires a more complex model that includes more equations and parameters.

To summarize, the minimal model is able to correctly describe the glucose-insulin system during an IVGTT experiment, using a parsimonious number of compartments, equations, parameters, and assumptions. Nevertheless, the model may be refined and extended to obtain more accurate descriptions. However, these extensions and refinements, usually, put aside the model minimality.

2.3.2 The Oral Minimal Model

Several research groups have extended and adapted the minimal model to describe the more physiological Oral Glucose Tolerance and Mixed Meal Tests (OGTT/MMT) [29, 31, 46, 47]. The ingestion of glucose is the main difference between the IVGTT and the OGTT/MMT, and it varies the way in which glucose appears in the blood. From the modeling perspective, in the IVGTT minimal model, the glucose appearance is described as a constant function during infusion. Although, the appearance follows more complex dynamics after the ingestion. This appearance is usually modeled using a function called *rate of appearance* (*Ra*). For example, in [29], the authors have tested different functions to model this appearance. They have compared a piecewise linear continuous function, the output of a dynamical model and a cubic spline function. In terms of model accuracy and complexity, the authors indicated the piecewise continuous function as the best candidate [29]. However, such a function requires several parameters to describe the glucose appearance and this increases the model complexity.

Modifying the glucose compartment of the IVGTT minimal model by including the *Ra* function leads to the following equations.

$$\begin{cases} \frac{d}{dt}G(t) = -(p_1 + X(t))G(t) + p_1 G_b + \frac{Ra(t)}{V_G} & , G(0) = G_b \\ \frac{d}{dt}X(t) = -p_2 X(t) + p_3(I(t) - I_b) & , X(0) = 0 \end{cases} \quad (2.4)$$

As in the IVGTT minimal model (Eq. 2.1), G is the plasma glucose concentration, X is the remote insulin compartment, and I is the plasma insulin concentration. G_b and I_b indicate the glucose and insulin basal concentration. The equations for insulin compartment are the same as those in the IVGTT minimal model (Eq. 2.2). V_G is the apparent glucose distribution volume.

The function Ra (rate of appearance of the glucose in the plasma) is assumed to be a piecewise linear function with n sub-domains:

$$Ra(t) = \begin{cases} \alpha_i + \frac{\alpha_i - \alpha_{i-1}}{t_i - t_{i-1}}, & t_{i-1} \leq t \leq t_i, \quad i = 1, \ldots, n \\ 0 & \text{otherwise.} \end{cases} \tag{2.5}$$

In (Eq. 2.5), the $t_i, i = 1, ..., n$ is a partition of the time of the experiment, with $t_0 = 0$ and $\alpha_0 = 0$. The $\alpha_i, i = 1, ..., n$ are the parameters that are estimated from the glucose experimental data. Their identifiability is guaranteed by the assumption that the AUC of Ra is equal to the fraction of the ingested dose that is actually absorbed. This fraction is commonly assumed to be equal to the 86% of the total amount [29,48], and it accounts for the splanchnic extraction [49].

As for the IVGTT minimal model, to obtain the identifiability of the model parameters, certain parameters are set to values obtained by population studies. For example, in [29,46], V_G and p_1 are set such that $p_1 V_G = 0.024$ dl kg^{-1} min^{-1}.

Successive studies have refined and simplified the Ra function. In particular, it has been proved that 8 time-points are sufficient to model the glucose appearance, and consequently to estimate the eight parameters $\alpha_i, i = 1, \ldots, 8$. Further analysis has reduced these parameters to 4 by considering an exponential decay after 120 minutes [29].

We may derive the insulin sensitivity index S_I for the oral minimal model, by considering the same calculation of the IVGTT (Eq. 2.3) [29]. Nevertheless, the orally derived S_I tends to overestimate this value even though it correlates well with the IVGTT S_I [2,12,50].

In analogy with the IVGTT minimal model, many extensions and refinements of the oral minimal model have been proposed. For example, in [51], the authors present a different Ra function that models, using partial differential equations, the process of digestion. In [52], the authors have extended the IVGTT description by dividing the digestive system into three compartments and by considering delay equations [39]. In the context of a mixed meal test for diabetes type 1 patients, in Chapter 3, we present a novel model that includes an original solution for the Ra [15]. In [44,47,50], the authors have extended the oral minimal model with the β-cell description, and in [12,53], the radio-labeled glucose has been considered.

As for the IVGTT, there is often a trade-off between each extension or refinement and the minimality of the oral minimal model.

Chapter 3

A Novel Insulin/Glucose Model after a Mixed-Meal Test in Patients with Type 1 Diabetes on Insulin Pump Therapy

Diabetes type 1 patients suffer a pathology that impairs their pancreas. As a result of this impairment, the pancreas does not secrete insulin anymore. As a consequence, the body cannot control the levels of glucose in the blood. To support the development of devices that are able to substitute this pancreas functionality, we need to refine robust control algorithms that aim at delivering the right amount of insulin according to a registered amount of glucose. As a first step in this direction, researchers are developing dynamical models that are able to reproduce the patient' curves of insulin and glucose levels, at least in very controlled scenarios.

In this framework, this chapter describes a new dynamical model. This model characterizes the glucose-insulin system in patients with diabetes type 1 that are on insulin pump therapy. The pump in such a therapy provides a continuous subcutaneous insulin infusion, mimicking the normal basal levels. Patients on such devices, are the natural candidates for testing any fully automated insulin delivery system. Nevertheless, the devices that are actually in use are not yet able to adjust the insulin amount according to the measured level of glucose.

To this end, we have developed and refined two dynamical models for a mixed meal test and a hyperinsulinemic euglycemic clamp test. We tested our models with a dataset on ten patients that have undergone a mixed meal test. In this test, they had a typical north Italian meal, "polenta" and Parmesan. Their blood glucose and insulin level were collected, as well as their standard clinical parameters. For some of the patients, the test was repeated with a same or doubled size meal. In addition to this test, a hyperinsulinemic euglycemic clamp (HEC) test was performed. This test is considered the gold standard to assess insulin sensitivity of patients.

Mixed meal tests provide an abstraction of our everyday life meals. These abstractions are very important for the development of an automated insulin delivery device. In fact, such devices are meant to be initially tuned by using patient-specific parameters that are estimated using models or *ad-hoc* experiments. They should then work without any other tuning process.

The models were used to reproduce the data and the unknown parameters were inferred using a multi-start approach together with a least squares method. This and other techniques for parameter estimation are described in detail in Appendix A. The parameter estimates for the HEC model have driven the inference of the unknown parameters for the mixed meal test model. The integration of the two experiments and their parameter estimates have provided a reliable and reproducible description of the glucose-insulin system in T1D patients on pump therapy.

What follows is the content of the article, published in the journal of Scientific Reports in November 2016. It describes the minimal model inspired new model and the HEC model.

3.1 Introduction

The glucose-insulin (G/I) system is a physiological closed-loop, which is able to maintain the plasma glucose levels within a narrow physiological range, as a result of a complex interaction among many components [19, 20]. Of them, only a limited number (namely, plasma glucose, insulin and C-peptide levels) is directly accessible for measurement in the bloodstream. Thus, either the closed-loop is experimentally interrupted under strictly controlled conditions, i.e. by the glucose clamp technique [41], or dedicated mathematical models [5, 6] are needed to estimate the intimate components of the G/I system [22, 42–47, 51, 54–62].

Variable	Patient 1	Patient 2	Patient 3	Patient 4	Patient 5	Patient 6	Patient 7	Patient 8	Patient 9	Patient 10
Sex	M	F	F	M	M	M	M	M	F	M
Age (years)	63	44	53	43	24	37	47	32	31	25
BMI (Kg·m^{-2})	26.43	20.60	24.75	19.27	24.73	25.54	23.29	23.27	21.80	22.89
BSA (m^2)	1.91	1.47	1.63	1.72	1.80	1.97	1.99	1.89	1.73	1.83
HbA1c DCCT (%)	8.0	8.3	7.1	7.2	7.8	8.7	8.6	7.3	7.8	7.2
HbA1c IFCC (mmol/mol)	63.9	67.2	54.1	55.2	61.7	71.6	70.5	56.3	61.7	55.2
Duration of diabetes (years)	9	18	12	34	8	24	40	19	22	13
Duration of CSII therapy (years)	4	11	7	1	3	9	4	2	3	1
Insulin Sensitivity (M clamp) (μmol/min/m^2 BSA)	165	64	127	83	82	115	71	82	186	965
Insulin analogue	aspart	lispro	aspart	glulisine	aspart	aspart	glulisine	aspart	lispro	lispro
MMT1 (292 Kcal)	•	•	•	•	•	•	•	•	•	•
MMT2 (292 Kcal)	•	•	•	-	-	-	-	-	-	-
MMT2 (600 Kcal)	-	-	-	•	•	•	-	-	-	-

Table 3.1: *Clinical and metabolic features of the MMT-T1D Pilot Study population sample. Abbreviations: BMI, Body Mass Index; BSA, Body Surface Area; HbA1c DCCT, Diabetes Control and Complication Trial-Aligned Hemoglobin A1c; HbA1c IFCC, International Federation of Clinical Chemistry-Aligned Hemoglobin A1c; CSII, Continuous Subcutaneous Insulin Infusion; MMT, Mixed Meal Test.*

Over the past four decades a number of experimental protocols have been

developed to assess the dynamics of the G/I system in vivo [41–43, 46, 47, 54, 63, 64], often analyzed by multi-compartmental modeling techniques [44, 45, 65]. In such models the G/I dynamics are described through a set of ordinary differential equations (ODEs) according to well validated modeling strategies, which often require complex experimental settings, including the use of a variable number of glucose tracers to exactly track the glucose dynamics [2, 12, 42]. In order to mitigate the burden of both experimental and modeling complexity, more parsimonious models have been proposed and successfully employed [21, 29–31, 40, 47, 50, 54, 64]. These "minimal models" have been thus far applied most frequently to the intravenous glucose tolerance tests (IVGTT) with the primary aim of measuring insulin sensitivity [40, 54, 58]. Their extension to more physiological settings, such as oral glucose tolerance tests (OGTT) [51, 64] and mixed meal tests (MMT) [31, 66], although feasible and widely in use, relies, when no glucose tracer(s) is (are) used, on an additional number of assumptions, especially regarding the dynamics of oral glucose appearance into the peripheral circulation [29], plus glucose effectiveness, volume of distribution [2, 67] and splanchnic extraction [29, 68]. Although the insulin sensitivities yielded by the oral models are well correlated to those obtained by the IVGTTs, they may overestimate insulin sensitivity, as assessed by the IVGTT [2, 13, 29, 50]. Furthermore, insulin sensitivity provided by the OGTT model is lower than insulin sensitivity measured by the insulin clamp [69] and higher than insulin sensitivity estimated by the MTT model [70]. Current evidence, however, indicates that, when measured with appropriate tools, i.e. tracer aided models of glucose dynamics, insulin sensitivity is relatively constant, regardless of the route of glucose/carbohydrate entry in the body [2, 69]. Thus, current minimal modeling of glucose/carbohydrate meals with no tracer(s) aid, even though calibrated to successfully handle the oral glucose rate of appearance with a set of constrained parameters [29, 68], provides estimates of insulin sensitivity which, albeit correlated to those obtained with reference methods, display significant deviations from all other methods for somewhat unclear reasons [2, 13, 29, 50, 69, 70].

Modeling the G/I system is particularly relevant nowadays in the therapeutic area of type 1 diabetes (T1D), specifically in those patients treated with continuous subcutaneous insulin infusions (CSII) coupled with continuous glucose monitoring (CGM). A considerable research effort has resulted in G/I models based on the results of complex tracer studies [53, 71] and growing experience has been accrued to successfully close the loop with control algorithms of the G/I system derived from them [46, 72]. Recent real-life clinical trials have reported very promising results towards the development of a reliable, wearable closed-loop insulin delivery system [73–75]. For the reasons described above, published parsimonious models may be of limited help for these specific applications. We reasoned that some limitations of the most parsimonious G/I models (e.g. inaccurate estimation of insulin sensitivity, multiple assumptions in key parameters of the G/I system) could be overcome by combining the assessment of insulin sensitivity yielded by a gold standard technique, i.e. the

hyperinsulinemic euglycemic clamp (HEC), with minimal modeling previously applied by us to unlabeled IVGTTs [76] with slight modifications inspired by our experience with labeled IVGTT [45]. This paper presents a novel mathematical model (GLUKINSLOOP 2.0) aimed at characterizing the G/I time-courses and quantitating the components of the G/I system during a standardized meal test. The GLUKINSLOOP 2.0 model builds on previous experience in our lab [45,76] and provides a comprehensive description of the G/I system by introducing an original solution to model glucose dynamics after meals, which is usually accommodated with either a piecewise linear continuous function, partial differential equations, or delay compartments, or a combination of them [29,50,51,59]. Owing to the special relevance of this work in the field of T1D, the GLUKINSLOOP 2.0 model has been used to describe the G/I system during a mixed meal test (MMT) in patients with T1D on insulin pump therapy. Among the ten patients considered, six were studied twice in separate days with MMTs of variable size in order to explore both the performance and the reproducibility of GLUKINSLOOP 2.0. Our results might be relevant to strategies aimed at improving the architecture of upcoming closed-loop insulin delivery systems.
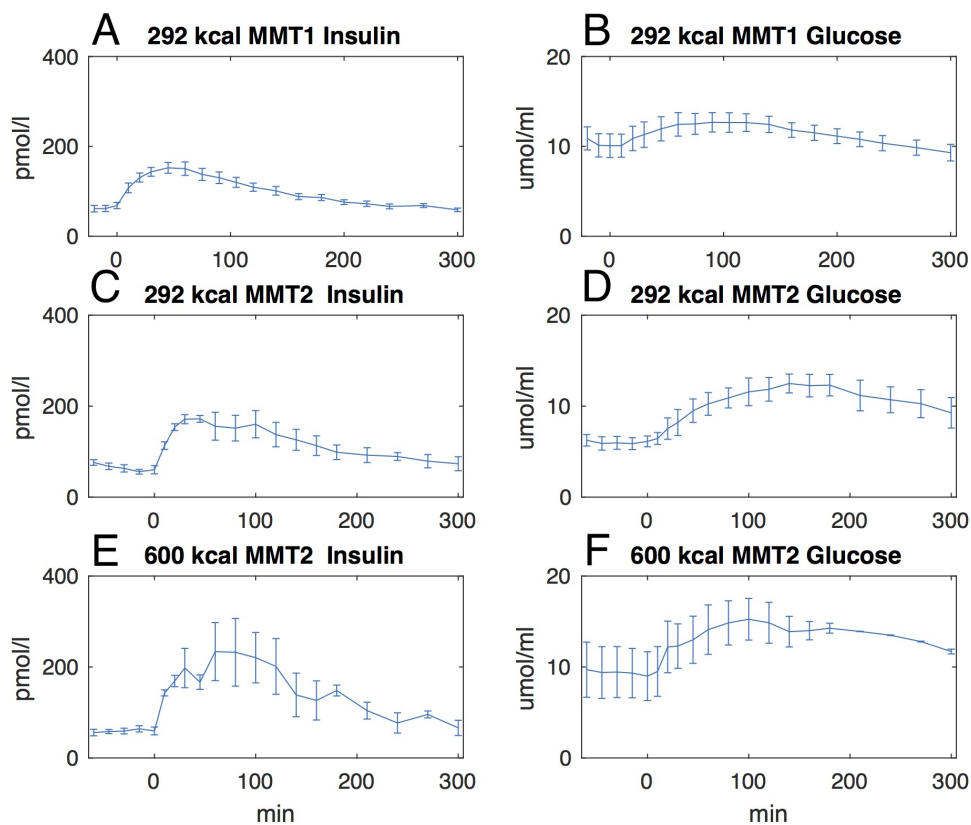
Figure 3.1: *Time courses of plasma insulin and glucose levels during the 292 Kcal and 600 Kcal MMTs. Panels A-B: mean (±SEM) plasma insulin and glucose concentrations at each time point during the 292 Kcal MMT (MMT1) in the 10 study participants. Panels C-D: MMT2, n=3, MMT=292 Kcal. Panels E-F: MMT2, n=3, MMT=600 Kcal.*

3.2 Results

The main clinical and metabolic features of the study patients are shown in Tab. 3.1. A quite large heterogeneity was evident in terms of age, body size, glucose control, duration of diabetes and time since the initiation of CSII therapy. When compared to historical healthy controls, the study patients had somewhat lower insulin sensitivity [77]. Figure 3.1 shows the time courses of plasma insulin and glucose concentrations during the 292 Kcal MMTs and during the 600 Kcal MMT, calculated as the average (±SEM) of the insulin and glucose concentrations at each time point during the MMTs for each group of patients undergoing the metabolic studies. As expected, plasma glucose/insulin time-series were higher in the latter (panels E-F) than in the former (panels A-D) set of MMTs. Figure 3.2 provides a simplified description of the GLUKINSLOOP 2.0 model herein applied to describe the G/I system and to identify its (unknown) parameters. The figure highlights the inherent conciseness of this new modeling solution, which is based on a parsimonious core set of ordinary differential equations (ODEs), as further detailed in the Methods section. A more detailed scheme and an accompanying thorough explanation of the GLUKINSLOOP 2.0 model equations are provided in the Section 3.6 (Fig. 3.5 and Section).
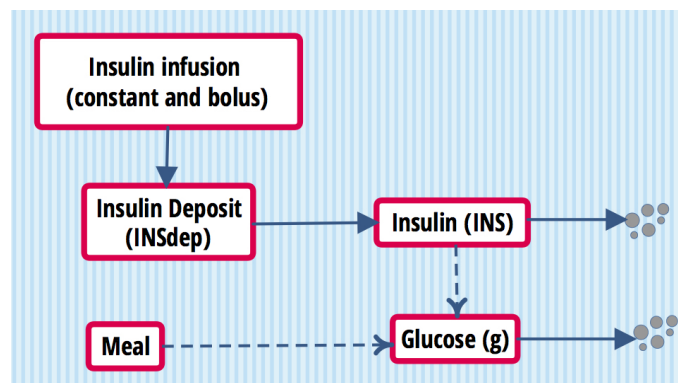
Figure 3.2: *The GLUKINSLOOP 2.0 model. In this schematic representation [1] of the model continuous arrows indicate transformations and dashed ones indicate regulations. Arrows pointing towards grey dots indicate degradation. A more detailed figure and an accompanying thorough explanation of the model are provided in the Section 3.6 (Fig. 3.5).*

Visual inspection of weighted residuals indicates a good fit of the model to the experimental data (Fig. 3.3). The simulation outputs, expressed as model fits to the insulin and glucose curves, are provided in Figures 3.6-3.15. In Figures 3.6-3.15the curves for each repeated study patient, during the 292 Kcal and 600 Kcal meals, are labeled as MMT1 and MMT2, respectively. Figure 3.4 shows the mean behavior (mean±SEM) of the Oral Glucose Input function (OGI), among the patients for the different meals. The shape and the peak of the curve agree with existing literature [2]. Repeated MMTs showed a good degree of reproducibility of the key physiological parameters (Tab. 3.2 and Tab. 3.7). Importantly, reproducibility was fairly good even when comparing meals of different sizes (Tab. 3.2 and Tab. 3.7, patients 4, 5 and 6). Mean transit time

of insulin (Insulin MTT) in the s.c. deposit were 112±56 (min) for MMT1 and 131±66 (min) for MMT2, respectively (Tab. 3.2); its within-subject coefficient of variation (±SD) was 28±18% (Tab. 3.2I). The apparent mean transit time of the oral glucose load from ingestion to the appearance in the accessible glucose pool (Glucose MTT) were 117±35 (min) for MMT1 and 109±35 (min) for MMT2, respectively (Tab. 3.2); its within-subject coefficient of variation (±SD) was 11±6% (Tab. 3.2I).
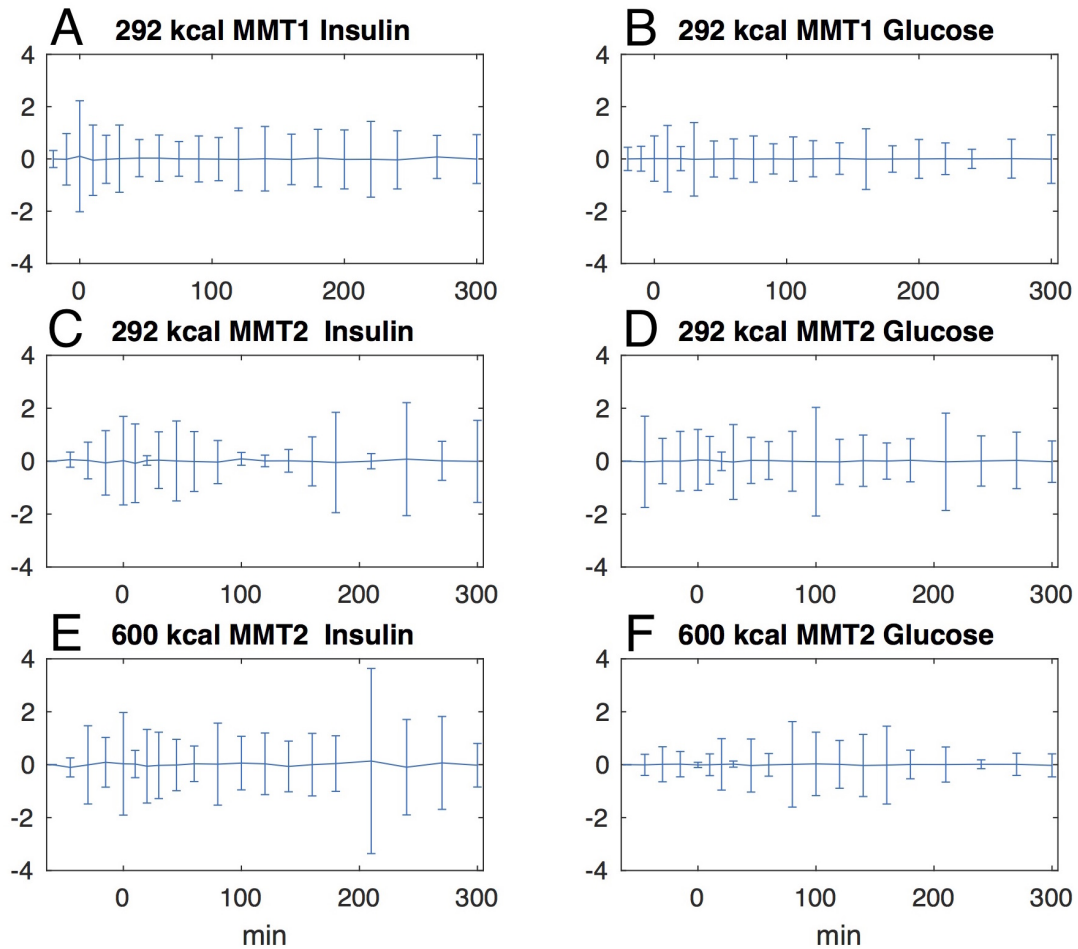
Figure 3.3: *Mean weighted residuals of the model fit to experimental insulin and glucose time courses during MMT1 and MMT2. The weighted residuals are a quantitative point-by-point assessment of the goodness-of-fit of the model to the experimental data: a theoretically perfect fit should generate weighted residuals with mean 0 and SD of 1, reflecting the distribution of errors during the experimental sampling. Panels A-B: mean ±SD of weighted residuals at each time point during the 292 Kcal MMT (MMT1) in all 10 study participants. Panels C-D: MMT2, n=3, MMT=292 Kcal. Panels E-F: MMT2, n=3, MMT=600 Kcal.*
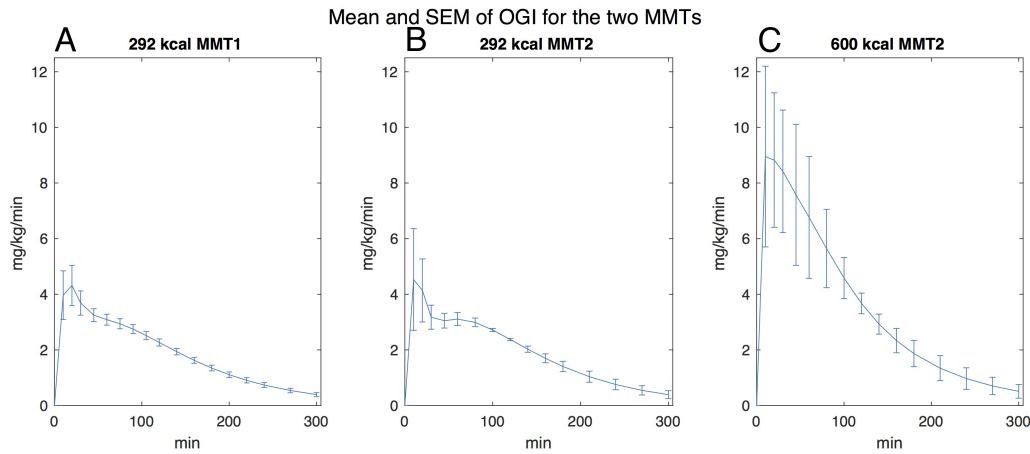
Figure 3.4: *The Oral Glucose Input function. Panels A-C show the output of the OGI function layered by different MMTs. The OGI function, i.e. the predicted glucose rate of appearance in the bloodstream at each time point after the MMT ingestion, is provided as mean±SEM of the individual OGI values for the study patients undergoing the MMT1 and MMT2 and is expressed as mg/Kg/min (see Fig. 3.16 for the same panels expressed as µmol/min) . Curve shapes and peaks are consistent with analogous functions in literature [2]. Detailed description of the function can be found in Section 3.6.*

3.3   Discussion

In this study, we successfully tested the hypothesis that, with the aid of the "external" assessment of insulin sensitivity by the HEC, the G/I system would be amenable to be successfully reconstructed in T1D patients, in whom modeling of the G/I system has become a key component of therapeutic innovative strategies [73–75]. Differently from previous models, which need to fix a number of parameters (glucose effectiveness, volume of distribution, fractional splanchnic extraction of glucose) to estimate meal insulin sensitivity, we exploit clamp-derived insulin sensitivity and parameters to reconstruct the G/I system during a mixed meal.

The novelty of our approach lies primarily in parsimony. Published models for OGTTs or meal tests were first based on more complex structures of the glucose system (typically two compartments were needed to accommodate glucose dynamics) and this, at variance with our proposal, entailed the need

Parameters	MMT1	MMT2
S_I , (ml/min)/(pmol/l)	0.78 ± 0.31	0.76 ± 0.38
S_G , ml/min	20.8 ± 18.4	24.2 ± 14.7
Glucose MTT, min	117 ± 35	109 ± 35
Insulin MTT, min	112 ± 36	131 ± 66

Table 3.2: *Model estimates (mean±SD) in all study participants of the key physiological parameters included in the GLUKINSLOOP 2.0.*

Parameters	Coefficient of Variation (%; mean $\pm$SD)
S_I	12 ± 17
S_G	23 ± 26
Glucose MTT	11 ± 6
Insulin MTT	28 ± 18

Table 3.3: *Day-to-Day within-subject coefficients of variation (%; mean $\pm$SD) of the key physiological parameters included in the GLUKINSLOOP 2.0.*

for tracer technology to identify the parameters governing the glucose system [2, 10, 22, 42, 44, 46]. In the last 15 years, single compartment models were introduced, both without and with the aid of tracer technology [21, 29, 29, 31, 50, 51, 56, 64, 66]. Single compartment models with no tracer aid require a number of assumptions to reconstruct a reliable estimate of the rate of appearance of oral glucose, but they may provide somewhat variable estimates of insulin sensitivity [2, 13, 29, 50, 69]. The single compartment model with oral tracer glucose performs better than in the absence of a glucose tracer; however, its estimate of endogenous glucose production is good when expressed as the ratio of basal endogenous glucose production, but it may be inaccurate in absolute terms [67]. Increasing the number of tracers to two or three yields the best available estimates of endogenous glucose production, insulin sensitivity and glucose disposal, but it considerably increases study complexity and costs [12]. Our approach transfers the single glucose compartment description of the time honored minimal model from the IVGTT [54] to the MMT [46]. So far, a parsimonious description of the OGTT [31, 64] was focused only on the use of the OGTT as a test to assess insulin sensitivity [30, 31, 64], at the cost of embodying a number of assumptions, of fixing numerical values for some parameters and of eventually providing insulin sensitivity values, which may be somewhat inaccurate. These limitations are overcome by the herein presented GLUKINSLOOP 2.0 model of the G/I system. The performance of our model, however, does not contradict the extensive previous experience with the single compartment OGTT (and MMT) models with no glucose tracer(s) [29–31, 50, 64]. Early experience taught us that, when insulin sensitivity is unknown, it can be estimated from the oral tests at the cost of several approximations and assumptions in the parameters governing glucose dynamics [29–31, 64]. Our present experience is logically coherent and complementary to the previous one, in that, if insulin sensitivity is known with the low uncertainty provided by the hyperinsulinemic euglycemic clamp (HEC), the key parameters of the G/I system can be safely estimated and a parsimonious description of the system can provide a good description of the glucose dynamics. As an added value, this evidence is obtained in patients with T1D, in whom new, parsimonious models of the G/I system may improve current efforts in building algorithms capable to safely and precisely deliver insulin in the context of closed-loop devices [72]. From this viewpoint, our model has the attractive feature of

showing a good degree of reproducibility of its key physiological parameters from day to day, and also with different meal sizes (Tab. 3.2). Of note, both the performance and robustness of the G/I dynamics estimates yielded by the GLUKINSLOOP 2.0 model were quite satisfactory despite the wide clinical heterogeneity of the study patients in terms of age, sex, diabetes duration and glycemic control. Some specific characteristics of our model are different from the original minimal models and need to be discussed in some detail. First, in contrast with some previous single-compartment models with no tracer(s), we explicitly deal with glucose fluxes, and not concentrations [30]. The latter ones may be more convenient to handle, at least for the sake of simplicity. For instance, we are forced to know exactly the amount of glucose equivalents ingested. On the other hand, working with extensive properties of the G/I system (fluxes, volumes) is unavoidable, if one wants to obtain a complete description of the system and of its capability to cope with meal challenges, as well as to predict its behavior in response to meals of different size. Second, we introduced a fixed flux of glucose utilization, which primarily reflects brain glucose utilization, in agreement with the two-compartment minimal models proposed for studies with glucose tracer [45,65], but not for single compartment models, such as the present one. In our opinion, the assumption of fixed glucose utilization (by the brain) is a perfectly tenable assumption and it is one of the improvements brought about by two-compartment minimal models for tracer glucose [65] over the minimal models for unlabeled glucose [11]. In our experience, there is no reason why this improvement in the description of the system should not be implemented also in the models for unlabeled glucose. Third, the combined presence of a fixed glucose utilization and glucose effectiveness (SG) forced the need for a glucose input in the basal, un-stimulated state, which exactly matches the combined effect of brain glucose utilization and SG and ensures the attainment of a steady state at baseline. Although it would be tempting to label this glucose input as endogenous glucose production - and its order of magnitude in our patients is indeed in the expected range - no measure of endogenous glucose production is available in our work and this glucose input should be considered as instrumental to the attainment of a steady state in the post-absorptive state. Fourth, as in all minimal models in which no glucose tracers are used, insulin sensitivity combines the net effect of insulin on glucose utilization and on glucose production [30,31,50,54]. Fifth, since no explicit endogenous glucose production is included in our model, the glucose input after meal ingestion should not be considered as a pure estimate of the appearance of oral glucose, because we cannot rule out the possibility that a minor fraction of it actually is due to an amount of residual endogenous glucose production, which is not captured by the insulin sensitivity parameter. Some limitations of our study should be recognized. First, only patients with T1D are presented in this study; hence, the performance of our approach in normal individuals or in other pathologic conditions currently remains unexplored. However, the class of patients included in this study is expected to directly benefit most from novel simplified glucose models. Secondly, the number of

studies herein presented is somewhat limited; however, this paper primarily aims at presenting the new GLUKINSLOOP 2.0 model, and it is not concerned with the report of novel pathophysiological insights. To this regard, it should be noted that the presentation of repeat studies (12 over a total of 16) with the same modeling methodology is a somewhat rare occurrence in this field and, as such, accounts for the stringent sensitivity analysis we applied to our data. Third, a separate insulin clamp (HEC) needs be performed to measure insulin sensitivity, thereby adding to the experimental burden one additional study day. In summary, we have introduced a HEC-supported minimal model of glucose dynamics after a mixed meal in patients with T1D. The GLUKINSLOOP 2.0 model apparently performs reasonably well and shows a good degree of reproducibility without employing labeled tracers. Hence, given the relevance of in vivo characterization of the G/I system dynamics, this model timely proposes itself as a useful step towards better algorithms to control glucose dynamics after meal ingestion in patients with T1D on sensor-augmented insulin pump therapy.

3.4   Methods

Subjects Ten (4 men/2 women) adult patients with C-peptide negative type 1 diabetes (T1D) were recruited for the study among those regularly attending the Diabetes Center of the Verona City Hospital. Their main clinical characteristics are shown in Tab. 3.1. All patients were on isocaloric dietitian prescribed diet and were free from any other disease except diabetes (only Patient 3 had autoimmune hypothyroidism and was euthyroid on 150 μg/day levotiroxin p.o. at the time of study enrollment). After a thorough explanation of the procedures and purposes of the study, a written informed consent was obtained from all patients to be included in the study. The study protocol (registered as NCT01800734 in December 3rd, 2013) was approved by the local Institutional Review Board (Comitato etico per la sperimentazione clinica delle Province di Verona e Rovigo) and was carried out according to the International Conference on Harmonisation Good Clinical Practice guidelines.

3.4.1   Phenotyping

Standard clinical parameters were assessed in all study patients. Metabolic tests were carried out at the Division of Endocrinology, Diabetes and Metabolism of the University of Verona Medical School (Verona, Italy), on three separate days, each test starting at 08:00 a.m., after a 10-12-h overnight fast. All patients were on CGM; the device had been in place and properly working (calibration with capillary blood glucose as measured by glucometer at pre-established hours of the day) for at least two days before metabolic studies. CGM data were collected for a companion experiment. During the entire study duration patients lay recumbent in bed. Two of the three studies were performed in random order. Study 1 - On one day, all patients underwent a hyperinsulinemic euglycemic insulin clamp (HEC). Study 2 - On a second occasion, all patients

were studied with a standardized mixed meal test (MMT1) of 292 Kcal. Study 3 - The third study (MMT2) was in 3 patients the repetition of the 292 Kcal MMT, whereas in other 3 patients it consisted of a 600 Kcal MMT, with the same relative macronutrient composition of the 292 Kcal MTT.

3.4.2 Assessment of Insulin Sensitivity (Study 1)

A standard HEC was carried out to assess insulin sensitivity, which was computed with standard formulae [41,78], and expressed as the amount of glucose metabolized during the last 60 min of the clamp. Subjects were instructed to use their usual nocturnal fast insulin analogue basal rate, to be left unchanged for at least five hours before the beginning of the test. Human insulin concentration was raised with an intravenous prime (0.8 U/m^2 BSA) and maintained constant by a constant intravenous infusion (40 mU/min·m^2 BSA). Plasma glucose was allowed to fall until it reached the physiologic range (i.e. < 5.6 mmol/l), after which it was clamped at 5.0 mmol/l for at least 60 min by appropriately changing an intravenous infusion of 20% dextrose.

3.4.3 Mixed-Meal Tests (Study 2 and 3)

The MMTs were performed to determine the time courses of plasma glucose and insulin during a mixed meal and to assess the pathophysiology of glucose control during a standardized physiological challenge. Subjects were instructed to be on an Indian corn free and cane sugar free diet for at least one week before each study and were instructed to use their usual nocturnal fast insulin analogue basal rate, to be left unchanged for at least five hours before the beginning of the test. A standardized mixed meal of maize polenta plus seasoned Italian Parmesan cheese (292 Kcal, 38.9 g carbohydrates, 8.9 g fats and 14 g proteins) was ingested by all study participants, and patients were monitored for 300 minutes thereafter. The time taken by the patients to ingest the meal was recorded. Right before meal ingestion, a fast subcutaneous insulin analogue bolus was administered through the pump, according to the individual insulin-to-carbohydrate ratio and correction dose. On a separate day, a MMT of the same size was repeated in three patients, while a MMT with the same composition, but of double caloric size, was administered in the other three patients. In both cases, the experimental procedures were identical to the first MMT. In all studies, blood samples were drawn at time intervals, put in ice and quickly spun at 1500 g at +4°C. Plasma/serum specimens were stored at -80°C.

3.4.4 Measurements

Plasma glucose was measured in duplicate with an YSI 2300 Stat Plus Glucose &Lactate Analyzer (YSI Inc., Yellow Springs, OH, USA), at bedside. Blood samples were collected at timed intervals to measure plasma insulin. Interstitial glucose monitoring was performed by the CGM device throughout the entire duration of insulin clamp for a companion experiment. Serum insulin

concentrations were measured by ELISA (Mercodia, Sweden) [78]. Glycosylated hemoglobin was measured by standard in-house methods. GAD-65 antibodies were measured by immunoradiometry (CentAK, Medipan, Germany), according to manufacturer's instructions (detection limit >1 KU/l).

3.4.5 Models

The MMT experiment, described in detail above, is modeled starting from the Minimal Model [11,54] ideas and its further refinements [11,29,29,40,45,46,50,65]. Figure 3.2 and Fig. 3.5 present a schematic representation of the model, which is tailored to consider T1D patients' conditions and presents an original and physiologically plausible function, called Oral Glucose Input (OGI), to model the glucose appearance in the plasma. The MMT model is used to reproduce the insulin-glucose time series obtained during two different MMT experiments, as explained in Mixed-Meal Tests (Study 2 and 3). Parameters are estimated by fitting experimental data using non-linear least squares and a multi-start approach to ensure a global optimum. To reduce the uncertainty of parameter estimates, a combination of clamp-derived, patient-specific and literature-based prior information have been considered to drive the optimization process (see sections 3.5 and 3.6). The robustness of the model has been also confirmed by the good reproducibility of parameter estimates on the two MMT experiments for all the physiological parameters (Tab. 3.2). To simplify the description, the MMT model has been conceptually designed as being composed by two submodels (the "insulin" and the "glucose" submodel), which interact as shown in Fig. 3.5. Since we are dealing here with T1D patients, the insulin submodel has been developed as a mono-compartmental model, where the beta-cell contribution to insulin secretion [43, 47, 79, 80] is removed. It describes the dynamics of the insulin deposit in tissues, due to the insulin injection, and the insulin concentration in the volume where insulin sampling takes place. The glucose submodel is realized through a mono-compartmental model as well, where insulin action regulates glucose metabolism according to the minimal model principles [46, 54]. The appearance of the ingested glucose in the system is obtained through the Oral Glucose Input function (OGI, see Section 3.6). Such a function is the output of two chains of compartments, representing fast and slow glucose absorption during the digestion, which produces exponential-shaped outputs combined into a one/two peak(s) shape with exponential decay, as depicted in Fig. 3.4. This function integrates and extends previous observations [29,51,52], by modeling the processes of digestion/absorption with just three parameters. For a more detailed description of the model, we refer to the Section 3.6. We refer to the section 3.5 for further details on the implementation and parameter estimation procedures.

3.5   Technologies

We implemented the GLUKINSLOOP 2.0 model in MATLAB v. R2016a (The MathWorks Inc., Natick, MA, USA) using ordinary differential equations (ODEs)

simulated according to a Runge-Kutta algorithm. Model equations include sixteen unknown parameters. We carried out parameter estimation by non-linear least squares using the lsqnonlin function (MATLAB Optimization Toolbox v. R2016a, trust-region-reflective algorithm [81,82]) with a 1e-10 tolerance and a multi-start approach to ensure a global optimum (MATLAB Global Optimization Toolbox v. R2016a). To take into account the differences in concentration of insulin and glucose without introducing a bias in the fitting procedure, squared-relative-errors weighted on experimental standard deviations have been considered for parameter estimation. In addition, for each parameter whose prior information was available, a penalty term proportional to the distance of the current parameter estimate from the prior has been added to drive the optimization process.

3.6 Supplementary Material

Models and Equations

The GLUKINSLOOP 2.0 model herein presented has been developed as a set of ordinary differential equations (ODEs), which describe the regulation of glucose and insulin during a Mixed Meal Test (MMT) in T1D patients on insulin pump therapy (CSII, continuous subcutaneous insulin infusion). The GLUKINSLOOP 2.0 model is designed to run as a whole during simulation and parameter estimation. However, for the sake of simplicity and only for descriptive purposes, the model was conceptually divided in two submodels: the "insulin" and the "glucose" submodel. The relationships among the compartments comprised in the GLUKINSLOOP 2.0 model and within its submodels are depicted in Fig. 3.5. The unknown parameters of the "insulin" and "glucose" submodels included in the ODEs (Tables 3.4-3.5) have been estimated in each subject (Tables 3.7-3.8) by fitting simultaneously the experimental time series of both circulating insulin and glucose (Figures 3.6-3.15). Paragraph 3.6 provides the formal description of the model employed to fit the Hyperinsulinemic Euglycemic Clamp (HEC) experiment. The parameters estimates of the HEC model (Tab. 3.6) are entered in the GLUKINSLOOP 2.0 model (specifically, in the "glucose" submodel) to drive the estimation of a number of unknown parameters according to the following description.

Mixed Meal (Insulin Submodel) The GLUKINSLOOP 2.0 is built on the assumption that insulin is provided through exogenous injection, since endogenous insulin secretion is not detectable in T1D. The Insulin Submodel (Fig. 3.1, purple box) aims at fitting the time course of circulating insulin concentration during the MMT. The Insulin Submodel is comprised of two equations. The first equation defines the INS_{dep} (μl of a 100 U/ml insulin solution) function, which represents the insulin deposit in tissues due to the exogenous CSII-driven

insulin injection:

$$\frac{d\,INS_{dep}(t)}{dt} = \begin{cases} INS_{ci} + INS_{bolus} - INS_{dep}(t) \cdot k_{01}(t), & 0 \le t \le Time_{bolus} \\ INS_{ci} - INS_{dep}(t) \cdot k_{01}(t), & \text{otherwise} \end{cases}$$

(3.1)

In the equation above INS_{ci} represents the constant insulin infusion ($\mu l \cdot min^{-1}$ of a 100 U/ml solution), while INS_{bolus} represents the insulin bolus injected before the mixed meal. Insulin transit from tissues to the bloodstream is modeled by the non-linear function $k_{01}(t) = 1/(SCAR \cdot \sqrt[3]{3/4\pi \cdot INS_{dep}(t)})$, which assumes that insulin diffusion is inversely proportional to the radius of a sphere with volume equal to INS_dep ($SCAR$ is a parameter regulating insulin exit from the subcutaneous depot).

The second equation of the Insulin Submodel defines the $INS(t)$ (pmol/l) function, which provides the insulin concentration dynamics in the compartment where the sampling of circulating insulin takes place:

$$\frac{d\,INS(t)}{dt} = CONV \cdot [INS_{dep}(t) \cdot k_{01}(t) - k_{03}(t) \cdot INS(t)$$

(3.2)

where $CONV$ is a conversion factor between INS and INS_{dep}, and $k_{03}(t) = INSCAT + INSCAT_2 \cdot [1 - \tanh(FEPER \cdot INS(t))]$. The parameter $k_{03}(t)$ represents the time-varying clearance of insulin from the sampling compartment, in which the hyperbolic function describes the inverse relationship between insulin concentration and insulin clearance [83] primarily due to nonlinearity and saturability of insulin extraction by the liver [33,84,85]. The unknown parameters of the Insulin Submodel are summarized in Tab. 3.4. For each parameter an initial estimate is provided, along with the optimization boundaries assigned to the system to compute the final parameter estimate.

Parameter	Initial Value	Lower Bound	Upper Bound
$Idep(0)$ (μl)	30	1	500
$SCAR$ ($min(\mu l/min)^{-1/3}$)	50	1	500
$CONV$ (unitless)	20	1	1500
$INSCAT$ (min^{-1})	0.05	0	10
$INSCAT_2$ (min^{-1})	0.05	0	10
$FEPER$ ($pmol/l)^{-1}$	0.002	0.0001	0.05

Table 3.4: *Unknown parameters of the Insulin Submodel.*

Mixed Meal (Glucose Submodel) This submodel is related to glucose dynamics and is highlighted in skyblue in Fig. 3.5. The glucose input into the plasma compartment, due primarily to the ingestion of the mixed meal, is modeled by means of the Oral Glucose Input ($OGI, \mu mol/min$) function, described further

below in paragraph 3.6. Glucose dynamics, g (μmol), are described by the following equations:

$$\frac{dg(t)}{dt} = \begin{cases} (CGU + S_G \cdot G_{SS} - k(0,G) \cdot g(t), & \text{if } (CGU + S_G \cdot G_{SS} - (1-SGE) \cdot OGI(t)) \geq 0 \\ (1-SGE) \cdot OGI(t) - k(0,G) \cdot g(t), & \text{otherwise} \end{cases}$$

(3.3)

$$K(0,G) = \begin{cases} CGU/g(t)k_G + q_2(t), & \text{if } G/t(< 10\mu mol/ml) \\ k_G + k_{guria}(t) + q_2(t), & \text{otherwise} \end{cases}$$

(3.4)

where SGE is the apparent fractional splanchnic glucose extraction, CGU is the constant glucose uptake, given by $203 \cdot BSA$ (body surface area); S_G is the glucose effectiveness, G_{SS} (μmol/ml) is the glucose concentration at the steady state (minimum value of the experimental data); $G(t)$ is the glucose concentration $(g(t)/V_G)$ at time t; $q_2(t)$ indicates the insulin action at time t (see Eq. 5); and $k_{guria}(t)$ represents the time varying rate constant of glycosuria (min^{-1}) derived from measured urinary glucose. Formally:

$$k_{guria}(t) = [RClearance/g(t)] \cdot (G(t) - 10),$$

where $RClearance = (Glycosuria)/\int [(G(t) - 10 + |G(t) - 10|)/2]dt$

and the $\int$ denotes the integral between the beginning and the end of the experiment. RClearance represents the renal clearance of glucose $((G_U \cdot V_U)/G_P$, with G_U urinary glucose concentration; V_U urine volume; G_P plasma glucose level), which comes into play above the renal threshold of glycosuria (about 10 mmol/l).

The insulin action $q_2(t)$ (min^{-1}) on glucose metabolism is described by the following equation:

$$\frac{dq2(t)}{dt} = \begin{cases} [INS(t) - INS_{AT}] \cdot p_2 \cdot (S_I/V_G) - p_2 \cdot q2(t), & \text{if } [INS(t) - INS_{AT}] \geq 0 \\ -p_2 \cdot q2(t), & \text{otherwise} \end{cases}$$

(3.5)

where $INS(t)$ is the circulating insulin concentration at time t, computed by simulating the Insulin Submodel; INS_{AT} is the concentration threshold above which insulin action takes place; p_2 is the rate constant of insulin action fading; V_G (milliliters, ml) is the apparent glucose distribution volume; and S_I is the insulin sensitivity at the steady state (see paragraph 3.6). The unknown parameters of the Glucose Submodel are summarized in Tab. 3.5. For each parameter an initial estimate is provided, along with the optimization boundaries assigned to the system to compute the final parameter estimate. Of note, the Glucose Submodel includes four additional parameters (Tab. 3.6), estimated from the HEC experiment as detailed further below in paragraph 3.6. The HEC-derived parameter estimates drive the multistart fitting of the mixed meal model by initializing one starting point to the values computed during the HEC fitting.

Moreover, the final estimates of V_G, S_G and S_I have been assumed to follow a normal distribution of mean equal to the HEC estimate and standard deviation (SD) of 20%, which accounts for the variability of patient metabolism and uncertainties in experimental measures. This has been implemented by including a penalty term $((MixedMeal_{estimate} - HEC_{estimate})/HEC_{SD})^2$ in the objective function for each parameter. Also the estimation of the parameters INS_{AT} and SGE followed the same approach, where the mean of the INS_{AT} distribution has been determined by the insulin basal and the mean of the SGE distribution has been inferred from population data [52, 86].

Parameter	Initial Value	Lower Bound	Upper Bound
$q_2(0)$ (min^{-1})	0.001	0	0.05
SGE (unitless)	0.14 with 20% of SD [52]	0	-
k_{fast} (min^{-1})	0.3	0.01	1
GTT_{fast} (min)	50	1	200
GTT_{slow} (min)	80	10	300
INS_{AT} (pmol/l)	insulin basal with 20% of SD	0	-

Table 3.5: *Unknown parameters of the Glucose Submodel. Parameter estimates from the HEC submodel are included according to paragraph 3.6*

Oral Glucose Input (OGI) function The OGI(t) function describes the dynamics of glucose input (μmol/min) into the plasma compartment after the ingestion of the mixed meal and accounts for the delay of glucose appearance in the bloodstream after meal ingestion and gut transit (see Fig. 3.16). The OGI function architecture rests on a multi-compartmental model constituted by two chains of 2 compartments (the minimum length required to build a delay chain):

$$OGI(t) = Comp^2_{fast}(t) \cdot kdiff_{fast} + Comp^2_{slow}(t) \cdot kdiff_{slow} \quad (3.6)$$

where:

$$\frac{d\,Comp^2_{fast}(t)}{dt} = kdiff_{fast} \cdot (Comp^1_{fast}(t) - Comp^2_{fast}(t))$$

$$\frac{d\,Comp^1_{fast}(t)}{dt} = k_{fast} \cdot Gload(t) - kdiff_{fast} \cdot Comp^1_{fast}(t)$$

$$\frac{d\,Comp^2_{slow}(t)}{dt} = kdiff_{slow} \cdot (Comp^1_{slow}(t) - Comp^2_{slow}(t))$$

$$\frac{d\,Comp^1_{slow}(t)}{dt} = k_{slow} \cdot Gload(t) - kdiff_{slow} \cdot Comp^1_{slow}(t)$$

and:

$$\frac{d\,Gload(t)}{dt} = \begin{cases} GlucoseLoad - Gload(t), & \text{if } t \in [0, MealTimeLength] \\ -Gload(t), & \text{otherwise} \end{cases} \quad (3.7)$$

In the equations above, GlucoseLoad (μmol/min) represents the averaged glucose (carbohydrates) mass that is ingested in a minute during the meal, while k_{fast} and k_{slow} (min^{-1}) are two kinetic parameters, representing the fraction of ingested glucose (carbohydrates) which follows the fast and slow route, respectively. As such, the net sum $k_{fast} + k_{slow} = 1$. The kinetic parameters $kdiff_{fast}$ and $kdiff_{slow}$ (min^{-1}) represent the rate constants at which glucose travels through each chain of compartments. The average time taken by glucose to travel through each chain of compartments is calculated as Ingested Glucose Transit Time (IGTT) of the fast and of the slow route, respectively ($IGTT_{fast}$ and $IGTT_{slow}$). Parameters $kdiff_{fast}$ and $kdiff_{slow}$ are computed as the number of compartments of the chain divided by the corresponding IGTT ($2/IGTT_{fast}$ and $2/IGTT_{slow}$). For each MMT, the Ingested Glucose Mean Transit Time (Glucose MTT1 and Glucose MMT2) provided in Table II of the main text and in Tab. 3.7, is computed by the weighted average of $IGTT_{fast}$ and $IGTT_{slow}$ according to their respective kinetic parameters, k_{fast} and k_{slow}, as follows: Glucose MTT = $k_{fast} \cdot IGTT_{fast} + k_{slow} \cdot IGTT_{slow}$.

Hyperinsulinemic Euglycemic Clamp (HEC Submodel) The MMT model introduced above has been coupled with a separate model describing the kinetics of glucose and insulin during the hyperinsulinemic euglycemic clamp (HEC) procedure in patients with diabetes, who are hyperglycemic in the fasting state. The HEC is the time-honoured gold standard to assess insulin sensitivity (S_I) [41]. As explained above in paragraph 3.6, the estimates of the four parameters included in the model (V_G, S_G, p_2 and S_I) are employed in the GLUKINSLOOP 2.0 to drive the estimation of the corresponding parameters in the Glucose Submodel. The kinetic of glucose and insulin during the HEC experiment are described by means of a mono-compartmental model (also referred as the "glucose metabolism" compartment), in which the dynamics of glucose (g) interact with the corresponding insulin action (q_2) over time (t). The glucose dynamics are described by the following equation:

$$\frac{d\,g(t)}{dt} = \begin{cases} (S_G \cdot (G_{SS} - G(t)) - q_2(t) \cdot g(t), & \text{if } (CGU + S_G \cdot G_{SS} - GIR) \geq 0 \\ GIR - CGU - S_G \cdot G(t) - q_2(t) \cdot g(t), & \text{otherwise} \end{cases} \tag{3.8}$$

where CGU is the constant glucose uptake, given by $203 \cdot BSA$(body surface area); S_G is the glucose effectiveness; G_{SS} is the glucose concentration at the steady state (i.e. the minimum value of the experimental time series); GIR is the intravenous glucose infusion rate; $G(t)$ is the glucose concentration ($g(t)/V_G$) at time t; and $q_2(t)$ is the insulin action at time t. Insulin action $q_2(t)$ is described by the following equation:

$$\frac{d\,q_2(t)}{dt} = [INS(t) - INS_{SS}] \cdot p_2 \cdot ((S_I)/V_G) - p_2 \cdot q_2(t) \tag{3.9}$$

where $INS(t)$ is the linear interpolation of insulin's experimental data at time t, $INS_S S$ is the insulin concentration at baseline, p_2 is the rate constant of insulin

action fading, V_G is the apparent glucose distribution volume and S_I is insulin sensitivity at steady state hyperinsulinemia. In order to enhance the reliability of the estimation of S_I, we refined its value starting from the initial estimate [2]:

$$S_{I\text{Intial}} = \frac{\text{Insulin Dependent Glucose Clearance}}{\Delta_{INS}} \qquad (3.10)$$

where:

$$\text{Insulin Dependent Glucose Clearance} = (M - CGU)/G_{HEC_{SS}}$$

and

$$\Delta_{INS} = INS_{HEC_{SS}} - INS_{SS}$$

The value of M (μmol $\cdot$ min^{-1}) is the HEC-derived measure of whole-body insulin action and is defined as the average glucose infusion rate over the last 60 minutes of the HEC. $G_{HEC_{SS}}$ is the average glucose concentration at steady state of the HEC, $INS_{HEC_{SS}}$ is the average insulin concentration at steady state of the HEC and INS_{SS} is baseline insulin concentration. The unknown parameters of the HEC Submodel are summarized in Tab. 3.6. For each parameter an initial estimate is provided, along with the optimization boundaries assigned to the system to compute the final parameter estimate.

Parameter	Initial Value	Lower Bound	Upper Bound
V_G (ml)	10000	4000	20000
S_G (ml/min)	40	0	250
p_2 (min^{-1})	0.1	0.0001	1
S_I ((ml/min)/(pmol/ l))	S_I Initial (Eq. 10)	S_I Initial -20%	S_I Initial +20%

Table 3.6: *Unknown parameters of the HEC Submodel.*

		S_I	S_G	Ingested Glucose MTT	Subcutaneous Insulin MTT
Patient 1	MMT1	0.80	14.01	115	50
	MMT2	0.80	31.11	107	108
Patient 2	MMT1	0.40	8.67	136	70
	MMT2	0.42	17.66	152	77
Patient 3	MMT1	1.36	5.49E-13	144	178
	MMT2	1.30	5.49E-13	87	130
Patient 4	MMT1	0.59	37.37	73	27
	MMT2	0.29	46.28	62	53
Patient 5	MMT1	0.66	9.07	191	183
	MMT2	0.67	9.29	147	221
Patient 6	MMT1	1.09	16.12	75	136
	MMT2	1.08	16.49	99	196
Patient 7	MMT1	0.55	60.27	105	129
Patient 8	MMT1	0.61	27.70	92	170
Patient 9	MMT1	1.15	13.61	127	100
Patient 10	MMT1	0.60	4.54E-08	108	76

Table 3.7: *Estimates of key physiological parameters of the GLUKINSLOOP 2.0 model during MMTs in each study participant. S_I: (ml/mol)/(pmol/l); S_G: ml/min; MTT: min.*

Patient		V_G	p_2	$I_{dep}0$	$SCAR$	$CONV$	$INSCAT$	$INSCAT_2$	$FEPER$	$q_2(0)$	SGE	k_{fast}	GTT_{fast}	GTT_{slow}	INS_{AT}
Patient 1	MMT1	6317	0.00062	5.53	47.78	20.14	3.4E-02	3.4E-08	1.1E-04	1.1E-03	0.12	0.09	9	126	64.56
	MMT2	7937	0.00182	25.51	106.36	66.93	1.1E-07	1.6E-01	3.1E-03	2.4E-14	0.14	0.16	12	125	66.08
Patient 2	MMT1	10994	0.99979	12.16	76.12	42.17	4.2E-03	1.4E-01	4.3E-03	1.1E-02	0.12	0.97	136	137	46.95
	MMT2	8024	0.07434	21.08	83.77	183.30	1.5E-08	6.8E-01	4.3E-03	1.1E-02	0.07	0.07	37	160	55.57
Patient 3	MMT1	12225	0.00249	232.01	193.34	359.51	5.7E-01	2.3E+00	9.7E-03	1.9E-03	0.14	0.17	19	168	56.38
	MMT2	12487	0.00113	60.15	133.19	166.30	1.7E-01	6.0E-01	8.7E-03	4.0E-14	0.18	0.18	11	103	59.65
Patient 4	MMT1	17250	0.00313	1.04	25.35	7.15	3.1E-07	2.3E-02	2.3E-03	3.4E-14	0.13	0.19	11	88	36.05
	MMT2	20600	0.99473	10.45	40.57	20.11	8.6E-09	6.4E-02	3.4E-02	2.3E-02	0.13	0.06	3	66	50.80
Patient 5	MMT1	4290	0.00856	298.49	203.55	159.65	2.9E-04	1.3E+00	6.3E-03	1.7E-03	0.14	0.18	43	225	35.20
	MMT2	6345	0.16826	414.32	203.69	677.68	1.6E+00	1.0E+01	1.3E-02	2.5E-14	0.14	0.15	30	168	47.34
Patient 6	MMT1	18874	0.00150	36.90	114.25	72.75	3.5E-07	3.1E-01	4.2E-03	1.2E-04	0.14	0.38	21	108	45.32
	MMT2	21505	0.00059	111.36	172.93	267.20	2.4E-01	1.0E+00	6.7E-03	1.3E-03	0.14	0.24	17	125	63.88
Patient 7	MMT1	6353	0.00061	64.48	121.38	126.83	2.0E-01	8.7E-01	1.2E-02	6.2E-13	0.14	0.07	18	112	35.21
Patient 8	MMT1	16578	0.08556	383.92	177.62	200.92	2.6E-01	1.9E+00	7.2E-03	8.8E-03	0.13	0.21	24	111	70.81
Patient 9	MMT1	12587	0.09404	90.31	108.30	1312	1.3E+00	5.9E+00	6.1E-03	2.4E-14	0.12	0.06	4	134	63.52
Patient 10	MMT1	8160	0.01144	32.25	73.43	84.60	1.0E-01	3.5E-01	7.2E-03	2.5E-14	0.14	0.24	16	137	59.39

Table 3.8: *Estimates of the other parameters of GLUKINSLOOP 2.0 model during MMTs in each study participant (key physiological parameters are in Tab. 3.7). V_G: ml; p_2: min^{-1}; $I_{dep}0$: μl; SCAR: $min(\mu l/min)^{-1/3}$; CONV: unitless; INSCAT: min^{-1}, $INSCAT_2$: min^{-1}; FEPER: $(pmol/l)^{-1}$; $q_2(0)$: min^{-1}, SGE: unitless; k_{fast}: min^{-1}; GTT_{fast}: min; GTT_{slow}: min; INS_{AT}: pmol/l*

BSA	Body Surface Area
CGM	Continuous Glucose Monitoring
CGU	Constant Glucose Uptake
$Comp_{Fast}$	Fast route of ingested glucose from mouth to systemic circulation
$Comp_{Slow}$	Slow route of ingested glucose from mouth to systemic circulation
$CONV$	Scaling factor
$CSII$	Continuous Subcutaneous Insulin Infusion
$FEPER$	Parameter regulating nonlinear insulin clearance
g	Glucose mass (μmol)
G	Glucose concentration (μmol/l)
$G_{HEC_{SS}}$	Average glucose concentration at steady state of the HEC
GIR	Intravenous Glucose Infusion Rate
G_P	Plasma glucose level
G_{SS}	Glucose concentration at the steady state
GTT_{fast}	Mean Transit Time of glucose in CompFast
GTT_{slow}	Mean Transit Time of glucose in CompSlow
G_U	Urinary glucose concentration
HEC	Hyperinsulinemic Euglycemic Clamp
$I_{dep}(t)$	Volume of Insulin Depot at time t
$IGTT$	Ingested Glucose Transit Time
INS	Plasma Insulin concentration
INS_{AT}	Insulin Action Threshold
INS_{bolus}	Insulin Bolus as infused by the insulin pump
$INSCAT$	Insulin Clearance (linear component)
$INSCAT_2$	Insulin Clearance (non-linear, saturable component)
INS_{ci}	Constant Insulin Infusion by the insulin pump
INS_{dep}	Subcutaneous Insulin Depot
$INS_{HEC_{SS}}$	Average insulin concentration at steady state of the HEC
INS_{SS}	Insulin Concentration at baseline
$IVGTT$	Intravenous Glucose Tolerance Test
$kdiff_{fast}$	Rate constant of glucose through CompFast
$kdiff_{slow}$	Rate constant of glucose through CompSlow
k_{fast}	Fraction of Ingested Glucose traveling through CompFast
$k_{guria}(t)$	Time varying rate constant of glycosuria
k_{slow}	Fraction of Ingested Glucose traveling through CompSlow
$k_{(m,n)}$	Kinetic parameters
M	HEC-derived measure of whole-body insulin action
MMT	Mixed Meal Test
MTT	Mean Transit Time
ODE	Ordinary Differential Equation
OGI	Oral Glucose Input Function
$OGTT$	Oral Glucose Tolerance Test
p_2	Rate Constant of Insulin Action Fading
$q_2(t)$	Insulin Action at time t
$RClearance$	Renal Clearance of Plasma Glucose
$SCAR$	Parameter regulating insulin exit from the subcutaneous depot
S_G	Glucose Effectiveness
SD	Standard deviation
SGE	Splanchnic Glucose Extraction
S_I	Insulin Sensitivity at Steady State
$T1D$	Type 1 Diabetes
V_G	Apparent Glucose Volume of Distribution
V_U	Urine volume

Table 3.9: *Table S6 - Abbreviations and acronyms.*
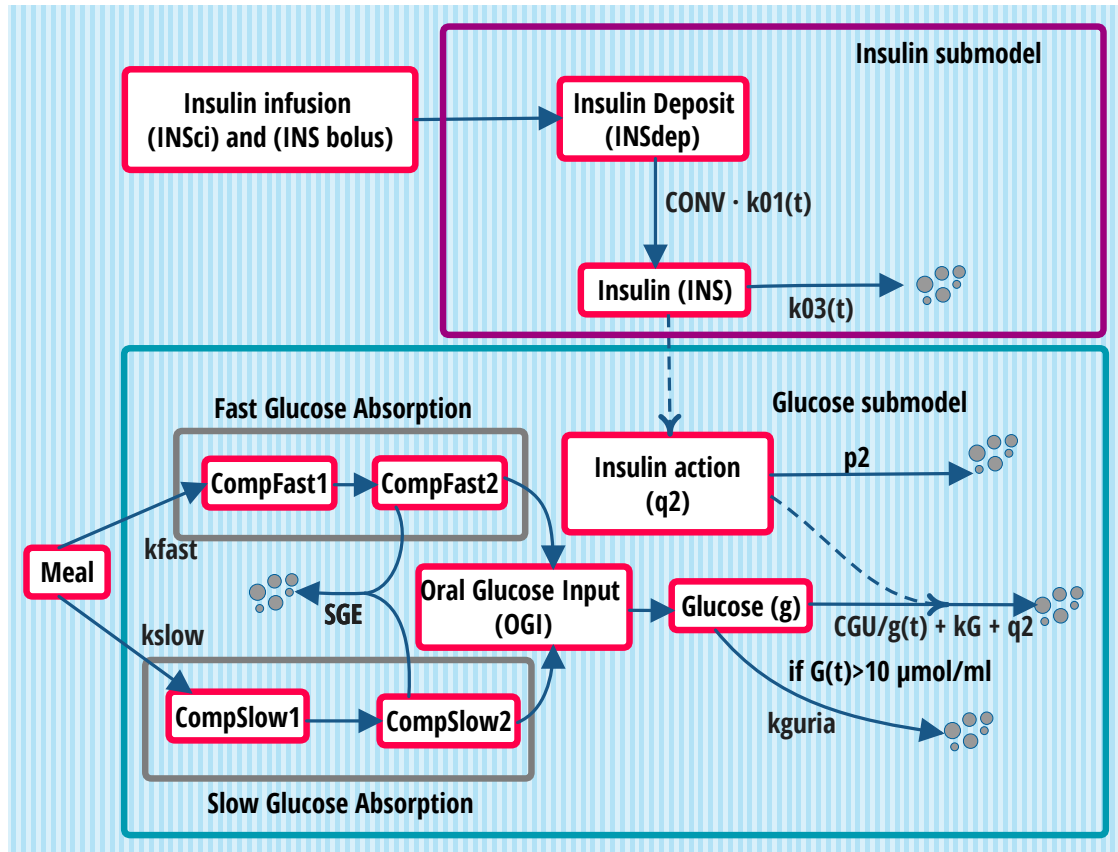
Figure 3.5: *The GLUKINSLOOP 2.0 model. The continuous arrows indicate mass transfers whereas the dashed arrows connecting insulin to the insulin action compartment and then insulin action to the irreversible loss of the glucose compartment symbolize the control exerted by insulin on glucose metabolism. The arrows pointing toward gray dotted material are used to indicate irreversible losses. INS, plasma insulin concentration; INSci, constant insulin infusion by the insulin pump; INS bolus, insulin bolus infused by the insulin pump; INSdep, subcutaneous insulin deposit; CONV, scaling factor; k, kinetic parameters; t, time; CompFast1-2, fast route of ingested glucose from mouth to systemic circulation; CompSlow1-2, slow route of ingested glucose from mouth to systemic circulation; q2, insulin action; p2, rate constant of insulin action fading; SGE, Splanchnic Glucose Extraction; OGI, Oral Glucose Input function; g, glucose mass; G, glucose concentration; CGU, Constant Glucose Uptake; $kG = S_G/V_G$.*
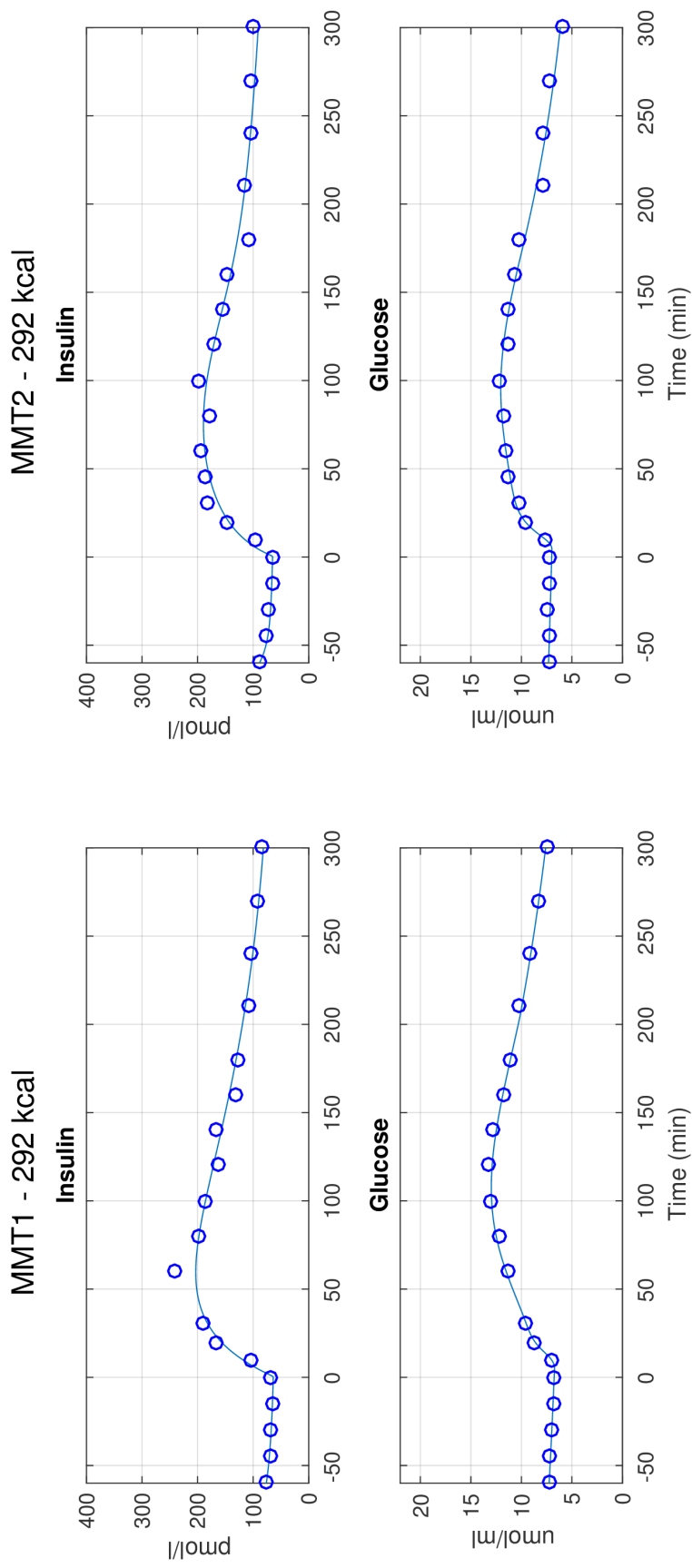
Figure 3.6: *Simulation outputs of the GLUKINSLOOP 2.0 (patient 1). The figure shows the time courses of plasma insulin and glucose concentrations during the MMT1 (left panel) and MMT2 (right panel) in the first study participant. Experimental data are shown as blue dots, whereas the simulated time courses are provided as a continuous blue line.*
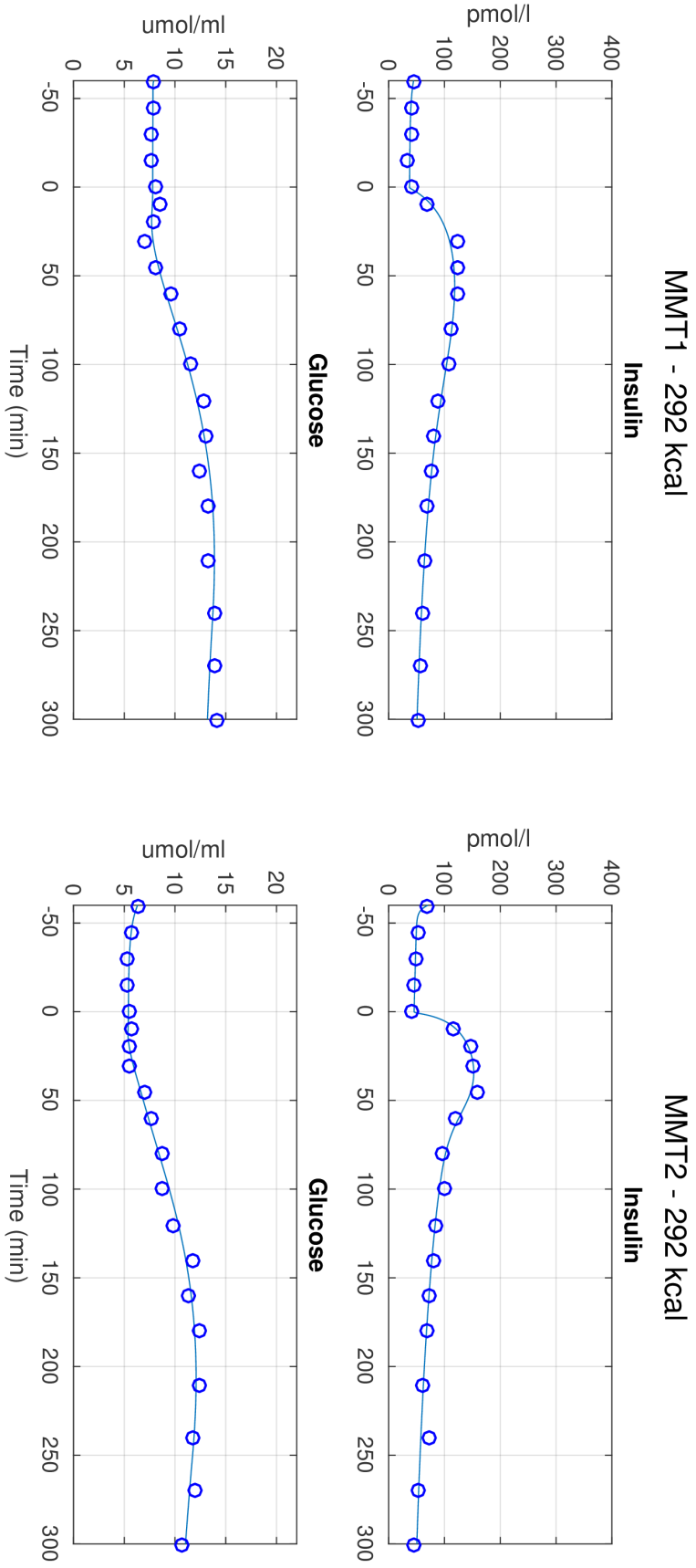
Figure 3.7: *Simulation outputs of the GLUKINSLOOP 2.0 (patient 2). The figure shows the time courses of plasma insulin and glucose concentrations during the MMT1 (left panel) and MMT2 (right panel) in the first study participant. Experimental data are shown as blue dots, whereas the simulated time courses are provided as a continuous blue line.*
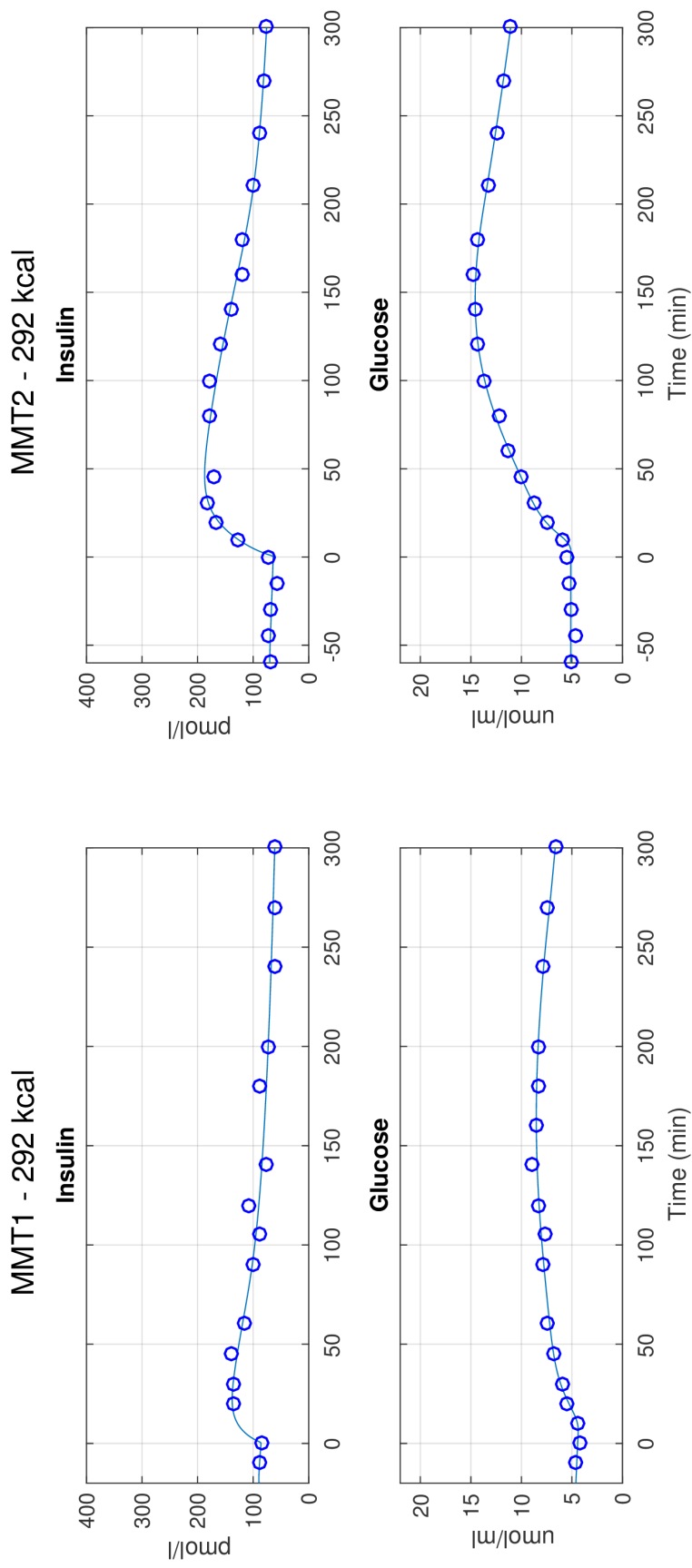
Figure 3.8: *Simulation outputs of the GLUKINSLOOP 2.0 (patient 3). The figure shows the time courses of plasma insulin and glucose concentrations during the MMT1 (left panel) and MMT2 (right panel) in the first study participant. Experimental data are shown as blue dots, whereas the simulated time courses are provided as a continuous blue line.*
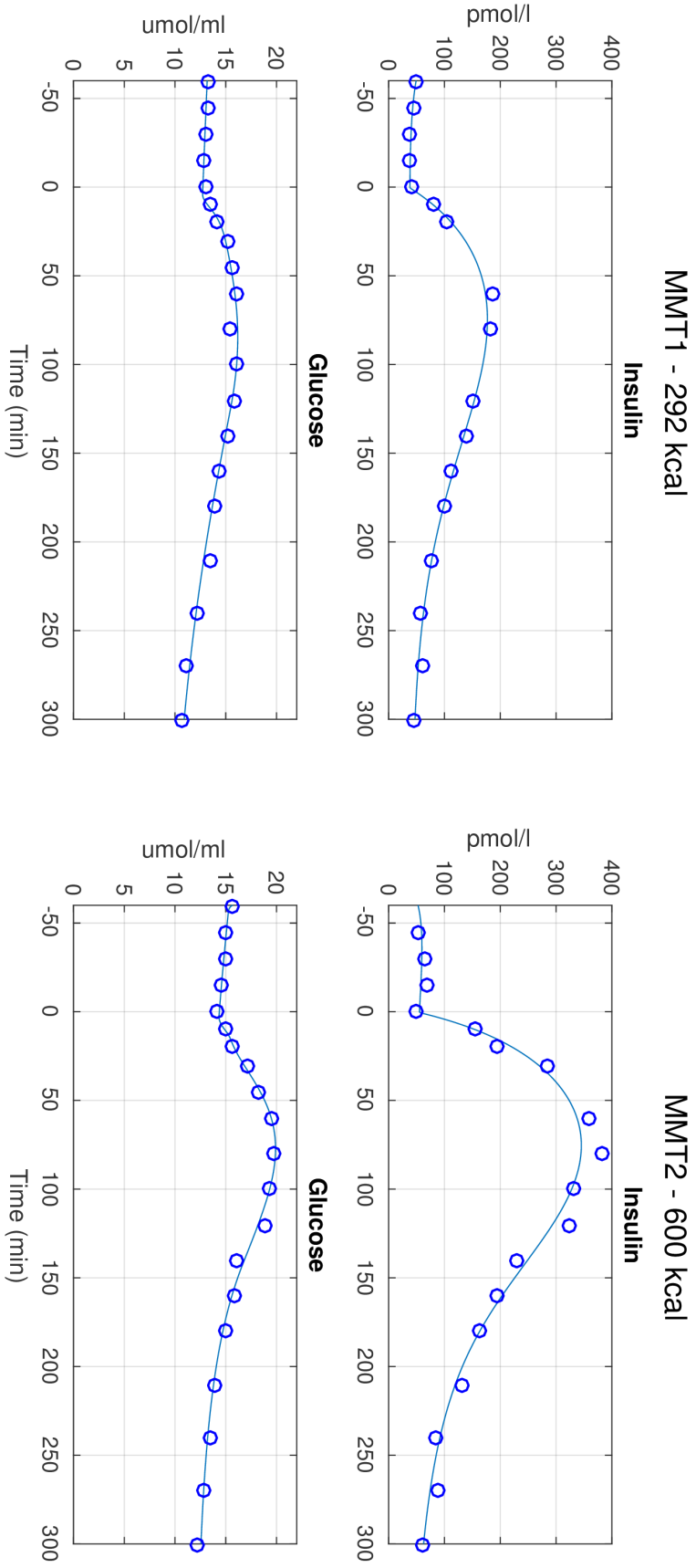
Figure 3.9: *Simulation outputs of the GLUKINSLOOP 2.0 (patient 4). The figure shows the time courses of plasma insulin and glucose concentrations during the MMT1 (left panel) and MMT2 (right panel) in the first study participant. Experimental data are shown as blue dots, whereas the simulated time courses are provided as a continuous blue line.*
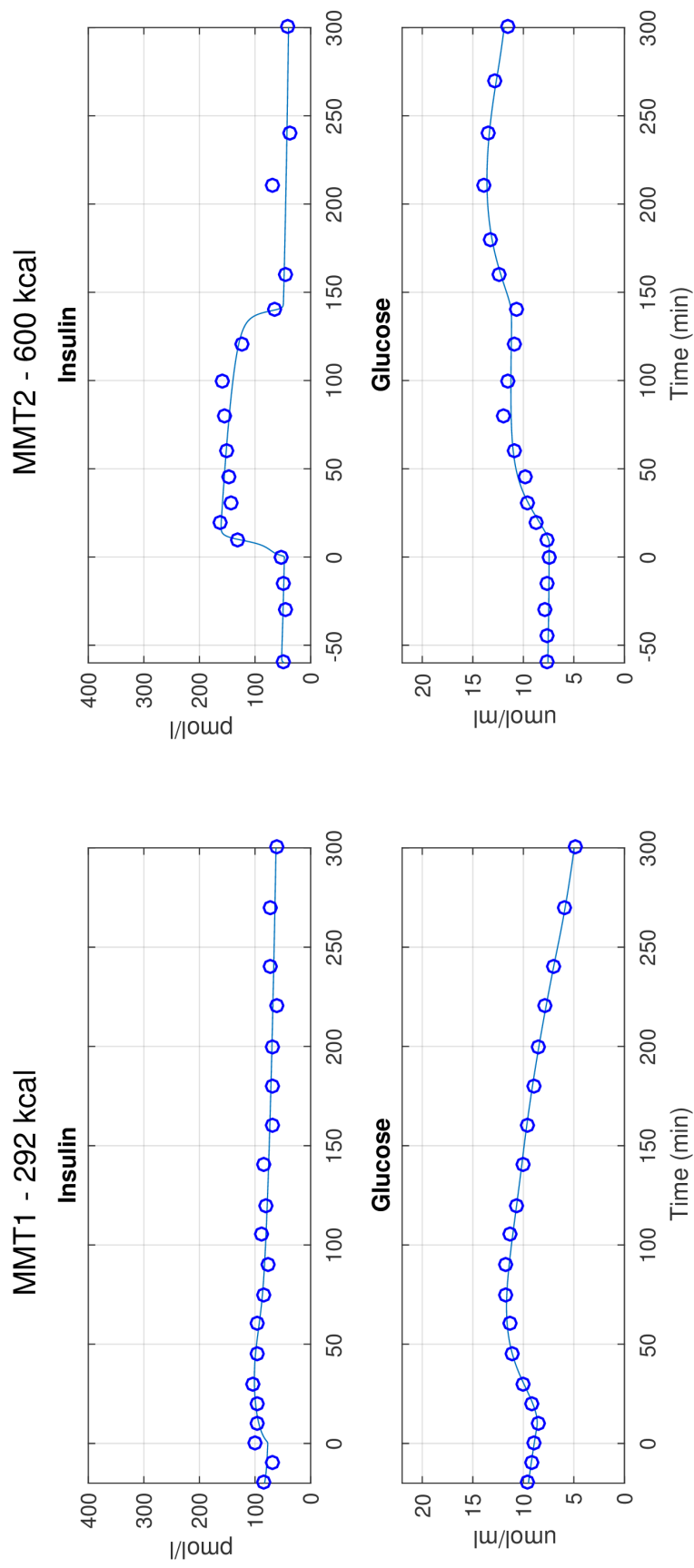
Figure 3.10: *Simulation outputs of the GLUKINSLOOP 2.0 (patient 5). The figure shows the time courses of plasma insulin and glucose concentrations during the MMT1 (left panel) and MMT2 (right panel) in the first study participant. Experimental data are shown as blue dots, whereas the simulated time courses are provided as a continuous blue line.*
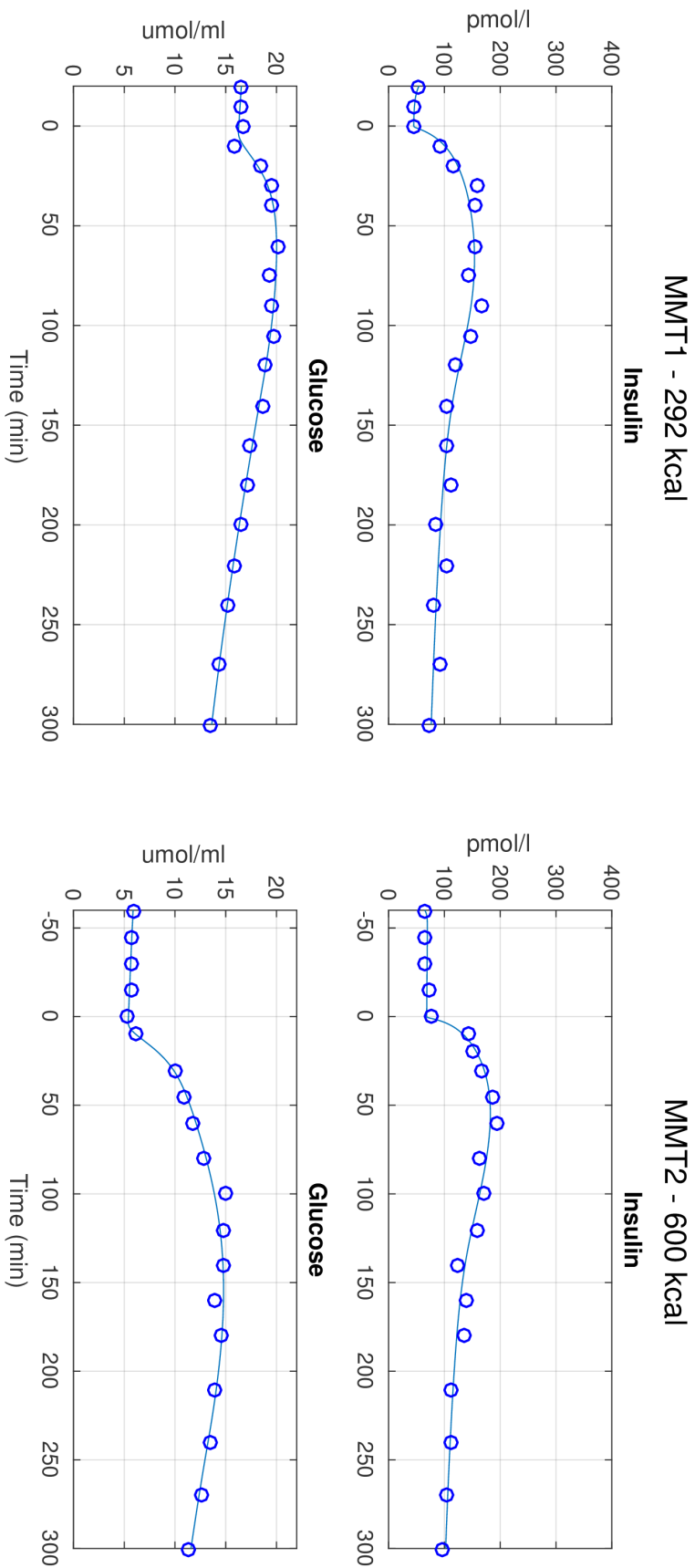
Figure 3.11: *Simulation outputs of the GLUKINSLOOP 2.0 (patient 6). The figure shows the time courses of plasma insulin and glucose concentrations during the MMT1 (left panel) and MMT2 (right panel) in the first study participant. Experimental data are shown as blue dots, whereas the simulated time courses are provided as a continuous blue line.*
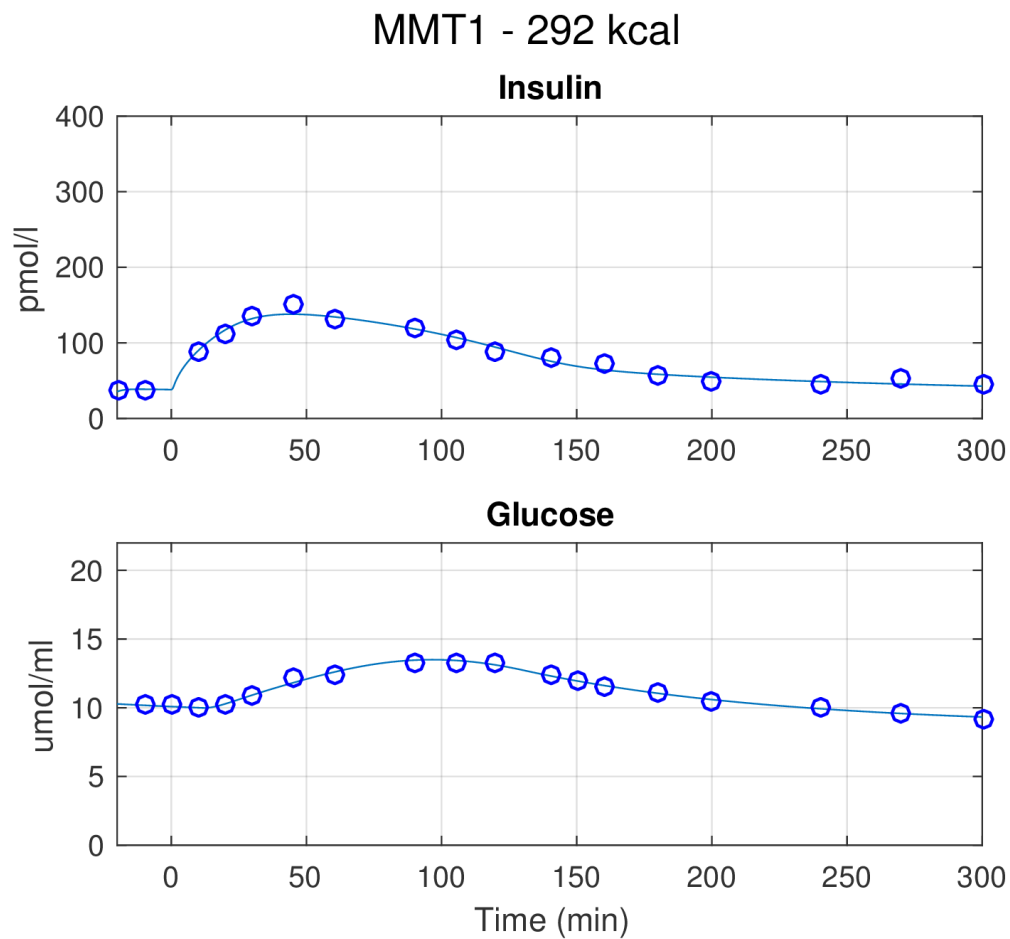
Figure 3.12: *Simulation outputs of the GLUKINSLOOP 2.0 (patient 7). The figure shows the time courses of plasma insulin and glucose concentrations during the MMT1 in the seventh study participant. Experimental data are shown as blue dots, whereas the simulated time courses are provided as a continuous blue line.*
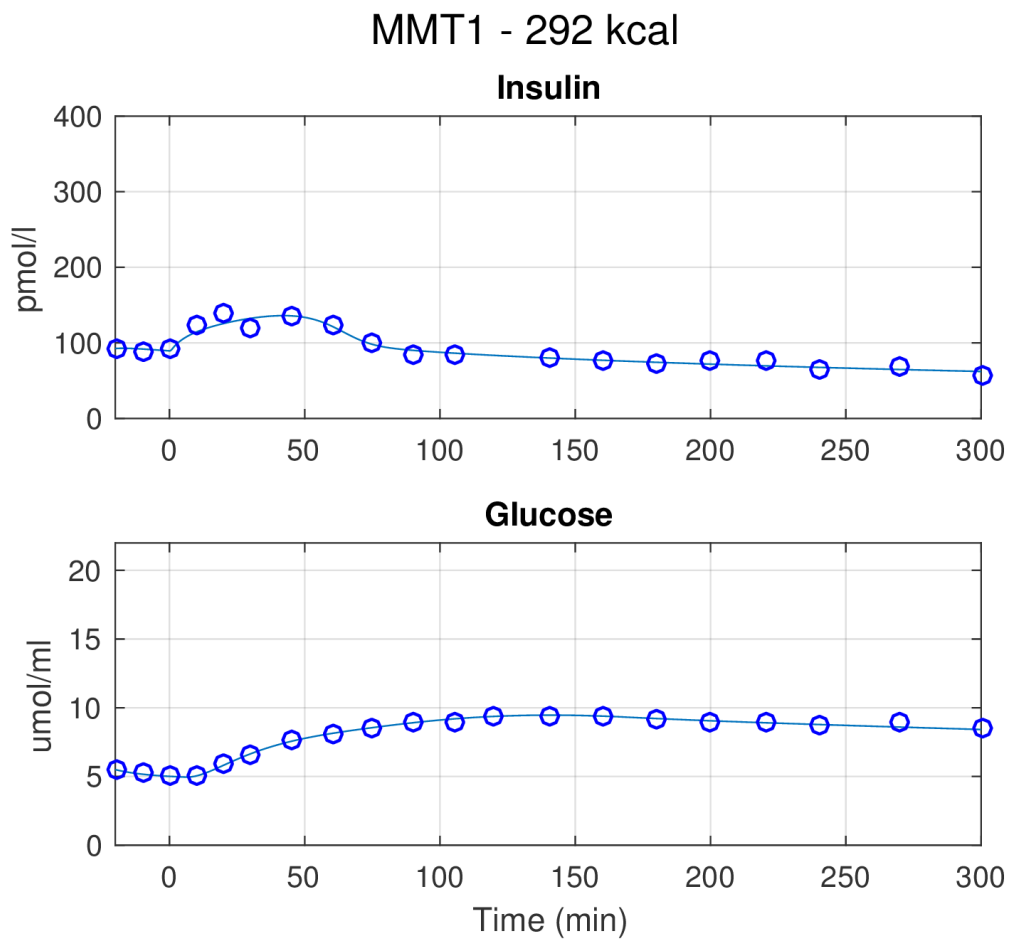
Figure 3.13: *Simulation outputs of the GLUKINSLOOP 2.0 (patient 8). The figure shows the time courses of plasma insulin and glucose concentrations during the MMT1 in the seventh study participant. Experimental data are shown as blue dots, whereas the simulated time courses are provided as a continuous blue line.*
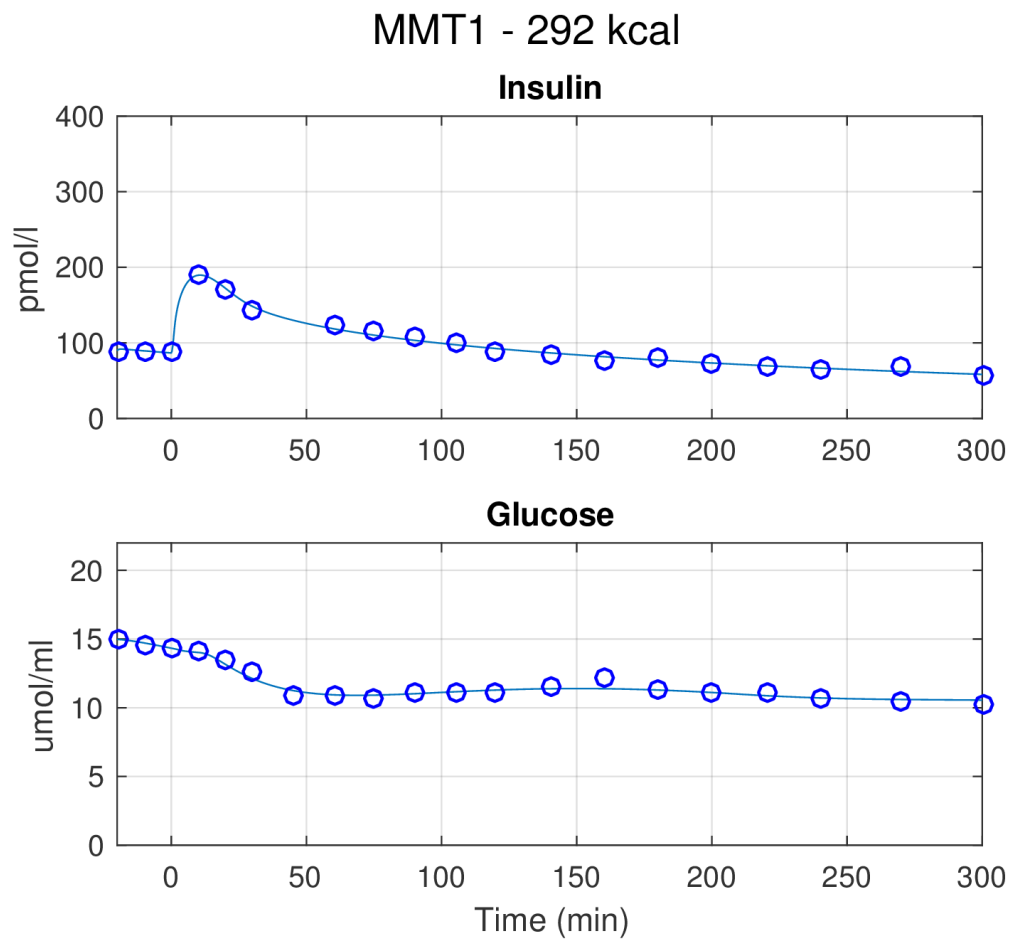
Figure 3.14: *Simulation outputs of the GLUKINSLOOP 2.0 (patient 9). The figure shows the time courses of plasma insulin and glucose concentrations during the MMT1 in the seventh study participant. Experimental data are shown as blue dots, whereas the simulated time courses are provided as a continuous blue line.*
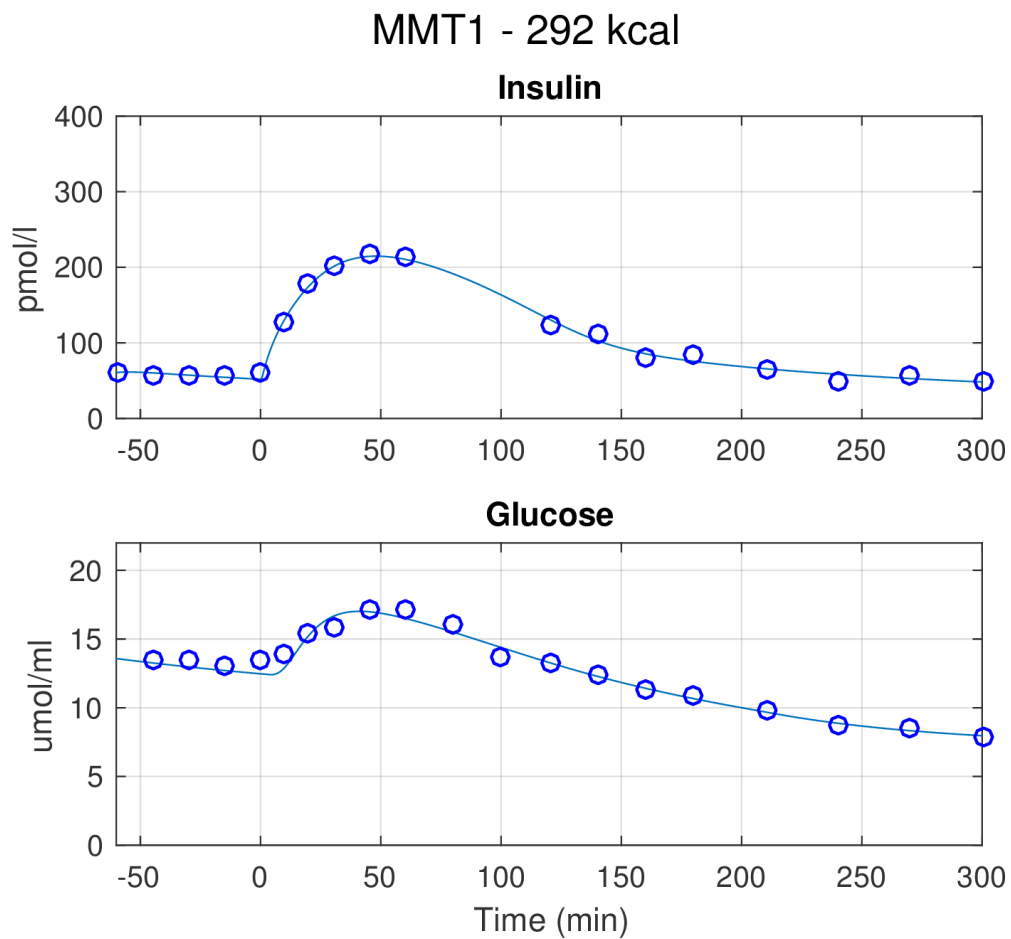
Figure 3.15: *Simulation outputs of the GLUKINSLOOP 2.0 (patient 10). The figure shows the time courses of plasma insulin and glucose concentrations during the MMT1 in the seventh study participant. Experimental data are shown as blue dots, whereas the simulated time courses are provided as a continuous blue line.*
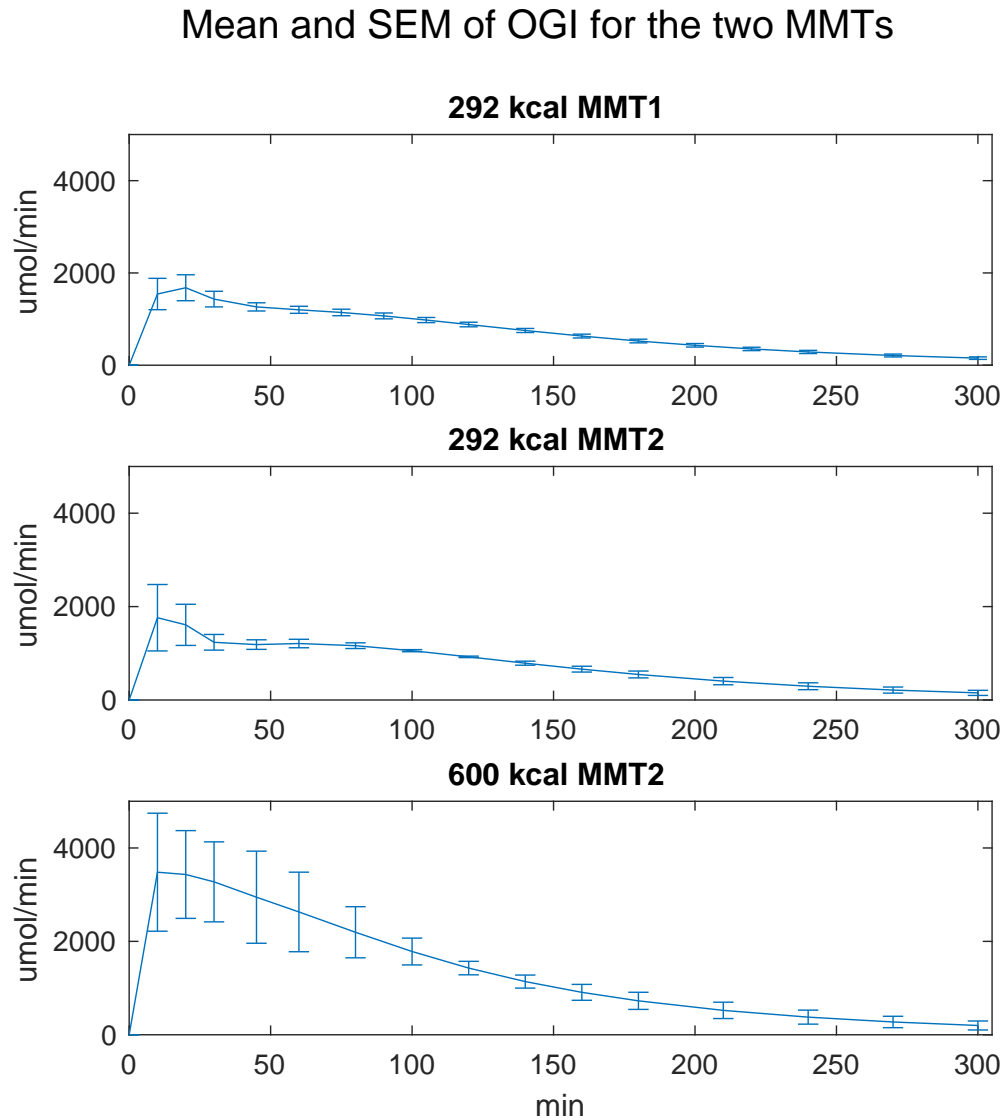
Figure 3.16: *The Oral Glucose Input function (OGI). The OGI function describes the rate of appearance of glucose that reaches the bloodstream after oral ingestion. The plots depict mean±SEM of the OGI functions (expressed in µmol/min) during the different MMTs.*

Author contributions

This work is the result of a collaboration between COSBI and the research group of Ricardo Bonadonna at the University of Verona, School of Medicine. The article is the result of the joint effort of the two institutions. In particular, Luca Marchetti and I, under the supervision of Corrado Priami and Riccardo Bonadonna, participated in the development of the mathematical model, computed parameter estimates and model dynamics. I contributed to the writing of the paper by providing a first draft of the paper and by editing the manuscript. In addition, I wrote and edited the supplementary material, under the supervision of Corrado Priami, Luca Marchetti and Riccardo Bonadonna. Marco Dauriz discussed the results, completed the first draft of the manuscript and edited the manuscript. Enzo Bonora and Riccardo Bonadonna designed the study and wrote and edited the manuscript. Corinna Brangani and Giulia Ceradini supervised and carried out the experimental studies, and revised the first draft of the manuscript. Linda Boselli and Riccardo Bonadonna developed a preliminary version of the mathematical model, and applied it to a preliminary analysis of the experimental studies.

Chapter 4

Mechanistic interplay between ceramide and insulin resistance

According to the 2014 data provided by the World Health Organization, 39% of the global adult population is overweight and 13% is obese. This is a consequence of physical inactivity due to the increasingly sedentary nature of many forms of work, as well as increased intake of fatty foods. Most of the scientists agree that excess of weight and lack of physical activity cause insulin resistance that increases the risk of developing type 2 diabetes.

Insulin resistance is the impairment of the normal crosstalk between insulin and the cells, whereby cells do not respond adequately to normal levels of insulin. As a result, they require always more insulin to stimulate the glucose uptake. This process leads to severe consequences for the organism.

Recently, many studies have elucidated the essential role of ceramides and sphingolipids in the glucose homeostasis and insulin signaling. However, the mechanistic interplay between various components of ceramide metabolism remains to be quantified. To this end, we have resorted to dynamical modeling to gain insights into the sphingolipid metabolism and their role in the development of the insulin resistance. In particular, we have focused on the C16 ceramides family.

Our model extends and refines a previously published model by including those reactions that connect sphingolipids *de novo* synthesis with the salvage pathway. The latter recycles complex sphingolipids by transforming them in ceramides and it accounts for a significant part of the total ceramide production. We estimated unknown parameters of the model using mice macrophage cell line data. For the parameter estimation, we have used a multi-start approach with a least squares method, as described in Appendix A.

We have validated this extended model on an independent dataset for the same tissue in mice. We have integrated the model with transcriptomic data from a different experiment in obese/diabetic murine macrophages at 5 and 16 weeks. Our in silico experiments of the behavior of ceramide and related bioactive lipids, in accordance with the observed transcriptomic changes, support the

observation of insulin resistance at the later phase. Our model has suggested the key role of ceramide, glucosylceramide and S1P in the development of insulin resistance.

In addition, sensitivity analysis on the model allowed us to quantify the effect of the availability of each enzyme involved in the metabolism on each sphingolipid. We have visualized such interactions using an interaction network. These visualizations should guide wet lab scientist in identifying new potential drug targets. In addition, the visualizations may help in identifying collateral effects by highlighting the nontrivial interactions among all the metabolites.

Our analysis suggests the pivotal role played by the enzymes ceramide synthase, serine palmitoyltransferase, and dihydroceramide desaturase. These enzymes are involved in the *de novo* synthesis and the salvage pathways in influencing insulin resistance versus its regulation. Moreover, in agreement with recent studies in rodents and humans, these enzymes are fundamentally linked to metabolic health.

This chapter contains the article published in the journal of Scientific Reports in January 2017.

4.1 Introduction

Ceramides (Cer) are a family of lipid molecules that play an active role in glucose homeostasis, insulin signaling and, ultimately, the diabetic phenotype [17, 87]. Two primary pathways through which ceramides are produced in the cell are the condensation of palmitate and serine (called *de novo* synthesis) and re-acylation of sphingosine (salvage pathway). In both cases, ceramide (dihydroceramide, in the case of the de novo synthesis pathway) is produced by ceramide synthase (CERS) through N-acylation of a sphingoid base. Mammalian CERS occurs in 6 isoforms (CERS1-6) with differing binding preference for specific fatty acid chain lengths. CERS6, in particular, is specific to C14 and C16 acyl chain lengths, and has been associated with obesity and insulin resistance [88].

The primary mechanism through which ceramide promotes insulin resistance is by inhibiting the activity of Akt/PKB, which is an essential facilitator of glucose transport into the cell. Ceramide blocks the activity of Akt/PKB by two independent mechanisms, i.e., by stimulation of Akt dephosphorylation via protein phosphatase 2A (PP2A) and blocking the translocation of Akt via PKCζ [89]. Ceramide activates PP2A, which inhibits the action of Akt/PKB by impairing Akt serine phosphorylation. The result of this inhibition is decreased translocation of glucose transporter type 4 (GLUT4) to the plasma membrane and hence decreased uptake of glucose.

In this study, we extended the dynamic model of the *de novo* synthesis of C16:0 ceramide (from here on we omit the C16:0 notation) in [3] (Tab. 4.1) with the salvage pathway (Tab. 4.2). The deterministic extension of the model in [3] is used to tune a stochastic version of the same model implemented in ℓ: a stochastic imperative, domain specific language [6, 90]. The quantitative parameters of

our model are extracted from lipidomic data on RAW264.7 cells [91] (a mouse leukemic macrophage cell line) and validated on primary macrophages [92] (bone marrow derived macrophages, BMDM). The cells were treated with the pro-inflammatory compound Kdo(2)-lipid A (KLA). RAW264.7 cells experiment was assessed at 0, 0.5, 1, 2, 4, 8, 12, and 24 hrs, whereas BMDM experiment at 0, 0.25, 0.5, 1, 2, 4, 8 and 20 hrs. Following [3], we assume that there are diacylglycerol (DAG)- and phosphatidylcholine (PC)- mediated reactions that transform dihydroceramide to dihydrosphingomyelin and vice versa. These reactions are analogous to the reactions involving ceramide and sphingomyelin, which connect ceramide *de novo* synthesis with the sphingomyelinase pathway.

We simulated our model both deterministically and stochastically to account for low abundances of metabolites. The outcome of the simulations predicts the trend of sphingolipid accumulation in CERS6 knockout mice [88] as well as the insulin resistance aetiology in *ob/ob* mice [93]. Finally, we performed a sensitivity analysis to identify the key enzymes and reactions that regulate sphingolipid metabolism.

4.2   Results

Working with an extended model of the one presented by Gupta et al. [3] to include the interplay between ceramide and sphingosine, the main result is the ability of our model to explain mechanistically the interplay between sphingolipid metabolism, specifically ceramide, and insulin resistance. We experimented on our model by focusing on two cases: (i) the availability of CERS6, and (ii) the groups of enzymes that are identified as significantly differentially-expressed in obese mice. The data on obese mice is from isolated adipose tissue macrophages from 5 and 16 week *ob/ob* (i.e., genetically obese) and wild type C57BL/6 mice, both fed standard chow diets (for detailed study methods, see [93]). We then performed a sensitivity analysis of the model.

4.2.1   CerS6 availability

We investigated the response to variation in CERS6 fold change (FC), as this enzyme plays a central role in the *de novo* production of (primarily C16:0) ceramide, catalyzing dihydroceramide (dhCer) starting from sphinganine, and in the salvage production, recycling ceramide from sphingosine. A substantial reduction of CERS6, for example, as a result of the effects of drugs such as fumosin B1, has the effect of blocking both *de novo* and salvage pathways, leaving only the ceramide production that occurs by sphingomyelinase. Moreover, as shown in [88], among all CERS enzymes, only CERS6 adipose tissue expression is significantly correlated with BMI, hyperglycemia and glucose infusion rate in human subjects.

Our model provides a mechanistic explanation of the results of [88]: the contribution of CERS5 in ceramide synthesis in macrophages is three orders of magnitude smaller than the one of CERS6. As a consequence, the extended

model includes a reaction that merges the effect of CERS5 and CERS6. In our analysis, in agreement with [3], we thus consider only the FC of CERS6, as it is the main contributor for the dynamics in the sphingolipid pathway, and FC of CERS5 remains negligible in comparison. Figure 4.1 shows results of the simulation, in particular with figure 4.1 **c**) showing that decreasing CERS6 results in an decrease in ceramide as well as an increase in sphingosine-1-phosphate.

4.2.2   Differentially expressed enzymes in *ob/ob* mice

While CERS6 plays a known role in the diabetic phenotype, dysregulation of biological systems is often the result of altered behavior in many interacting components. Therefore, we focused our analysis on multiple enzymes that were found to be differentially expressed in macrophages of *ob/ob* and wild type mice.

Results from simulations suggest that sphingolipid metabolism in the obese mouse is affected after 5 weeks (Fig. 4.2**c**). However, the sphingolipids related to insulin action, ceramide, glucosylceramide (GluCer) and S1P are balanced: GluCer and S1P, are either stable or decreasing, ceramide increases and the mechanisms of insulin resistance due to Akt activity remain unaffected. These observations are in agreement with [93]: after 5 weeks, ob/ob mice show signs of early insulin resistance, compared with wild-type mice, however show well-controlled glycemia. Moreover, the model indicates that the affected sphingolipid metabolism maintains a balance between sphingolipids involved in insulin signaling.

Simulations suggest that *ob/ob* mice metabolism is highly affected after 16 weeks with a general up-regulation of sphingolipids, including the ones involved in insulin signaling (Fig. 4.2**d**). This suggests potential impairment of insulin signaling and the development of insulin resistance and glucose intolerance. The model indicates an impairment of the ratio between the sphingolipids involved in insulin signaling. In agreement with Prieur et al. [93], this can be the cause of the obesity-induced insulin resistance [94, 95], which is stronger at 16 weeks than at 5 weeks, leading to severe insulin resistance and glucose intolerance.

4.2.3   Sensitivity analysis

We performed parametric sensitivity analysis to test the model and to highlight the key reactions and enzymes for the behavior of the system and estimate the effect of each rate or enzyme on the concentration of each sphingolipid. Figure 4.3 illustrates the results of sensitivity analysis as a network, with the width of edges indicating the strength of effect of enzymes on metabolite abundance. Our results demonstrate that while the concentrations of enzymes like ceramide-activated protein phosphatase (CAPP), ceramide kinase (CERK), sphingosine-1-phosphate lyase (SGPL1) and sphingosine-1-phosphate phosphatase (SGPP1) have strong effect on specific sphingolipids, other enzymes like CERS, ceramide glucosyltransferase (UGCG), dihydroceramide desaturase (DEGS), sphingomyelin synthase (SMS), ceramidase (ASAH), sphingomyeli-

nase (SMA) and serine palmitoyltransferase (SPT) have a more diffuse effect throughout the model.

4.3 Discussion

We used a combination of deterministic and stochastic simulations to provide a dynamic account of the mechanistic processes of sphingolipid metabolism. We extended and refined the model by Gupta et al. [3] to include the interplay between ceramide and sphingosine. We used our model to test different conditions for CERS6 availability and various combinations of enzymes that are differentially expressed in *ob/ob* mice after 5 and 16 weeks. We quantified the effect of each single enzyme in the pathway, through sensitivity analysis, identifying the main regulators of sphingolipid production.

The data used to identify the parameters of the model are taken from cell cultures, where fast and slow metabolic interactions co-occur, and this is a source of intrinsic noise; stochastic simulations are useful in capturing the fluctuations due to these variations in reaction rates. Moreover, the measurements of metabolite concentrations in this system vary in orders of magnitude. Stochastic simulations are instrumental for capturing the noise that emerges in experimental observations [96] (see Fig. 4.7). Figure 4.1**b** shows that the stochastic simulations are closer to experimental observations than deterministic simulations on both RAW 264.7 and BMDM cells. Deterministic simulations, on the other hand, are better for sensitivity analysis and monitoring the average behavior.

We then extended the model to analyze the cross-talk between ceramide *de novo* synthesis and the salvage pathway, where ceramide is produced by recycling sphingosine [97] (Fig. 4.1**a**). Sphingosine is involved in Cer synthesis inside lysosomes and mitochondria, and sphingosine-1-phosphate (S1P) plays a central role in insulin signaling and inflammatory response [24]. By including sphingosine and S1P, the extended model is a comprehensive exposure of the processes that link ceramide metabolism to the diabetic phenotype. Moreover, the extended model takes the role played by ceramide-1-phosphate phosphatase (CAPP) into account, which produces ceramide from ceramide-1-phosphate [98].

Our simulations showed that the decrease of CERS6 results in a decrease of ceramide, as expected, as well as an increase in sphingosine-1-phosphate (Fig. 4.1 **c**). Sphingosine-1-phosphate (S1P) can be reversibly produced from ceramide via sphingosine, and plays a well-studied role in insulin signalling. Recent work by Mullen et al. [99] demonstrated that combined knockdown of CERS2, CERS5 and CERS6 resulted in elevated levels of S1P in an adenocarcinoma cell line. The interplay between the levels of ceramide and sphingosine-1-phosphate (S1P) plays a role in the control of the Akt pathway, which in turn influences insulin action as well as the fate of the cell [100–102]. This suggests that, for macrophage sphingolipid metabolism, the balance of these two sphingolipids may explain why even with high-fat diet, CERS6-knockout mice did not show significant differences in insulin action and glucose tolerance in comparison with wild type high-fat diet-fed mice [88]. Conversely, as CERS6 abundance increases,

the simulations suggest that the increase of both ceramide and glucosylceramide (GluCer) affects the Akt/PKB insulin signaling pathway, which is correlated with increased CERS6 expression.

In [3] the abundances of the four metabolites DAG, phosphatidylcholine, sphinganine and palmitoyl-CoA are modeled with time-dependent variables obtained as linear interpolations of the experimental data. This approach is based on the physiological observation that KLA treatment primarily affects these four components, and the treatment induced variation of concentrations is enough to capture the effect of the treatment for most of the metabolites. Our extended model refines the representation of *de novo* synthesis by replacing the time-dependent functions for sphinganine with mechanistic components and, as a consequence, provides a characterization of the underlying biochemical processes. We aggregated the reactions between same metabolites that are mediated by different enzymes, thereby assessing of the aggregated influence of each sphingolipid over other sphingolipids without compromising accuracy. We initially assumed that the enzyme levels remain constant during the experiments, as in [3]. Furthermore, we successfully tested the consistency of the results in the presence of significant perturbations on enzyme concentrations (Fig. 4.11). We were able to significantly reduce the number of rates to fit without affecting the precision of the model, and avoid compensation effects of parallel reactions. The stochastic simulations are performed using ℓ, a domain-specific modeling language. The results of the deterministic and stochastic simulations compared with experimental data for RAW 264.7 and BMDM cells are in Fig. 4.1.

The sensitivity analysis of the enzymes highlighted a strong role for SPT, which showed positive effects on the abundance of a range of metabolites. The reaction carried out by SPT - the condensation of serine and palmitoyl CoA to produce dihydrosphingosine (dhSph) - has been shown to be a rate-limiting step in de novo sphingolipid biosynthesis [103]. Humans possess three variants of SPT (SPTLC1, SPTLC2, SPTLC3), and SNPs in all three have been found to be significantly associated with type 2 diabetes and related phenotypes [104–110]. Likewise, treatment with myriocin (a specific inhibitor of SPT) substantially reduces ceramide synthesis and ameliorates insulin resistance in diabetic rodents [111, 112].

The sensitivity analysis also highlights the diffused effect of DEGS, the enzyme that catalyzes the transformation of dhCer into ceramide, and connects the dh and non-dh parts of the pathway. A significant reduction of this enzyme removes the dhCer contribution from ceramide production, and an increase in DEGS promotes ceramide production. Recent work has shown that signaling targets of ceramide are not affected by similar levels of dhCer, which suggests that the enzyme DEGS is essential in cell regulation [18] and plays a role on glucose homeostasis as well: multiple SNPs in DEGS are significantly associated with 2 hour glucose, mice lacking DEGS are resistant to dexamethasone-induced insulin resistance and DEGS-knockdown mice myoblast are protected from palmitate-induced ceramide-mediated insulin resistance [104, 110, 111, 113].

Collectively, our results illustrate patterns in sphingolipid metabolism that mechanistically link ceramides and related bioactive lipids to insulin resistance. By perturbing CERS6 we observed changes in sphingolipid abundances that are consistent with improvement in insulin signalling, however further work would be required to assess how this may affect whole-body glucose homeostasis. Furthermore, in agreement with recent studies in rodents and humans, sensitivity analysis of our model highlighted a strong functional role of SPT and DEGS in regulating abundance of multiple sphingolipid metabolites that are fundamentally linked to metabolic health.
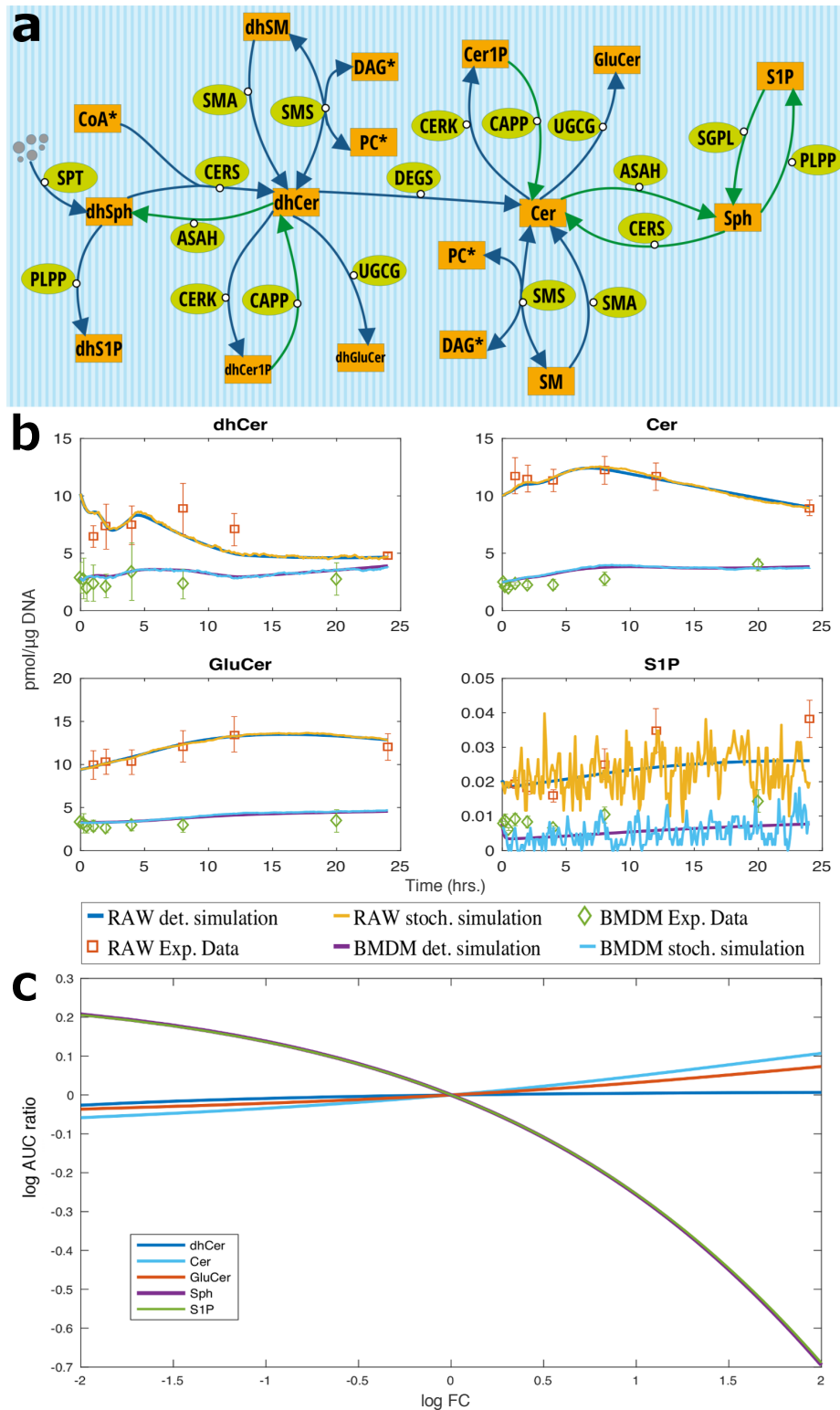
Figure 4.1: *a The model extends the one in [3] with additional reactions identified in the literature in green. Degradation and production reactions are omitted. Metabolites with time-dependent variables are marked with the symbol '*'. b Simulation results of the extended models, both deterministic and stochastic, for the concentrations in RAW 264.7 cells and BMDM measured in pmol/μg DNA. The model simulates all the sphingolipids involved in the ceramide pathway. For the stochastic simulations a scaling factor 1000 is used.* x-axis: *time in hours. c The $\log_2$ AUC-FC/AUC-Control ratio for the sphingolipids in the legend. The fold-change is varied from 0.25 to 4.*

Figure 4.2: *a and b) the up (red boundary) and down (green boundary) regulated enzymes in obese mice, according to genes significantly differentially expressed, after 5 (Tab. 4.3) and 16 weeks (Tab. 4.4) of chow diet. c and d) the $\log_2$ AUC-FC/AUC-Control ratio for the sphingolipids in the legend. The fold-change of the enzymes highlighted in a and b are varied from 1 to 4.*

Figure 4.3: *The network of interactions obtained from the sensitivity analysis for enzymes. Edges are red if the increase of the rate causes an increase of the concentration of the sphingolipid node; green if the concentration decreases. The thickness of the edges is proportional to the $\log_2$ of the AUC ratio. Orange rectangles and blue circles, respectively, are the sphingolipids and the enzymes.*

4.4 Methods

We implemented two versions of the model for deterministic and stochastic simulations. Because both of these implementations are based on mass action kinetics, they can be considered as two equivalent implementations of the same model. The stochastic simulations capture some fluctuations that are not captured by the deterministic simulations. The deterministic simulations, on the other hand, are more efficient and enable fitting procedures.

Deterministic implementation. We implemented the deterministic version of the model using ordinary differential equations (ODE) in Matlab, and we used the built-in ODE solver functions ode23 and ode45. Sometimes we used a lower order Runge-Kutta method to speed up the simulation, and compared the results with higher order methods to quantify the error. Time dependent variables are included as in [3]; they are encoded as linear interpolation of the related experimental concentrations.

Stochastic implementation. We implemented the time-continuous discrete stochastic version of the model using the domain specific ℓ language designed to model chemical reactions and biological systems [6, 90]. ℓ is equipped with a built-in stochastic simulation engine, based on Gillespie algorithm [114]. The mass action kinetics allowed us to use the deterministic rates also for the stochastic implementation by using conversion factors, see, e.g., [6]. The number of molecules required for the stochastic simulation are thus obtained by using the transformation from the concentration $pmol/\mu g$ of DNA to number of molecules, that is, by multiplying with the expression $AvogadroNumber \cdot 10^{-12} \cdot 10^{-6}/ScalingFactor$. We performed simulations with different stochastic seeds and scaling factors that emphasize the stochastic noise, and we compared these results with the experimental data. The yellow plots in Fig. 4.1**b** and Fig. 4.7 are obtained with a scaling factor 1000. Time dependent variables were included in the propensity calculation of the reactions, and their amounts are determined as linear interpolation of the related experimental number of molecules. For example, the propensity function at time t of $dhSph + CoA + CERS \xrightarrow{\text{kf1}} dhCer$, is

$$\#dhSph(t) \cdot CoA(t) \cdot \text{kf1} \qquad (4.1)$$

where $\#dhSph(t)$ is the simulated number of molecules of $dhSph$ at time t, kf1 is the stochastic rate constant, and $CoA(t)$ is the time dependent function that accounts for the number of CoA molecules at time t.

Enzyme concentrations. The concentrations of the enzymes in the model are initially kept constant during the duration of the experiments as in [3], and their amounts are calculated by parameter estimation. For example, the estimated parameter kf12 of $dhCer + DEGS \xrightarrow{kf12} dhCer$ is $[DEGS] \cdot \text{kf12}'$, where $\text{kf12}'$ is the actual kinetics value and $[DEGS]$ is the enzyme concentration.

Enzyme Availability. To validate the model results with respect to the variations in the availability of the enzymes, we have quantified the effect of reducing each enzyme on each metabolite. To measure the accumulated effect of these changes on the metabolites, we used the Area Under the Curve (AUC) of the simulated time-series. We used the $\log_2$ of the AUC ratio for the case with reduced enzyme availability and the AUC for the control case, that is, $\log_2$(AUC-Reduced/AUC-Control). This allowed us to quantify and compare the variations in AUC, depicted as heatmaps. We performed this by scaling the reaction rate constants that are mediated by the selected enzyme from 0.1 to 1. These results are depicted in Fig. 4.9.

To further assess the robustness of the model, we dynamically perturbed the concentration of the enzymes. We first considered the perturbations at random time points. Following this, we applied perturbations at fixed time points in order to compare the two behaviors, and verify that they are in agreement. For this, at each time point, we considered random normally distributed fold changes (FC) for all the enzymes. These fold changes are included in the rate constant as a factor of 2^{FC}. For the perturbations, we tested a variety of time points and standard deviations from 6 to 240 and from 0.1 to 1, respectively. Fig. 4.10 and Fig. 4.11 depict the results for 10000 different simulations with a standard deviation of 0.5. As expected, varying the standard deviations result in proportional variations of the outputs. Fig. 4.9 shows that the output of the model is consistent with the dynamics we have considered as control, also in the presence of significant perturbations on enzyme concentrations (Fig. 4.10 and Fig. 4.11). The dynamics of all the sphingolipids in our conclusions in the main text show good agreement with the experimental data (Fig. 4.10 and Fig. 4.11).

Parameter Estimation. The extended model includes 29 reactions, with unknown rates. We carried out a deterministic parameter estimation procedure, based on *non-linear least squares method*. To take the differences in concentration of the sphingolipids into account and to ensure that the fitting procedure is not used in a biased manner by the abundance of any sphingolipid, we used a weighted objective function, where for each sphingolipid and each time point we considered the squared-relative-error. The objective function that we minimized is

$$\sum_{t \in \text{TimePoints}} \left(\sum_{i=1}^{12} \left(\frac{X^i(t) - Exp^i(t)}{Exp^i(t)} \right)^2 \right) \tag{4.2}$$

where $X^i(t)$ and $Exp^i(t)$ are the simulated and experimental values for the i-th, non-time dependent, sphingolipid at the time point t, and TimePoints is the set of the experimental measurements at time $t \in \{0.5, 1, 2, 4, 8, 12, 24\}$ hours.

We minimized this expression using the *lsqnonlin* Matlab function (trust-region-reflective algorithm) by using a multi-start approach: the algorithm starts from a number of randomly generated starting points (our case 200) within the feasible regions and from each point it executes the *lsqnonlin* function. This procedure for parameter estimation provided excellent fitting results (Fig. 4.1**b**

and Fig. 4.7).

Validation.   Since the BMDM dataset does not include all the data, for the time dependent variables (Acyl-CoA 16, DAG and PC) we have used data from RAW 264.7 cells. The results of this simulation are depicted in Fig. 4.8. The model, tested on the new data, correctly reproduces the behavior of most of the metabolites, in particular these metabolites that are involved in our conclusions. However, the dynamics of dhSph is not correctly captured by the model. Our investigation on this highlights the role of the reaction that synthesizes dhSph (reaction 22). Since the concentration of dhSph is much smaller in the BMDM data than in RAW 264.7 cells, we varied its rate accordingly. As a consequence, the model results are closer to experimental data.

Microarray analysis.   A microarray dataset (accession number GSE36669) was obtained from Gene Expression Omnibus, representing isolated adipose tissue macrophages from 5 and 16 week *ob/ob* and wild type C57BL6 mice, both fed standard chow diets (for detailed study methods, see [93]). Data were normalized using the *rma* function from the oligo R library, then filtered to remove probes in the lowest 10% expression and lowest 10% variance. Data were then analyzed using the limma library, to identify probes that were significantly differentially expressed between *ob/ob* and wild type mice at 5 and 16 weeks. P values were corrected for multiple testing using the Benjamini & Hochberg method [115].

Fold change experiments.   In order to test how the model responds to the variations in the concentration of the enzymes that emerge in conditions related to obesity, we modeled the variation of the amount of certain enzymes in terms of their fold change (FC) with respect to the experimental microarray data. To cluster the enzymes we identified two sets of genes: those contained in our model and differentially expressed at 5 weeks (Tab. 4.3) those contained in our model and differentially expressed at 16 weeks (Tab. 4.4). In the FC experiments, we included the variation in fold change in the model as the product of $[DEGS] \cdot FC \cdot kf12'$, thereby assuming that the variations in the fold change of gene expression affect the concentrations of the related enzymes, and this affects the propensity of the reactions that involve these enzymes. In particular, if the enzyme is overexpressed FC is given as 2^x, if it is underexpressed as 2^{-x}, where x is the amount of change we simulated. To measure the accumulated effect of these changes, in accordance with the experimental data, we have considered the $\log_2$ of the ratio of AUC for the case with varied fold change of the enzymes and the AUC of the control case where FC=1, that is, $\log_2$(AUC-FC/AUC-Control). This provides an estimate of the cumulative effect over the whole experiment with respect to the varied fold change of the enzyme. Logarithm is used to highlight the cases in which the fold change has a decreasing effect on the accumulated effect of the metabolite.

Compartmentalization. Sphingolipid metabolism is a complex system that takes place in different parts of the cell, from the ER to the cell membrane [100, 116]. Regarding the specific compartmentalization of the metabolites, to the best of our knowledge, there is no data available that is suitable for modeling. Other approaches have been tested in the literature, such as in [117], where the authors proposed a model for sphingolipid metabolism that includes compartments. However, their results are neither compared with experimental data, nor quantitatively justified. Moreover, the model in [117], despite the lack of experimental verification, includes more than 120 free parameters, which introduces additional challenges in terms of interpretation of the results. In contrast, our model includes only 29 parameters, which are instantiated by using experimental data, and verified by independent data and sensitivity analysis.

We have, however, addressed the compartmentalization of certain components within the realm of our model. We tested our model in order to quantify how the effect of impairment on the transport mechanisms [100] would affect its output. To this end, we analyzed the sphingolipids that may be more affected by the transport impairment. In particular, we tested our results by varying the initial concentrations of the metabolites that are known to be subject to transport between compartments by a factor from 1 to 0.2. These results are depicted in Fig. 4.12. These simulations indicate that our results are not vulnerable to perturbations in the availability of sphingolipids due to alteration in transport.

Sensitivity Analysis. We performed a parametric sensitivity analysis, considering for each reaction the estimated rate and varying it under mass action law. We considered 4 orders of magnitude fold change interval starting from 0.01 up to 100 that covers possible metabolic perturbations of the system. The parameter fold changes are included in the model in the same way as for the enzyme fold changes. We ran simulations by varying these fold change values, and we measured the impact of these changes to the system in terms of AUC ratio for each sphingolipid. We performed the same kind of analysis for enzymes, with varying FC from 0.01 up to 10.

This data is used to produce a network of interactions. We used orange rectangular nodes to represent the sphingolipids and blue circles to represent the rates or the enzymes. The dimension of the nodes is proportional to the number of incident edges. We used color edges to differentiate the effect of rates on sphingolipids: an edge is red if the rate increase causes concentration of the lipid increase; it is green if the concentration decreases. Undirected edges are chosen for increasing readability, however they are directed from the rates or the enzymes to the sphingolipids (Fig. 4.3 and Fig. 4.4).

We weighted the edges of the network proportionally to the base two logarithm of the AUC ratio. Therefore an edge has the same width if the effect on a sphingolipid is doubling or halving its concentration. In particular, we determined the value to use for this representation with respect to the results of the sensitivity analysis. We identified a value in the range where the concentrations vary in

a monotone way according to FC. In this case, we choose a fold change of 4. To improve the readability of the network we represented only the interaction such that $| \text{ AUC ratio } -1| > 0.01$. We produced in the same way the interaction network for the enzymes and chose the interactions such that $| \text{ AUC ratio } -1| > 0.001$.

The networks are obtained from simulation data, and processed using the igraph R library [118]. Finally the network figure was produced using Cytoscape, and the organic layout algorithm was used to improve the readability.

4.5   Supplementary Material

Reaction N.	Reaction	Rate Identifier	Deterministic Rate	Stochastic Rate
1	dhSph + CoA16 + CERS6 → dhCer	kf1	13	2.158751e-05 · sf
2	dhSph + CoA16 → dhCer	kf2	5.940000e-02	9.863833e-08 · sf
3	dhCer →	kf3	1.060000e-03	1.060000e-03
4	dhSph + Sphk1 → dhSph1P	kf4	3.740000e-04	3.740000e-04
5	dhSph + Sphk2 → dhSph1P	kf5	1.570000e-02	1.570000e-02
6	dhSph1P →	kf6	5.200000e-01	5.200000e-01
7	dhCer + UGCG → dhGlcCer	kf7	2.020000e-02	2.020000e-02
8	dhGlcCer →	kf8	2.900000e-01	2.900000e-01
9	dhCer + Sms1 + PC ⟷	kf9	1.160000e-01	1.926270e-07 · sf
	dhSM + Sms1 + DAG	kb9	3.900000e-01	2.856360e-06 · sf
10	dhCer + Sms2 + PC ⟷	kf10	1.720100e+00	6.476254e-07 · sf
	dhSM + Sms2 + DAG	kb10	1.080000e-01	1.429758e-06 · sf
11	dhSM + SMPD1 → dhCer	kf11	8.610000e-01	1.080000e-01
12	dhSM →	kf12	3.000000e-02	3.000000e-02
13	dhCer + CERK → dhCerP	kf13	1.180000e-04	1.180000e-04
14	dhCerP →	kf14	1.660000e-01	1.660000e-01
15	dhCer + DEGS1 → Cer	kf15	9.250000e-03	9.250000e-03
16	dhCer → Cer	kf16	8.000000e-01	8.000000e-01
17	Cer + CERK → CerP	kf17	1.180000e-04	1.180000e-04
18	CerP →	kf18	1.130000e-01	1.130000e-01
19	Cer + Sms1 + PC ⟷	kf19	1.160000e-01	1.926270e-07 · sf
	SM + Sms1 + DAG	kb19	3.900000e-01	9.282630e-08 · sf
20	Cer + Sms2 + PC ⟷	kf20	5.590000e-02	6.476254e-07 · sf
	SM + Sms2 + DAG	kb20	1.670000e-03	2.236632e-06 · sf
21	SM + SMPD1 → Cer	kf21	1.346900e+00	1.670000e-03
22	SM →	kf22	1.060000e-02	1.060000e-02
23	Cer →	kf23	0	0
24	Cer + UGCG → GlcCer	kf24	2.020000e-02	2.020000e-02
25	GlcCer →	kf25	3.170000e-03	3.170000e-03

Table 4.1: *Reactions and stochastic rates obtained from the deterministic rates in [3]. sf refers to the scaling factor.*

Reaction N.	Reaction	Rate Identifier	Deterministic Rate	Stochastic Rate
1	dhSph + CoA + CERS $\longrightarrow$ dhCer	kf1	1.2523e+01	2.0794e-05 · sf
2	dhCer $\longrightarrow$	kf2	5.3996e-01	5.3996e-01
3	dhSph + PLPP $\longrightarrow$ dhS1P	kf3	3.5455e-03	3.5455e-03
4	dhS1P $\longrightarrow$	kf4	1.5116e-01	1.5116e-01
5	dhCer + UGCG $\longrightarrow$ dhGluCer	kf5	6.8664e-02	6.8664e-02
6	dhGluCer $\longrightarrow$	kf6	3.2676e-01	3.2676e-01
7	dhCer + SMS + PC $\longleftrightarrow$	kf7	9.2076e-02	1.5290e-07 · sf
	dhSM + SMS + DAG	kf28	4.7810e-01	7.9390e-07 · sf
8	dhSM + SMA $\longrightarrow$ dhCer	kf8	2.0220e-08	2.0220e-08
9	dhSM $\longrightarrow$	kf9	4.1706e-02	4.1706e-02
10	dhCer + CERK $\longrightarrow$ dhCer1P	kf10	7.6142e-04	7.6142e-04
11	dhCer1P + CAPP $\longrightarrow$ dhCer	kf11	4.0986e-01	4.0986e-01
12	dhCer + DEGS $\longrightarrow$ Cer	kf12	1.3904e-01	1.3904e-01
13	Cer + CERK $\longrightarrow$ Cer1P	kf13	2.9955e-04	2.9955e-04
14	Cer1P + CAPP $\longrightarrow$ Cer	kf14	1.7897e-01	1.7897e-01
15	Cer + SMS + PC $\longleftrightarrow$	kf15	2.3484e-03	3.8996e-09 · sf
	SM + SMS + DAG	kf29	2.0752e-02	3.4460e-08 · sf
16	SM + SMA $\longrightarrow$ Cer	kf16	9.6067e-05	9.6067e-05
17	SM $\longrightarrow$	kf17	6.4391e-05	6.4391e-05
18	Cer $\longrightarrow$	kf18	1.0800e-02	1.0800e-02
19	Cer + UGCG $\longrightarrow$ GluCer	kf19	1.2546e-01	1.2546e-01
20	GluCer $\longrightarrow$	kf20	9.8926e-02	9.8926e-02
21	dhCer + ASAH $\longrightarrow$ dhSph	kf21	1.3685e-02	1.3685e-02
22	null + SPT $\longrightarrow$ dhSph	kf22	4.6336e+00	(2.7904e+06)/ sf
23	Cer + ASAH $\longrightarrow$ Sph	kf23	2.6853e-02	2.6853e-02
24	Sph + CERS $\longrightarrow$ Cer	kf24	2.4217e-02	2.4217e-02
25	Sph + SK $\longrightarrow$ S1P	kf25	3.7867e-02	3.7867e-02
26	S1P + SGPP1 $\longrightarrow$ Sph	kf26	4.9200e+00	4.9200e+00
27	S1P + SGPL $\longrightarrow$	kf27	3.7856e+00	3.7856e+00

Table 4.2: *Reactions of our extended model.*

logFC	adj.P.	symbol	aggregated symbol	AveExpr$_{WT}$	AveExpr$_{ob/ob}$
−0.452620099	0.008182273	Sgpp1	SGPP1	9.221666078	8.769045979
−0.224976984	0.091131914	Asah2	ASAH	7.750207047	7.525230062
−0.216372605	0.096486253	Asah1	ASAH	10.39519443	10.17882183
−0.180378296	0.09595853	Ugcg	UGCG	8.181176815	8.000798519
0.497378687	0.003163028	Degs1	DEGS	8.628122177	9.125500863
0.454196511	0.016684256	Smpd3	SAM	6.563311134	7.017507645
0.346984067	0.011837382	Sgms1	SMS	8.109475589	8.456459656
0.970942051	0.008430373	Sgms2	SMS	5.871574472	6.842516523
0.510300826	0.003532425	Cers6	CERS	8.087639879	8.597940705

Table 4.3: *Statistical analysis results for genes contained in our model. Differential expression values refer to the difference between wildtype (WT) and* ob/ob *mice at 5 weeks.*

logFC	adj.P.	symbol	aggregated symbol	AveExpr$_{WT}$	AveExpr$_{ob/ob}$
0.251283323	0.009757826	Asah1	ASAH, ASAH[1]	11.32289211	11.57417544
−0.400699156	0.000899179	Asah2	ASAH, ASAH[1]	8.618283842	8.217584686
−0.19660911	0.078807427	Acer1	ASAH[1]	5.177626666	4.981017556
−0.625195789	7.90e-05	Acer2	ASAH[1]	7.548612508	6.923416719
1.038252808	1.09e-07	Acer3	ASAH	7.721198262	8.75945107
0.588336958	1.34e-05	Cerk	CERK	8.527943995	9.116280954
0.60453069	7.26e-06	Degs1	DEGS	9.737870426	10.34240112
−1.883316456	1.12e-08	Ppap2b	PLPP	11.79434036	9.911023905
0.336052217	0.020480217	Ppap2c	PLPP	8.463706403	8.799758619
0.343115755	0.001608825	Sptlc1	SPT	9.044525454	9.38764121
−0.198809527	0.072928862	Smpd3	SMA	7.912221158	7.713411631
0.470062309	3.91e-05	Sgms1	SMS	8.633440478	9.103502786
0.182996148	0.05350511	Sphk2	PLPP	7.777322825	7.960318974
0.812523823	5.45e-07	Sgpl1	SGPL	10.93098122	11.74350504
0.947997388	1.04e-07	Cers6	CERS	8.718705273	9.666702661
0.206366580	0.025389854	Cers5	CERS	8.868672068	9.075038647

Table 4.4: *Statistical analysis results for genes contained in our model. Differential expression values refer to the difference between wildtype (WT) and* ob/ob *mice at 16 weeks. ASAH is the name that summarize enzymes that mediate reaction 21, ASAH[1] those which mediate reaction 23.*
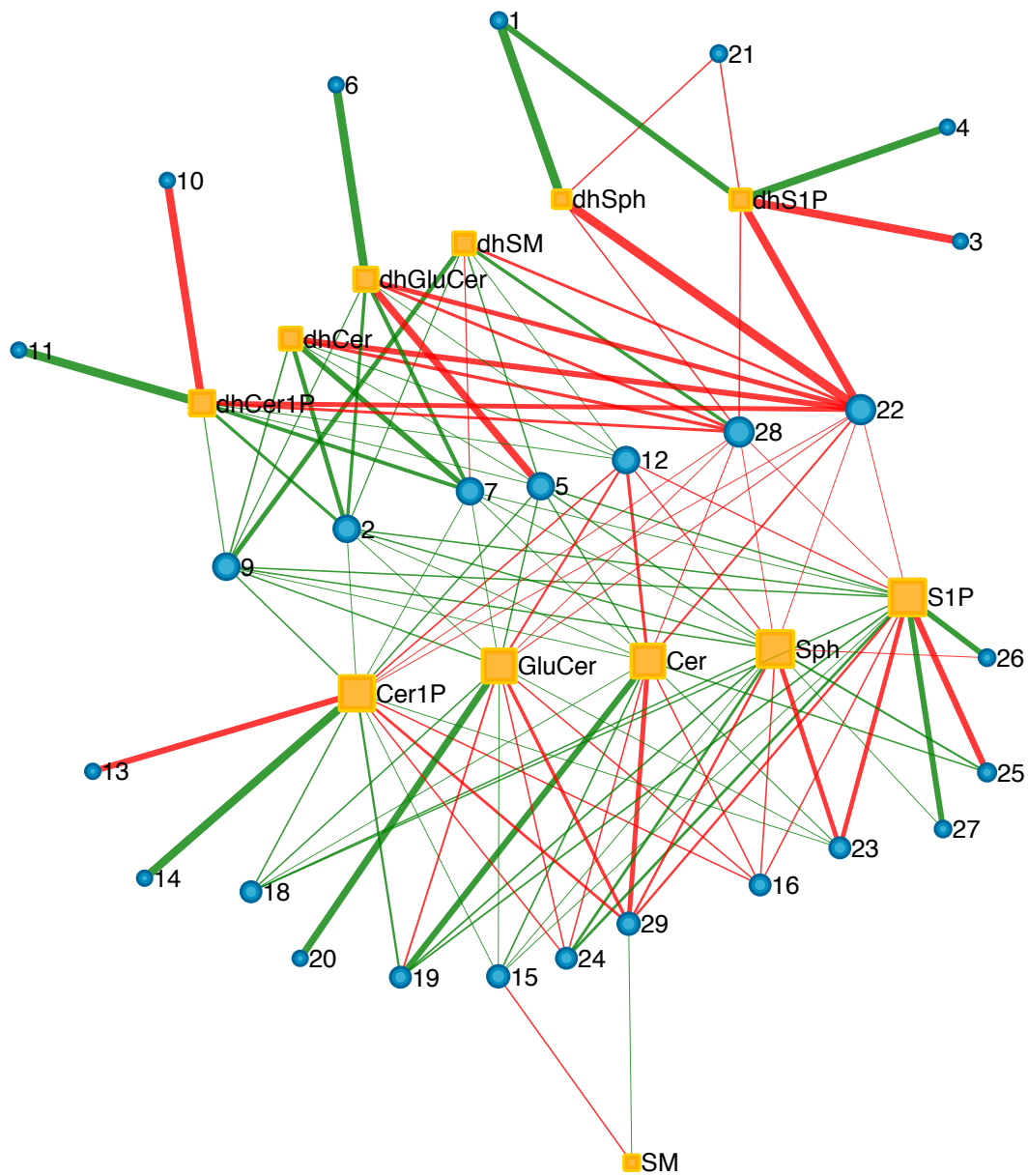
Figure 4.4: *The network of interactions obtained from the sensitivity analysis for rates. Edges are colored in red if the increase of the rate follows an increase of the concentration of the sphingolipid node, in green if the concentration decreases. The thickness of the edges is proportional to the log_2 of the AUC ratio. In orange rectangles and blue circles, respectively, the sphingolipids and the enzymes are represented. The label of the nodes are the reaction numbers in Tab. 4.2.*
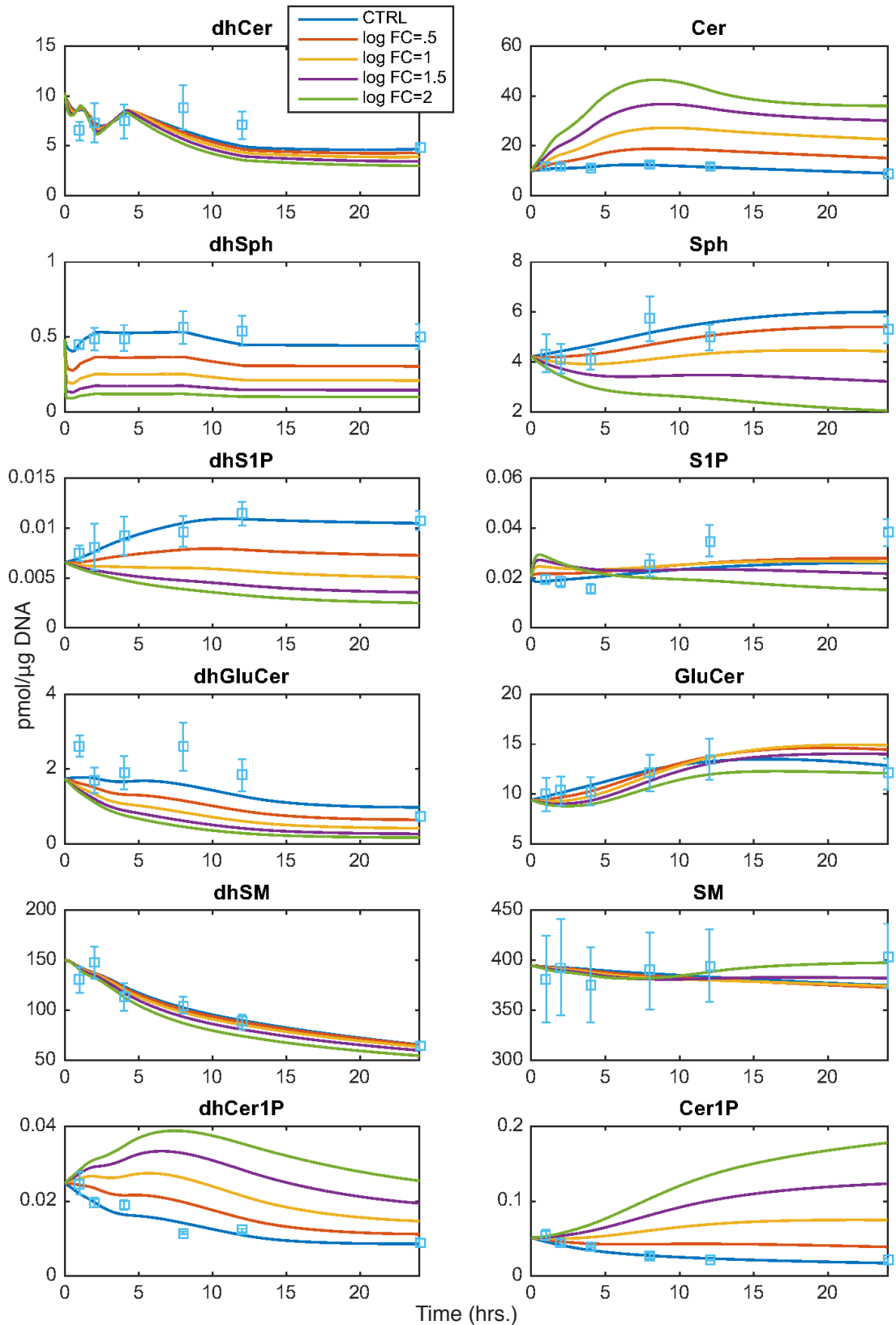
Figure 4.5: *Deterministic simulation of the main metabolites with varying fold changes to observe the effect of the perturbation compared with experimental observations of* ob/ob *mice at 5 weeks. Concentrations measured in pmol/μg DNA.* x-axis: *time in hours.*
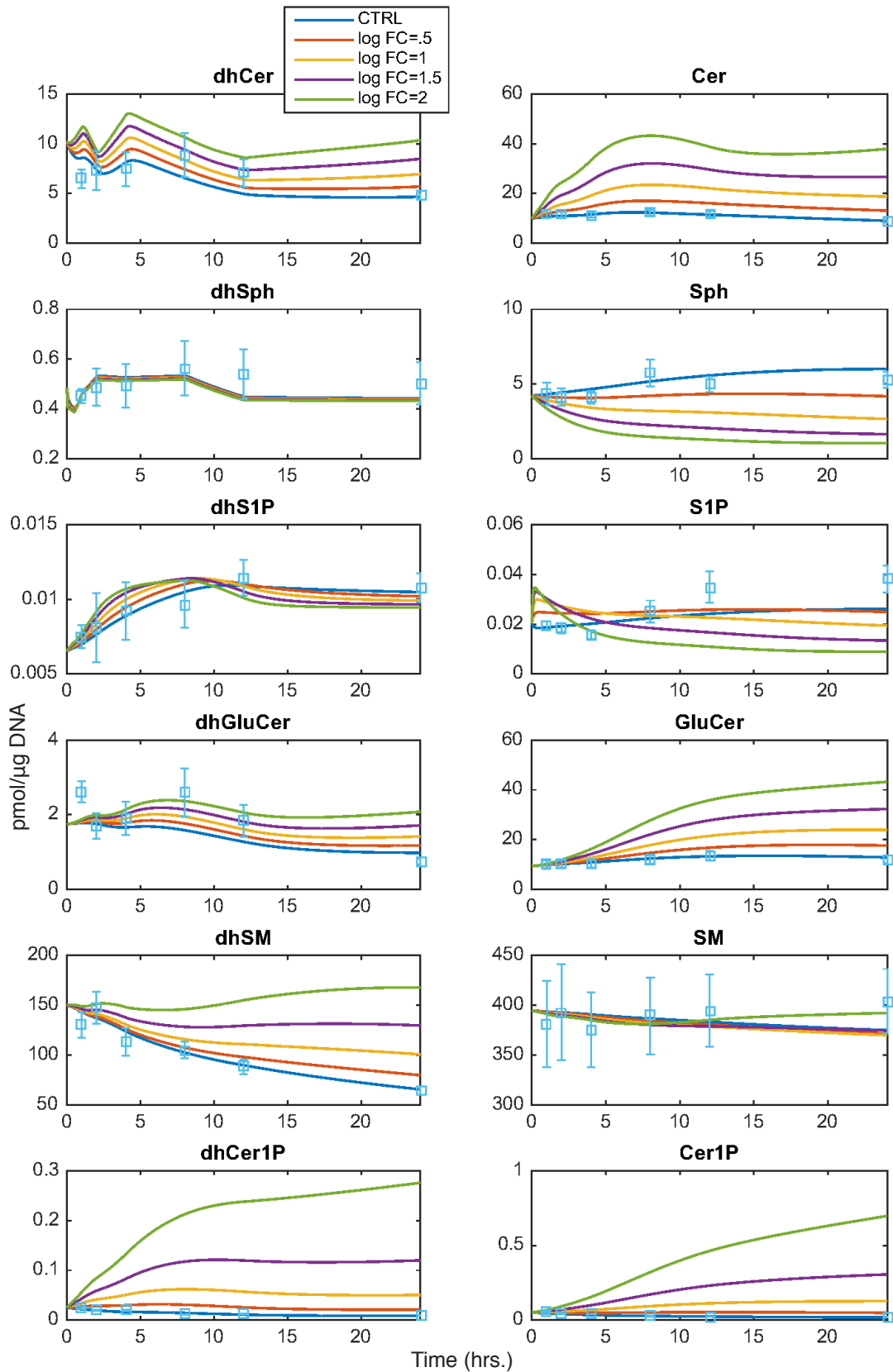
Figure 4.6: *Deterministic simulation of the main metabolites with varying fold changes to observe the effect of the perturbation compared with experimental observations of* ob/ob *mice at 16 weeks. Concentrations measured in pmol/µg DNA.* x-axis: *time in hours.*
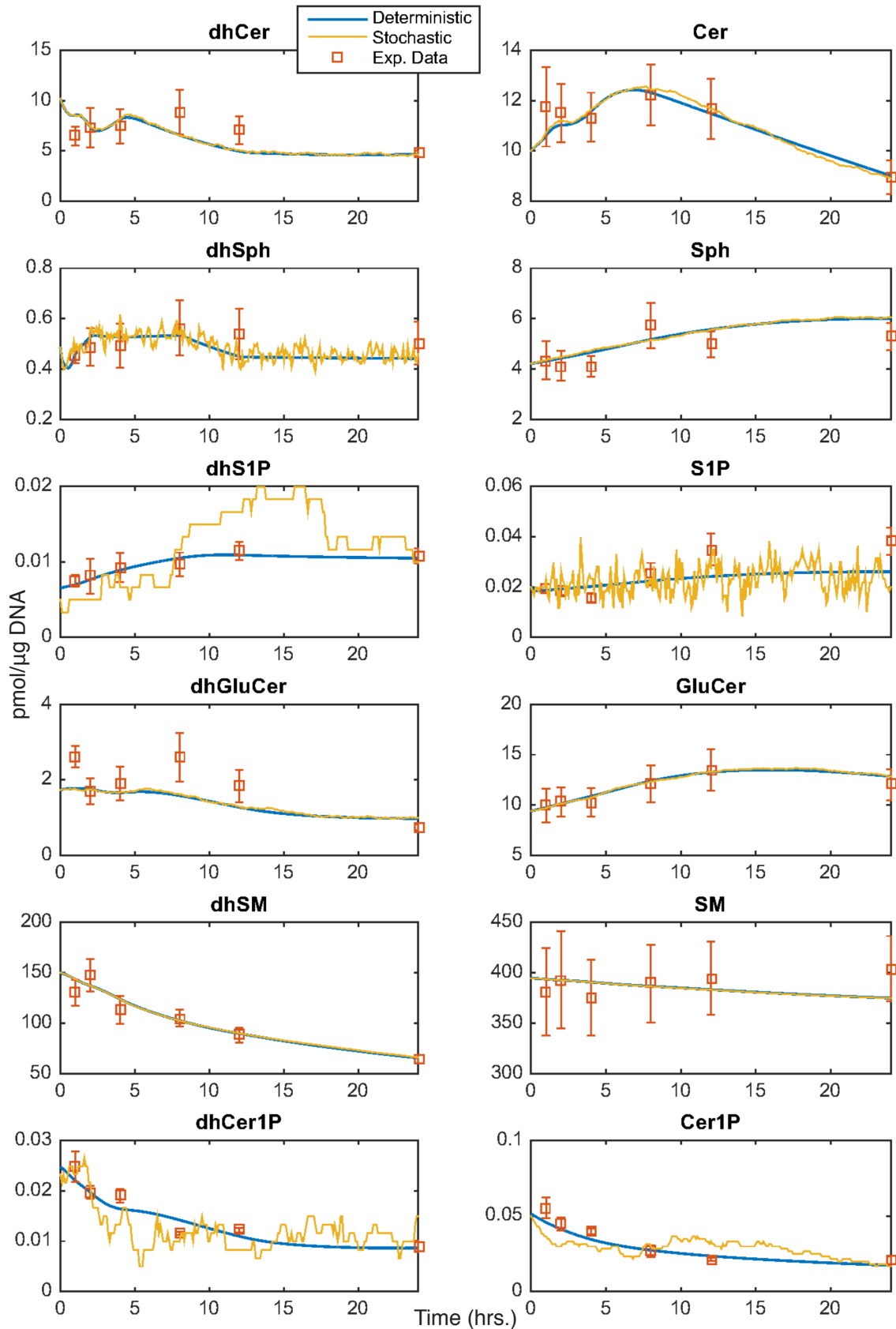
Figure 4.7: *Comparison of the deterministic and stochastic simulation outcomes of the main metabolites with the experimental observation, for RAW 264.7 cells. Note the fluctuation of the stochastic simulations when the abundance of the metabolites is very low,* e.g. *dhCer1P, Cer1P, dhS1P, S1P and dhSph. Concentrations measured in pmol/μg DNA.* x-axis: *time in hours.*
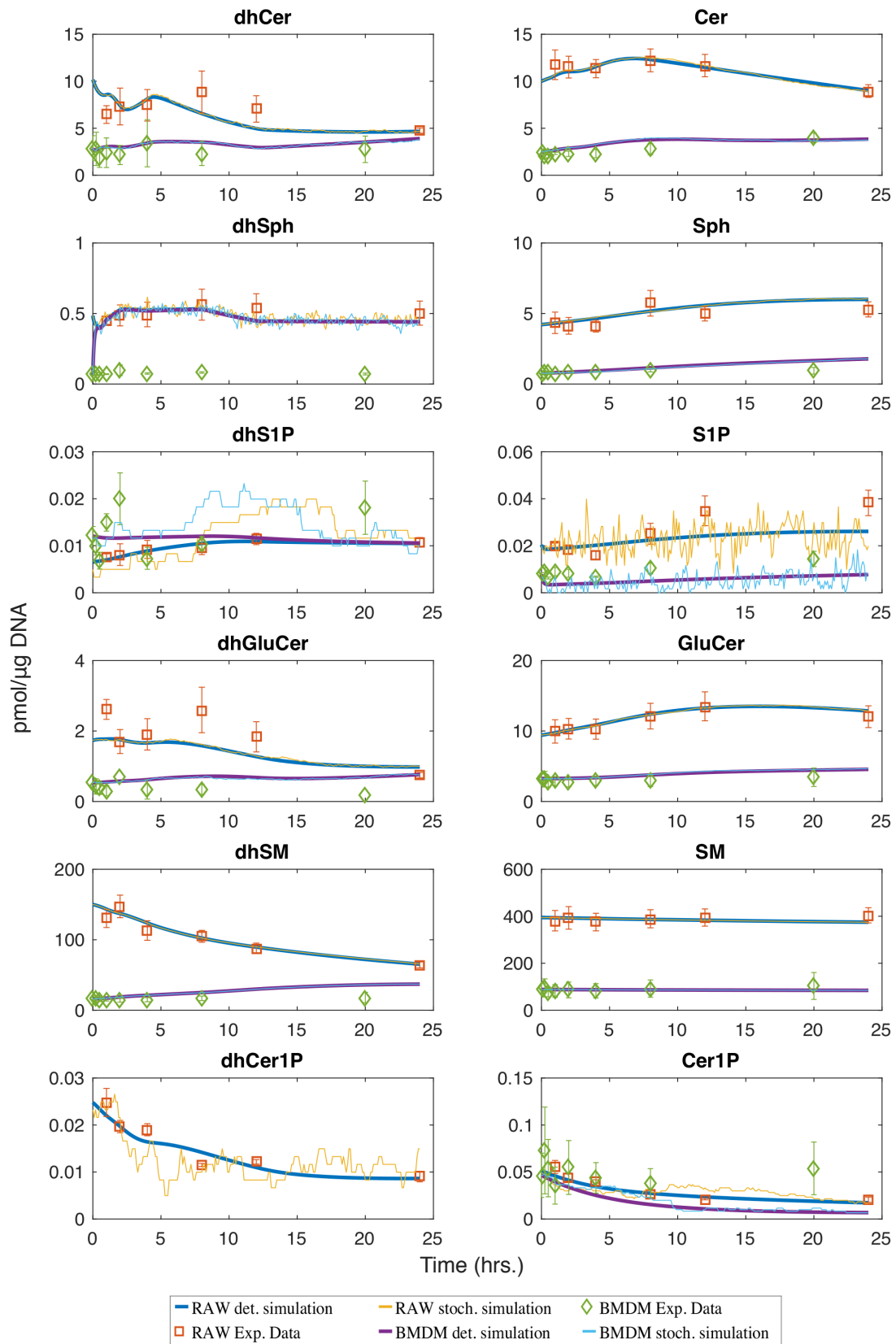
Figure 4.8: *Comparison of the deterministic and stochastic simulation outcomes, for both RAW 264.7 cells and BMDM. The BMDM dataset does not include data for dhCer1P. Concentrations measured in pmol/μg DNA.* x-axis: *time in hours.*
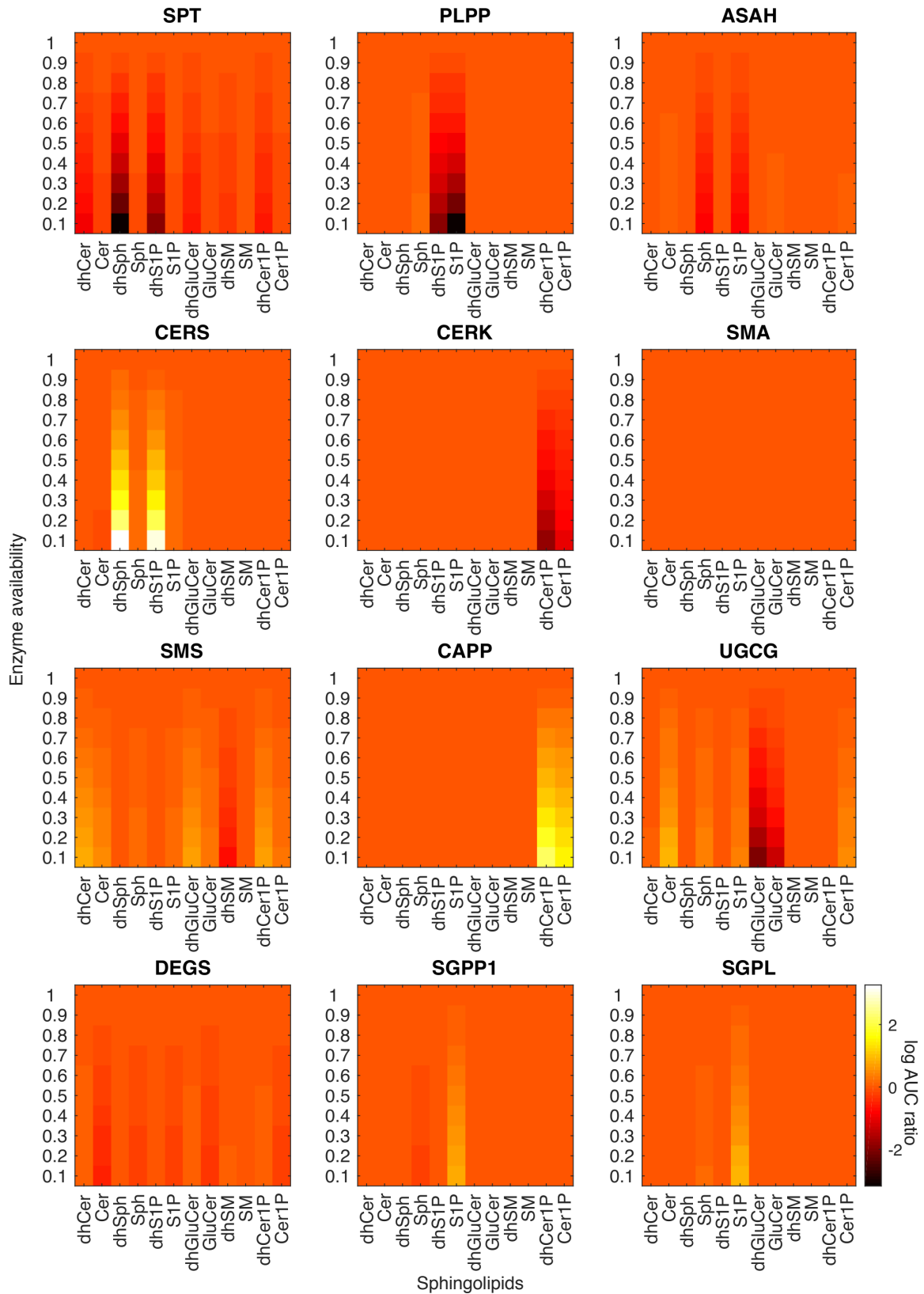
Figure 4.9: *Heatmaps quantifying the effect of the reduced availability of each enzyme on each metabolite. The effect is quantified in terms of* $\log_2$ *AUC ratio, as defined in the main text.*
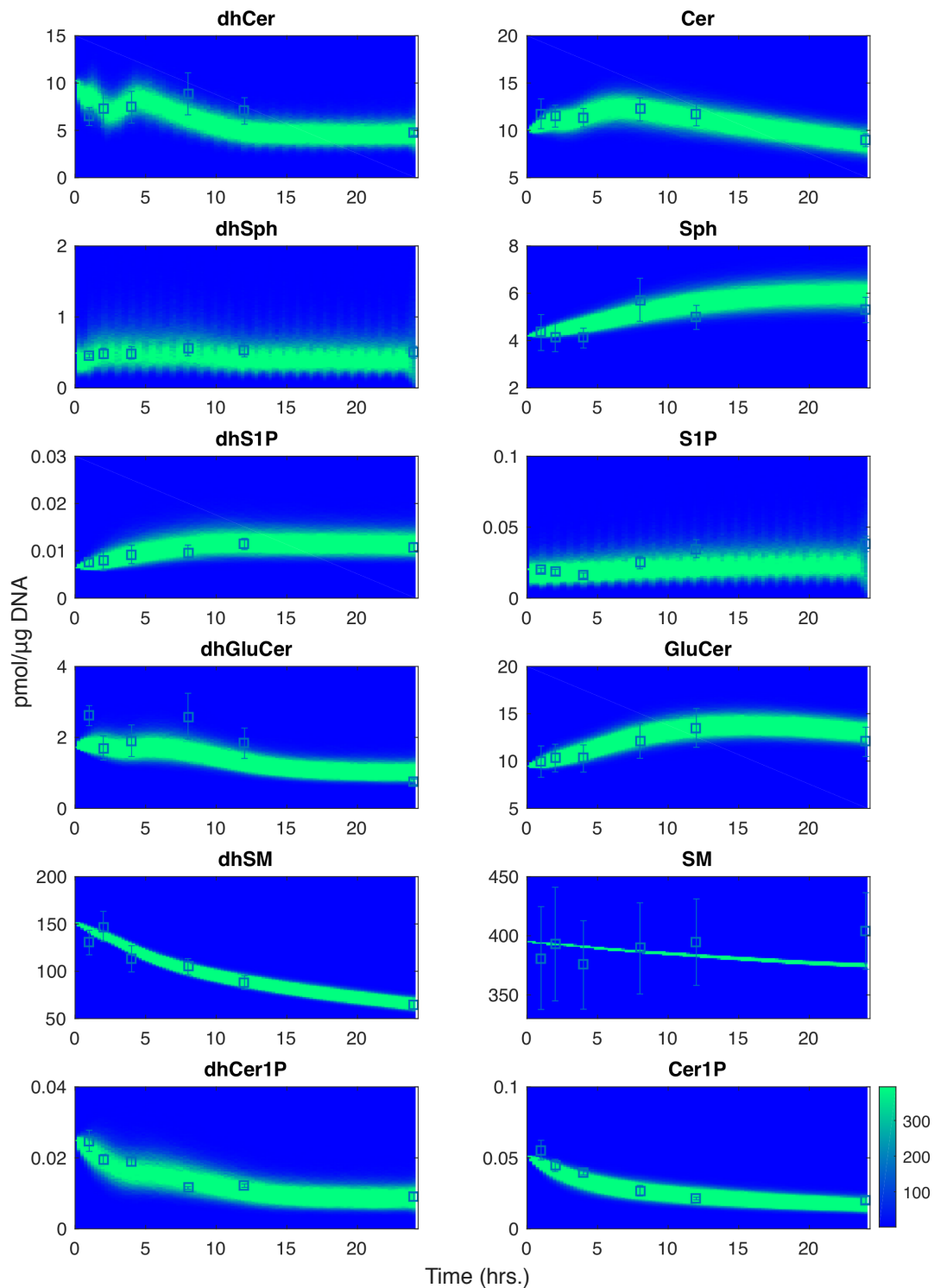
Figure 4.10: *The cumulative output of 10000 simulations under the effect of random perturbations on the fold change of the enzymes, compared with the experimental data. Every hour the enzyme fold changes are randomly varied. The colors are proportional to the number of simulations. Here the greener is the color, the more are the simulations that coincide with that trajectory. The random perturbations are obtained as the sampling of a normal distribution with mean 0 and standard deviation 0.5. Concentrations measured in pmol/μg DNA. x-axis: time in hours.*
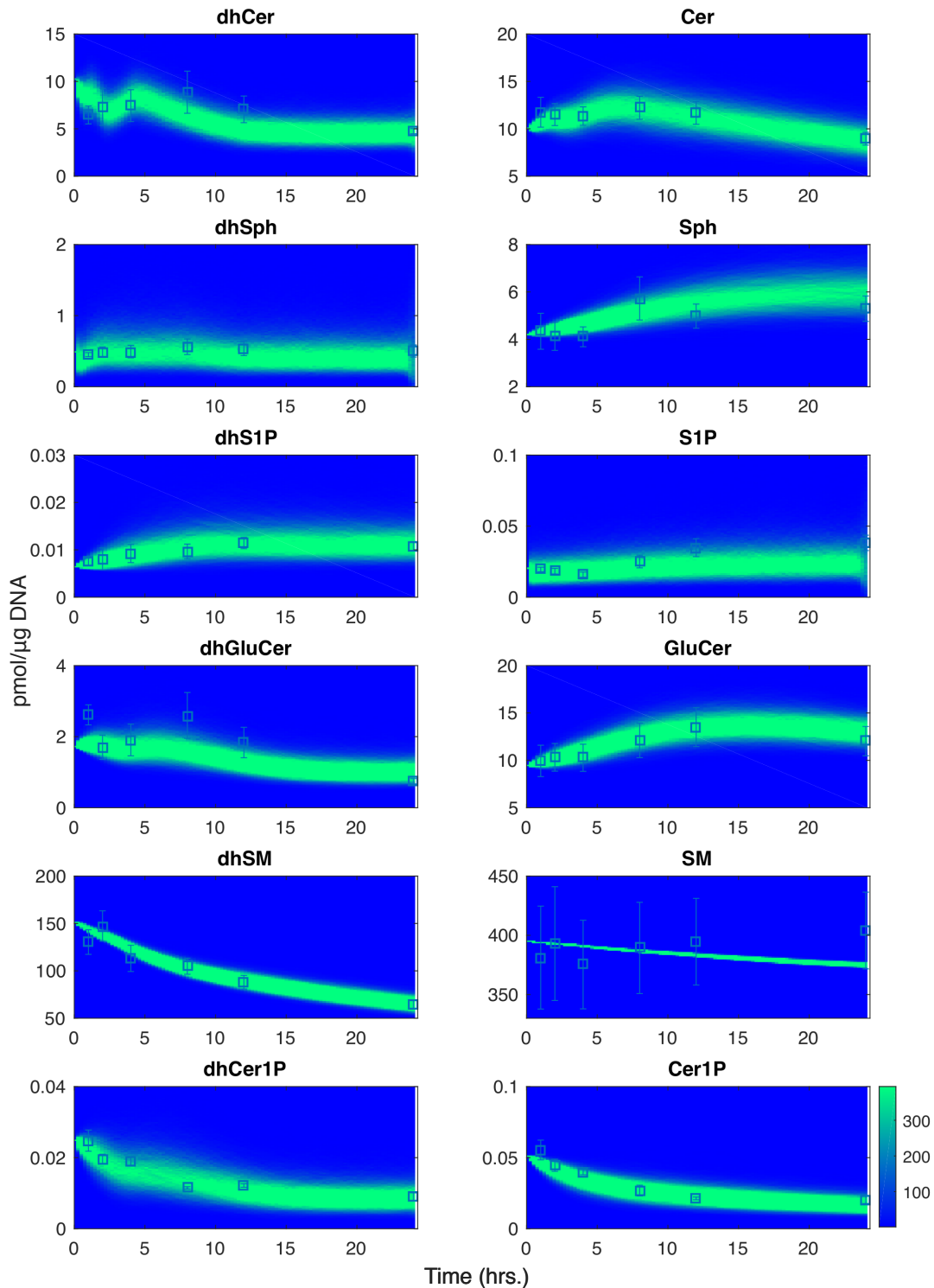
Figure 4.11: *The cumulative output of 10000 simulations under the effect of random pertur-bations on the fold change of the enzymes, compared with the experimental data. At random time points the enzyme concentrations are randomly varied. The colors are proportional to the number of simulations. Here the greener is the color, the more are the simulations that coincide with that trajectory. The random time points are obtained as the sampling of 15 points from an uniform distribution between 0 and 24. The random perturbations are obtained as the sampling of a normal distribution with mean 0 and standard deviation 0.5. Concentrations measured in pmol/μg DNA.* x-axis: *time in hours.*
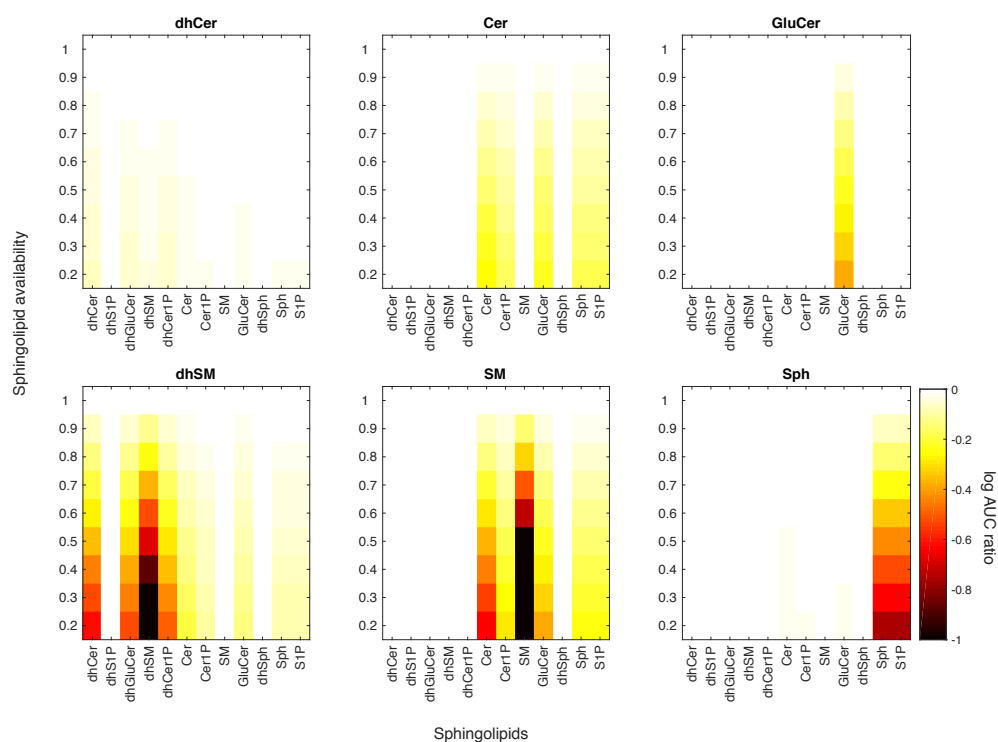
Figure 4.12: *Heatmaps quantifying the effect of the reduced availability of the metabolites due to, for example, impairment in transport between compartments. The reduced effect, displayed in the tiles of each metabolite, is quantified in terms of AUC ratio as defined in the main text.*

Author contributions

This work is the result of a collaboration between COSBI and Daniel Crowther's group at Sanofi-Aventis Duetschland GmbH, Frankfut am Main, Germany. Also the article is the result of the joint effort of both the institutions.

Ozan Kahramanoğulları and I designed and performed simulations and sensitivity analysis. Melissa J. Morine, Corrado Priami, Ozan Kahramanoğulları and I wrote and edited the manuscript. Melissa J. Morine and Corrado Priami performed literature mining and identified the reactions of interest. All the authors analysed the results and reviewed the manuscript.

Chapter 5

Discussion

Mathematical and dynamical models have been shown to provide a useful framework for the development of mechanistic descriptions of biological phenomena related to diabetes. The results included in this dissertation also highlight how these models may lead to useful biological insights. The models described here, as models in general, rest on assumptions and abstractions. They, thus, may be refined or extended according to the context they are used in. We discuss in this chapter some of the possible developments and further extensions.

Diabetes type 1 The development of an automated insulin delivery device is a long process that started in the late 70s with the first models for the glucose-insulin system [11,42], and the following developments [46]. In the following decades, more complex and accurate diagnostics procedures, such as the use of glucose tracers [12,53,71], have been introduced. As a consequence, the research effort refocused towards more complex representations and models, departing from the initial idea of a minimal model. These new procedures allowed the models to correctly identify parts of the processes involved with increasing precision. For example, the glucose trackers have helped in distinguishing the endogenous from the exogenous glucose measured in the bloodstream [12]. Nevertheless, these procedures have led to more complex models. These models are harder to tune and are not suitable for implementation on devices such as "artificial pancreas" that are required to be as simple as possible. For example, such a device is meant to work on data recorded from the patient in everyday life, where it is impossible to use radio-labeled glucose.

The need for simpler models has shed new light to those minimal approaches, such as the one we describe in Chapter 3. In this approach, we have focused on describing with a minimal number of equations and parameters, complex processes such as digestion and the insulin-glucose system [15]. Our model does not include some improvements, such as tracers, to be as close as possible to the scenario of application. To the same end, our model is a close-loop model, where the insulin and glucose compartments are simulated synchronously, as we expect in control algorithms. Moreover, our original solution to the appearance of glucose in the blood does not only require fewer parameters than other models in the literature [15,47], but it also requires only the approximate glucose content

of the meal. This is an important feature because such information may be easily quantified, whereas other information, for instance the glucose experimental data, is unlikely available *a-priori* for an everyday meal.

Our model and its results have been validated with repeated tests over the same patients. This has provided strong indications on the quality of the model. Nevertheless, extending the analysis to more patients would provide more solid evidence. By testing the model on an extended cohort, it may strengthen our results and, however, it may also provide modeling challenges. Such an extended cohort should include healthy patients, and, after the necessary adjustments, the model should reflect the patient conditions, ideally providing ways to discriminate them. In this respect, it would be important to develop shared databases that contain data for multiple experiments. However, such datasets are quite rare.

The data itself may provide a possible improvement of the model. Since any device such as the artificial pancreas would rely on glucose and insulin measurements taken from the tissues, it would be better to test the models with data from these tissues [75]. However, we have used measurements from blood. The use of tissue measurements would add complexity since the delayed appearance of glucose requires more equations and parameters than with data from blood [7]. Still, this may provide a more accurate description that is closer to the one that would actually be used.

Developing and implementing such models introduce also other challenges. An interesting challenge we have faced in the process of developing our model is the integration of data and parameters from two different experiments namely, the HEC and the MMT experiments. In particular, we have used the model for the HEC experiment to tune some parameters that are in common between the two models. The HEC experiment, which is considered the gold standard to assess the insulin sensitivity of patients [41], is described with less uncertainty. In fact, such a model is smaller and contains less parameters [45]. Its parameters are used to drive the estimation of some of the parameters of the MMT model [15]. The integration of data and models for different experiments is an important part of the development of models that autonomously regulate insulin and glucose. In fact, devices such as "artificial pancreas" are meant to be initially tuned by using patient specific parameters that are estimated using models or *ad-hoc* experiments. They should then work without any other tuning process [72].

Another important issue in the development of such control algorithms is the need for models that are commonly accepted by the research community. In fact, the development of such algorithms has been kept mostly secret due to intellectual property issues. However, our vision, as well as the vision of many research groups, lies in sharing the results in order to establish a consensus.

In conclusion, the development of a fully automated insulin delivery device may still be far. Nevertheless, with the joint effort of the research community, in a not so long future, these devices may become as common as pacemakers are now for cardiac diseases.

Insulin resistance   Modern age took not just great improvements in people's health and standard of living, but also serious changes in our everyday life. As a consequence of sedentary life and unhealthy habits, always more people suffer from weight problems or insulin impairment, such as obesity or insulin resistance and diabetes type 2 [17, 119]. It is possible to mitigate the impact of these diseases on our society promoting healthier lifestyles and habits, as well as designing specific new drugs.

In the endeavor of providing a better understanding of insulin resistance, we have developed the model described in Chapter 4. Our results have suggested mechanistic explanations for the role of sphingolipids in the development of insulin resistance for mice macrophage tissues. This may help in identifying potential drug targets [27]. However, to gain a better comprehension of this process, models need to be tested on several tissues by using data from different animal models and cell lines. For example, an accurate description of the sphingolipids metabolism in muscle and liver tissues may help in understanding their role in the whole-body glucose-insulin homeostasis [89]. As for diabetes type 1, this highlights the need for open access datasets that allow researchers to analyze their results and the quality of their models in the presence of heterogeneous data. Nevertheless, there are few available datasets also in this case.

One possible extension of our model is to take into account other molecules that are involved in the sphingolipids metabolism and in the insulin resistance development [17]. Building a model that captures certain interactions between the molecules of interest for these processes might help in quantifying their effect, unveiling unknown mechanisms. This could drive the research toward the design of effective drugs while minimizing the risk of side effects [6].

Another extension of the model may be to proceed in the direction we have started in Chapter 4, i.e., analyze the model using stochastic simulations. As detailed in Appendix A, this kind of simulations may precisely describe a possible evolution of a dynamical system. In addition, when certain species abundances are particularly small, it is the most appropriate way to simulate a model [120, 121]. In our case, we may apply stochastic simulations to precisely describe the interactions of the sphingolipids in a reduced section of the cell. For example, we may concentrate our attention on the cell membrane where sphingolipids interact with the insulin receptors and the insulin receptor substrates (Fig. 2.2). A mechanistic description of this process may produce valuable information that links this molecular regulation with the cellular sphingolipid metabolism [17, 122].

As in similar cases, tuning the parameters of the sphingolipid model has provided several challenges. For example, there is the computational effort to assure a solution that provides the best set of parameters that fit the experimental data. In addition, there is the effort to exclude that such estimates over-fit the data [123]. To this end, the sphingolipid model has undergone further analysis than the one described in Chapter 4. In fact, to assure the convergence to a reliable set of parameters, the solution of the multi-start non-linear least

squares approach was further analyzed by using a Markov Chain Monte Carlo method (Appendix A). This method permits to estimate the correlations and dependencies between the parameters [124] and it may have supported the biological validation of the model. In fact, the parameter set was robust enough to successfully describe the sphingolipid metabolism in a validation dataset from a different experiment [27].

During the development of the model presented in Chapter 4, we were also challenged by the need for integrating transcriptomic and lipidomic data. This integration is a necessary step, as well as the integration of different types of data in general, to fully develop the systems view that characterizes the systems biology approach [5,6]. To this end, some of our ongoing work, not included in this dissertation, focuses on the integration of these data to gain a better understanding of the interaction of these different biological levels, namely, genes and lipids. We are using this integration to understand the processes of the *de-novo* synthesis of various chain length ceramides. This may help in quantifying the contribution of each different ceramide, as well as the interaction between them [18].

Dynamical models are supporting the discovery of new drugs and they are key components towards the development of personalized medicine. Personalized medicine could be tailored to patients' needs and characteristics, thereby reducing the risk of side or collateral effects. This should have a remarkable effect on people's lives, also changing the way we develop and discover drugs.

Optimization in systems biology   Optimization is a key task in the development of models, and it has been a crucial part of the development of the models included in this dissertation. For example, the model for diabetes type 1 required to deal with a particular objective function that accounts for the previous knowledge [15]. In addition, in the sphingolipid model, the combination of different estimation techniques has enhanced the results' reproducibility [27]. Despite their role in the development of dynamical models, optimization tools are often seen as black-boxes [125]. Such an approach may lead to naive interpretations of the results or to poor choices of the algorithms to solve the problems.

With the aim of providing an accessible description that introduces (global) optimization techniques in systems biology, we have provided a review article that is reported in Appendix A. We have selected three algorithms that present some of the main family of optimization approaches. The three algorithms belong to the deterministic [126], stochastic [127], and heuristic [128] optimization techniques. Although this selection provides the general ideas behind these optimization areas, there exists a variety of sub-families that populates the optimization literature [124–128]. We have included a rich list of references to many of them, however, it would be impossible to list them all.

For the models we discussed, we have considered a multi-start approach for the non-linear least squares method. This choice follows different considerations on the models. First, the two models are formulated in terms of differential

equations and the sought parameters are continuous. Moreover, experimental time points are known. As a consequence, the objective functions may be expressed as a sum of squares and they are continuous. A natural candidate for solving this kind of optimization problems is the least squares method [129]. Second, since the problem is non-linear and different local solutions may exist, we have considered a multi-start approach and a non-linear method [130]. Third, the selected method is one of the few that may certify the convergence, thanks to its theoretically proved termination criteria [129]. Fourth, in both models the simulation is fast. This permits the use of this computationally demanding approach. Nevertheless, the combined use of this technique with a Markov Chain Monte Carlo method may have contributed to the results in the validation dataset of the sphingolipids' model.

These considerations are valid for problems that are similar to the one we have dealt with. However, each case should be carefully analyzed and the most suitable method to solve the problem should be identified for each specific task. For example, more complex models, whose simulation time is of the order of many seconds or minutes, may favor the use of other approaches [125, 131].

The algorithms that are included in Appendix A are available in many different implementations for different languages and platforms. For example, the multi-start non-linear least squares method is implemented in the Matlab Global Optimization Toolbox. For the results of the previous Chapters, we have considered this toolbox. Similarly, non-linear least squares algorithms have been implemented in many packages for different languages and included in different libraries. Among others, they are included in the Python *scipy* package [132], as well as in the R *nlstools* library [133], or in the *Ceres* C++ library [134]. However, the multi-start approach is not included in any of these libraries. The genetic algorithms, described in Appendix A, are implemented in Matlab, Python, R and many other languages, as well. In contrast, there is no Matlab built-in function or package for the Markov Chain Monte Carlo, whereas it is available for the other languages.

Even though some knowledge on optimization algorithms is often necessary for the development of dynamical models, optimization is only one part of a bigger process. One task it to correctly translate the problem and chose the adequate algorithm. A different, and necessary, task is to provide biological evidence that supports the results. The results cannot rely only on mathematical termination criteria and optimality conditions; successive tests should be carried out. For example, since the objective function may be formulated in different ways, there is no guarantee that the best fitting set of parameters would reflect the biologically expected properties. In our experience, it is not unusual that the varying of the objective function reflects on the biological meaning of the solutions. As a good practice, it is worth to compare the results of different optimization strategies and different objective functions to support the findings. In addition, the solution of the optimization problem should be a starting point for the biological interpretation. This phase requires to interpret and validate the results to assure their biological plausibility. For example, the results should

be validated by independent datasets or the simulations should consistently reproduce known perturbation of the system, such as diseases or impairments. Sensitivity analysis is another test that models should undergo [135]. It is a fundamental tool to mathematically assess the quality of a model, and it may provide both biological insights and validations, as shown in Chapter 4.

Optimization is a fundamental tool to support the results and the goals we discussed in the previous paragraph. However, the real strength of this tool comes when its techniques are combined with biological evidence and interpretation of the models.

Appendix A

Optimization algorithms for computational systems biology

Mathematical and dynamical models often need parameters, such as rate constants or scaling factors, to describe the phenomena they are representing. It is not unusual that some of those model parameters are unknown. In the absence of effective methods to determine parameter estimates, a model provided with the wrong set of parameters may produce a distorted representation of the observed phenomena. This may lead to the rejection of its mechanistic description.

In computational systems biology, parameter estimation is needed not just for model parameters, but also for data analysis. For example, it is used to determine the optimal length of biomarkers, as well as to determine the optimal number of clusters in which data should be divided.

This appendix presents three powerful methodologies for global optimization that fit the requirements of most of the computational systems biology applications. To provide a clear description of the methods, we have focused on presenting the general ideas behind them, without blurring the description with many details.

We include the multi-start approach for least squares methods, mostly applied for fitting experimental data. We illustrate Markov Chain Monte Carlo methods, which are stochastic techniques here used for the same purpose when a model involves stochastic equations or simulations. Finally, we present Genetic Algorithms, heuristic nature-inspired methods that are applied in a broad range of optimization applications, including model tuning and biomarker identification. Moreover, the here-presented approaches coexist with a vast literature of other methods, for which we have provided several references.

This appendix contains the review article that we submitted to the journal of Frontiers in Applied Mathematics and Statistics, special topic Optimization.

A.1 Introduction

The human desire to improve and to solve problems has been addressed using mathematical methods by the field of optimization. This field has become a

crucial aspect of our daily life, with servers and computers solving hundreds of optimization problems every second, determining the best solution for finance, engineering or computer science problems. From the assets to include in a portfolio, to the shape of a particular object, to the distribution of packages sent among networks and uncountable other applications, optimization problems are addressed and solved constantly.

Among the many branches of optimization, global optimization focuses on the development of techniques and algorithms to discover the best solution, according to specific criteria, when several local solutions are possible [127]. It has been intensively improved during the last decades in an exchange of ideas and applications from various fields, such as mathematics, computer science, biology and statistics. These improvements have had a tangible effect in terms of accuracy of the results and time of execution, allowing the use of this discipline to solve bigger and more complex problems.

In the meanwhile, the convergence of biology and computer science lead to the establishment of computational systems biology [5, 6]. Computational systems biology challenges, among the others, the non-trivial tasks of gaining knowledge from the vast amount of data produced by the omics technologies and to build, starting from static data, dynamical representations that elucidate the mechanistic insights of the phenomena. Since the occurrence of multiple local solutions is likely to take place in computational systems biology [136,137], in the following we provide a concise review of three methodologies for global optimization that are successfully applied in such a field [126].

The herein proposed selection of algorithms embraces three of the main optimization areas, which rely on deterministic, stochastic and heuristic methods, respectively [127]. We have chosen simple specific implementations that, in our opinion, help in communicating the ideas behind the algorithms and elucidate the corresponding areas. We avoided technical details or strict mathematical rigor to facilitate the reading also for scientists whose background is more focused on biology than in computer science or mathematics. Nevertheless, we provided technical details in the list of references, where a skilled reader can find all the resources for an in depth coverage of the matter.

A.2 Global optimization in computational systems biology

When challenged with computational systems biology problems, global optimization has to face a variety of scenarios. We focus on model tuning and *biomarker identification*. Models are here intended for *in-silico* simulations of biological phenomena. They are usually systems of differential or stochastic equations that quantitatively describe chemical reactions or other complex interactions. A model returns a vector of current values for all the variables, which can be reals (*e.g.,* average chemical concentrations) or integers (*e.g.,* number of molecules or individuals). For example, we may consider the Lotka-Volterra

model (Eq. (A.1)), also known as the *prey-predator* model [6].

$$\begin{cases} y' = \alpha y - ayz, & y(0) = y_0 > 0 \\ z' = -bz + \beta yz, & z(0) = z_0 > 0 \end{cases} \tag{A.1}$$

This set of ordinary differential equations describes the population dynamics of two species in which one of them, the predators z, consume the other one, the prey y. The Lotka-Volterra model depends on four parameters: the growth rate of the prey α, the death rate of predators b, the rate at which preys are eaten by predators a and the rate at which the predator population grows as a consequence of eating prey β.

It is not unusual that some of the model parameters are unknown, such as rate constants or scaling factors. In the absence of effective methods to determine parameter estimates, a model provided with the wrong set of parameters may produce a distorted representation of the observed phenomena. This may lead to the rejection of its mechanistic description. For example, Fig. A.1 shows two possible outcomes of the deterministic simulation of the Lotka-Volterra model, with different sets of parameter estimates.

(a)	(b)
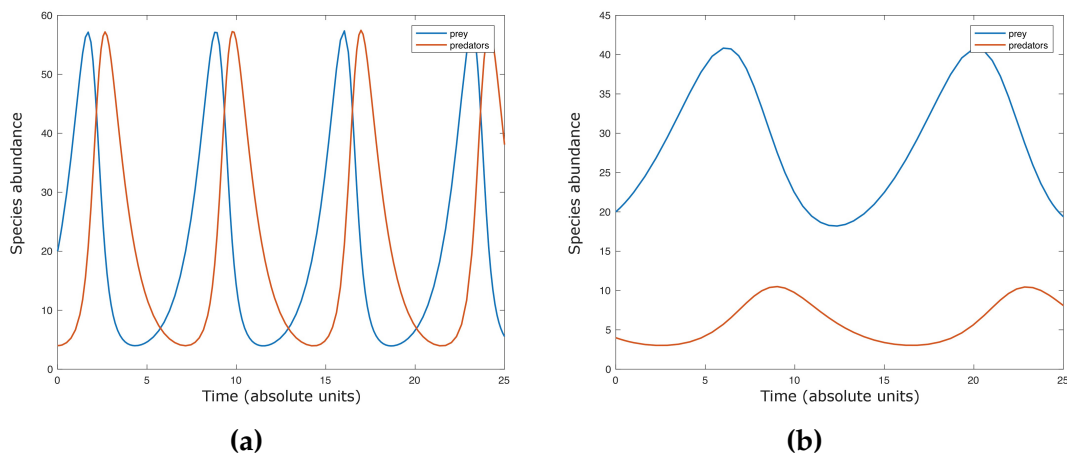
Figure A.1: *Two possible outcomes of the deterministic simulation of the Lotka-Volterra model with different sets of parameter estimates. Figure A.1a shows the dynamics with the parameters $\alpha = 1, a = 0.05, b = 1, \beta = 0.05$. Figure A.1b shows the dynamics with $\alpha = 0.3, a = 0.05, b = 0.7, \beta = 0.025$. Both the simulations start from the same initial state.*

Another common application of optimization in computational systems biology is biomarker identification, which is frequently related to the problem of classifying samples measured using the omics technologies (genomics, proteomics, lipidomics, metabolomics). These techniques produce a vast amount of data and researchers are challenged to infer knowledge from it [6]. In classification, certain characteristic sample properties, such as the expression level of some genes or proteins, are selected to separate the samples. Such selected properties, here generically called *features*, are then used to divide samples in categories. For example, respondent and non-respondent to a particular drug or healthy and unhealthy [138, 139]. Usually a sufficiently short list of features, called

biomarker, is sought to discriminate the samples. If this list of features is not optimally chosen, it may drive to poor classification accuracy.

Optimization problems can be formulated as follows:

$$\min c(\boldsymbol{\theta})$$
$$\mathbf{g}(\boldsymbol{\theta}) \leq 0$$
$$\mathbf{h}(\boldsymbol{\theta}) = 0 \qquad\qquad\qquad (A.2)$$
$$\mathbf{lb} \leq \boldsymbol{\theta} \leq \mathbf{ub}$$
$$\theta_j \in \mathbb{R} \text{ or } \mathbb{Z}, \; j = 1, ..., p$$

$\boldsymbol{\theta}$ is a vector of dimension $p \geq 1$ and it contains the parameter estimates that are sought. A solution of the optimization problem contains those parameter estimates that minimize the function c. We generically refer at them as *parameters*. The *cost function c*, also called *objective function*, translates the problem in mathematical equations and it undergoes the optimization process to estimate the optimal parameters. The objective function may also depend on other variables rather than $\boldsymbol{\theta}$, as initial values, forcing functions or other variables that are not optimized. For the sake of simplicity, such values are not explicitly included in Eq. (A.2). The objective function may depend linearly on $\boldsymbol{\theta}$, like in the case of routing or scheduling problems [140], or non-linearly, such as in many applications of computational systems biology [137].

Once these parameters are estimated, their values are fixed in the model. In contrast, the independent variables, here called just *variables*, remain free to vary after the optimization process. For example, in the Lotka-Volterra model (Eq. (A.1)) α, a, β, b are parameters, whereas y and z are variables. In addition, the problem may be subject to *constraints*, which can be bounds for the values that each θ_j can assume (**lb** and **ub** in (A.2)) or functional relations among the parameters (**g** and **h**). For instance, the parameters may represent biological rates or physical quantities that cannot be negative or that are admissible only inside a specific interval. In other cases, the value of certain parameters may depend on other parameters, as in the case when their sum should be smaller or equal to a certain threshold [15].

We refer to the space where the parameters $\boldsymbol{\theta}$ can vary, according to constraints, as the *space of parameters*. This set can include continuous or discrete parameters, or both, according to the problem and the constraints on $\boldsymbol{\theta}$. If we need to optimize certain rate constants of chemical reactions, parameter estimates are continuous values, whereas the number of genes to take into account to determine a biomarker is an integer (positive) value. During the identification of biomarkers, we may also need to consider a significance threshold associated to a specific statistical test. Therefore, some parameters of the problem may be continuous (significance threshold) whereas, at the same time, others may be integers (the length of the list).

In certain cases, optimization problems may be solved directly by studying the objective function. For example, if the problem depends on a limited number of parameters and variables, or the objective function is linear or convex (Fig. A.2a) [140, 141]. However, as soon as the number of variable increases

(a) *A convex objective function*

(b) *A non-convex objective function*
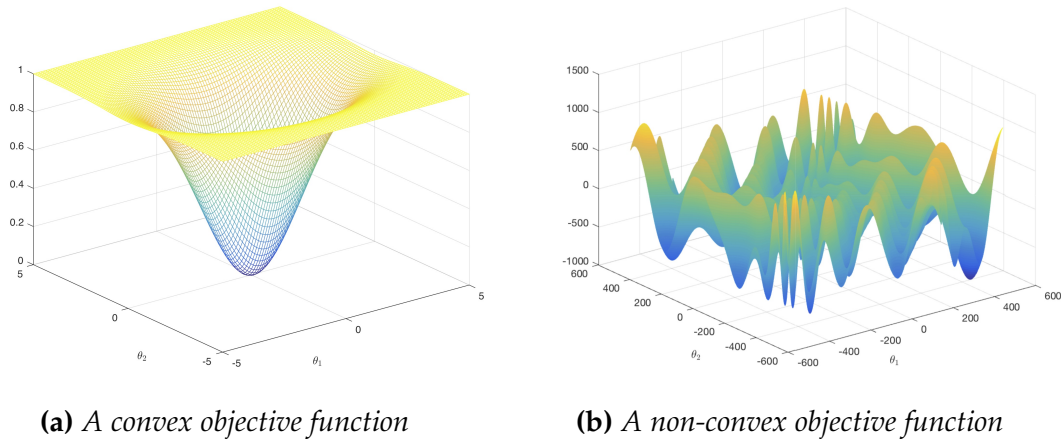
Figure A.2: *The plots for two possible objective functions depending on two parameters. Figure A.2a shows a convex function, whose minimum is easy to identify. On the contrary, Fig. A.2b shows the so-called* egg holder *function, which is non-convex and its minimum is hard to determine [4].*

or the function loses linearity or convexity (Fig. A.2b), the problem becomes intractable. Thus, the need for methods that permit the systematic research for optimal solutions arises.

In this article, we will focus on the case where the objective function is non-linear and non-convex and multiple solutions are possible. We have referred to the plural "methods" since there is no one-for-all method. As the No Free Lunch Theorem (NFL) states: *"for any algorithm, any elevated performance over one class of problems is offset by performance over another class."* [142].

In the following, we discuss the multi-start non-linear least squares method (ms-nlLSQ) based on a Gauss-Newton approach [129], mostly applied for fitting experimental data. We illustrate the random walk Markov Chain Monte Carlo method (rw-MCMC) [124], a stochastic technique used when a model involves stochastic equations or simulations. Finally, we present the simple Genetic Algorithm (sGA) [128]. It is a heuristic nature-inspired method belonging to the class of Evolutionary Algorithms, which is applied in a broad range of optimization applications, including model tuning and *biomarker identification*.

	ms-nlLSQ	rw-MCMC	sGA
Convergence	Proof to local*	Proof to global*	No proof
Support for continuous parameters	√	√	√
Support for continuous objective functions	√	√	√
Support for non-continuous objective functions	-	√	√
Support for discrete parameters	-	-	√

Table A.1: *Comparison of the described algorithms. Abbreviations: ms-nlLSQ multi-start non-linear least squares, rw-MCMC random walk Markov Chain Monte Carlo, sGA simple Genetic Algorithm. * convergence is assured under specific hypotheses.*

Table A.1 collects some important properties of the considered methods. Under specific hypotheses [124, 129], ms-nlLSQ and rw-MCMC are proved to converge

to local or global minimum, respectively. ms-nlLSQ is suitable only for problems where both model parameters and the objective function are continuous. On the other hand, rw-MCMC supports continuous and non-continuous objective functions, as well as sGA that also supports discrete parameters. All the considered optimization techniques require objective function evaluations at each iteration step, from just one evaluation in the case of rw-MCMC, to several as in the case of ms-nlLSQ and sGA.

A.3 Least Squares Methods

Model tuning is the estimation of model parameters to reproduce experimental time series. This problem is often formulated in the form of least squares. Among the others, in computational systems biology it has been considered for models related to diabetes [15, 57, 143], biological pathways [3, 27, 144, 145], and pharmacokinetics/pharmacodynamics [146, 147]. Least squares problems may arise in statistical regression as well [123, 148–152].

We denote the output of the model at a certain time instant t_i as $x^{\text{model}}(t_i, \boldsymbol{\theta})$, $i = 1, ..., n$. It may be the result, for instance, of integrating differential equations. When the experimental data at the same time point $x^{\text{experimental}}(t_i)$ is known, we can compute the *residual* function $\boldsymbol{r}$, which can be defined as a vector of components

$$r_i(\boldsymbol{\theta}) = x^{\text{model}}(t_i, \boldsymbol{\theta}) - x^{\text{experimental}}(t_i). \tag{A.3}$$

We refer to a *least squares problem* [153] when the objective function is obtained as the squared sum of these residuals for all the time points:

$$c(\boldsymbol{\theta}) = \sum_{i=1}^{n} r_i(\boldsymbol{\theta})^2. \tag{A.4}$$

In addition, c may include weights (w_i) that multiply the r_i

$$c_W(\boldsymbol{\theta}) = \sum_{i=1}^{n} w_i r_i(\boldsymbol{\theta})^2 \tag{A.5}$$

and in this case we have a *weighted least squares problem* [154]. This is often the case when experimental standard deviations are known and their reciprocal can be used as weights. For example, biological measures are often collected in triplicate. In such a case, experimental points can be computed by the mean of these measurements and by a dispersion index, such as the standard deviation. This helps in quantifying the confidence in the measures and the objective function will weight more the residual of those experimental points that have less uncertainty. The distance of a model output from the experimental data may always be quantified as a least squares problem. However, least squares methods mostly address problems involving continuous parameters and objective function [129]. In the following, we embrace these assumptions. The least squares methods exploit the properties of the particular objective function to obtain *ad-hoc* implementations. For example, the structure of its

derivatives permits to approximate the objective function without the computation of the second order derivatives [129]. Due to this and other attractive features, many applied unconstrained problems are formulated in the least squares terms. Besides their prominent role in unconstrained optimization, some implementations allow solving constrained problems.

According to the way in which the objective function depends on the parameters, least squares problems are divided in linear and non-linear. Linear least squares problems admit unique solution and fast solving algorithms [129], whereas non-linear least squares problems admit in general more solutions and the methods return local solutions. In order to circumvent these limitations and provide a global solution, the procedure is repeated starting from different set of parameter estimates, hereafter called *starting points*. The best solution among the results of the repeated procedure is then selected to ensure that the result is global. This procedure is known as *multi-start* approach. However, as the number of starting point increases, the overall procedure slows down. Thus, it is crucial to determine an adequate number of initial points N, such that the space of parameters is properly explored and the problem is still tractable. In addition, multiple runs of the procedure may lead to the same set of parameter estimates, weakening its efficiency.

Input: n experimental data points; the corresponding residual function r, whose components are defined as in (A.3); an objective function c as in (A.4); the number of starting points N; a *threshold* for the termination criterion.

Output: the vector θ providing the global minimum.

1 Randomly select N vectors of dimension p in the space of parameters $\{\theta^1, ..., \theta^N\}$ as starting points;

2 Compute the function $J(\theta) = \left[\frac{\partial r_i(\theta)}{\partial \theta_j} \right]_{i=1,...,n; j=1,...,p}$;

3 **foreach** θ^i, $i = 1, ..., N$ **do**

4   **repeat**

5   Evaluate $\tilde{J} = J(\theta^i)$;

6   Compute the search direction $\mathbf{q}$ such that $\tilde{J}^T \tilde{J} \mathbf{q} = -\tilde{J}^T r(\theta^i)$;

7   Compute $\vartheta = \theta^i + \mathbf{q}$;

8   Compute $\varepsilon = \left\| \frac{\theta^i - \vartheta}{\theta^i} \right\|$;

9   Update $\theta^i = \vartheta$;

10   **until** $\varepsilon > threshold$;

11   save in memory θ^i;

12 **end**

13 Determine the best solution $\bar{\theta}$ such that $c(\bar{\theta}) = \min_{i=1,...,N} c(\theta^i)$;

Algorithm 1: Multi-start non-linear least squares method based on the Gauss-Newton approach.

Algorithm 1 provides a multi-start implementation for solving unconstrained non-linear least squares problems by exploiting a simple Gauss-Newton approach [153]. The global search procedure begins defining N starting points for the method. These starting points can be selected randomly in the space of parameters (Alg.1, line 1), or using more elaborated procedures. For example, the Latin hypercube technique samples near-randomly the space of parameters trying to reduce the clustering of points that may happen in random selection. We refer to [155–157] for a complete description of Latin hypercube and other sampling techniques. Once the starting points are determined, for each of them the least squares procedure is computed (Alg.1, lines 2-13). Remarkably, each run of this approach is independent from the others, and the procedure naturally supports parallel implementation. This may allow a consistent speed-up.

The here-described Gauss-Newton approach for unconstrained non-linear least squares problems adopts a linearization of the objective function through a first order approximation (Alg.1, lines 2 and 5). At each iteration it proceeds identifying a new search direction by solving a linear least squares problem for the linearized objective function (Alg.1, line 6). This step requires a model simulation to compute the residuals $r(\theta^i)$ and an evaluation of $J(\theta^i)$. However, in modeling the analytical expression of J is often unknown, and at each step $J(\theta^i)$ needs to be approximated, requiring more model simulations [129]. Once the new search direction is determined, the parameters are updated along that direction (Alg.1, line 9) and these steps are repeated.

The optimization procedure runs until termination criteria are met. Among the many termination criteria [158], here we considered a common criterion that stops the procedure when the relative distance of the update is smaller than a certain threshold (Alg.1, line 10). Notably, the gradient of the objective function may provide termination criteria, which may be used to certify the local convergence to a stationary point. However, less computationally demanding procedures, as the one we considered, are usually preferred. When all the runs are terminated, the results are compared and the best one is selected, for instance considering the smallest value of c (Alg.1, line 13).

The Gauss-Newton method shows some drawbacks. In particular it does not support constraints on θ and requires some hypotheses to ensure the local convergence. As a consequence, more robust implementations have been proposed, including some that could manage linear or bound constraints [129, 153,159]. Some improvements have been obtained by determining the step length for the update using line search [129] or by adopting more accurate second order approximations of the objective function, such as in the Levenberg-Marquardt algorithm [130,160]. As a further extension, the trust region approach calculates the region of the space of parameters where the approximation is reliable [161,162]. Nevertheless, all these implementations are more computationally demanding, for example requiring more objective function evaluations and therefore more model simulations. In spite of these limitations, the Gauss-Newton method is very efficient when its convergence hypotheses are met [129]. Consequently, there is a trade-off between the expensive computations required

at each iteration and the small number of iterations guaranteed by the fast convergence.

A.4 Markov Chain Monte Carlo Methods

Markov chain Monte Carlo methods (MCMC) are a family of general purpose techniques that have been applied for a variety of statistical inferences [163]. Among their many applications, they have been used for parameter estimation in the context of Bayesian inference [164] and for maximizing likelihood, especially when stochastic processes and simulations are involved. Likelihood refers to a probability density function that in modeling is used to evaluate the goodness of how a model reproduces the data. Under the assumption that each experimental measurement is independently effected by Gaussian noise, the likelihood and the objective function in (A.5), are connected by the formula:

$$L(\boldsymbol{\theta}) = s_1 e^{-c_W(\boldsymbol{\theta})/2s_2},\tag{A.6}$$

where s_1 and s_2 are normalization factors.

Stochastic algorithms simulate each event in an asynchronous and separate way. This strategy allows an accurate investigation of the biological phenomena [6,165]. However, it can be slower than deterministic algorithms when several events have been generated per unit of time. This is often the case in the simulation of chemical reaction networks. In such cases, stochastic simulation of fast reactions may require more time than the deterministic approach [121,166]. On the other hand, when the model includes particularly low abundances of certain species, *e.g.*, few individuals, considering average behaviors may not accurately describe the phenomena, and hence deterministic simulation cannot be applied [6,167]. Consequently, stochastic simulation has been often applied, among the others, in the simulation of chemical reaction networks [120,168,169], population dynamics [170,171] and infectious diseases spreading [7,172–174]. Despite in both cases the parameter estimates are the same as in Fig. A.1a, Fig. A.3 shows how the outcome of stochastic simulations may vary substantially. For example, the results in Fig. A.3a are comparable with the deterministic simulation in Fig. A.1a, whereas Fig. A.3b shows a dramatically different scenario, with the extinction of the prey and the consequent extinction of the predators. Even though this kind of outcomes are both biologically plausible, deterministic simulations cannot predict the latter.

MCMC methods implement Markov chains, *i.e.*, stochastic processes that determine the next step using only the information provided by the current step, and a modified Monte Carlo step to determine the acceptance or rejection of each set of parameters [124]. The convergence of these methods is guaranteed, under specific hypotheses that are often met in modeling problems, by the central limit theorem and its extensions [175]. Therefore, MCMC methods converge asymptotically to stationary distributions of the Markov chains. However, this result does not provide the order of convergence or termination criteria, and in general the convergence is slow since it is not guaranteed that the optimization
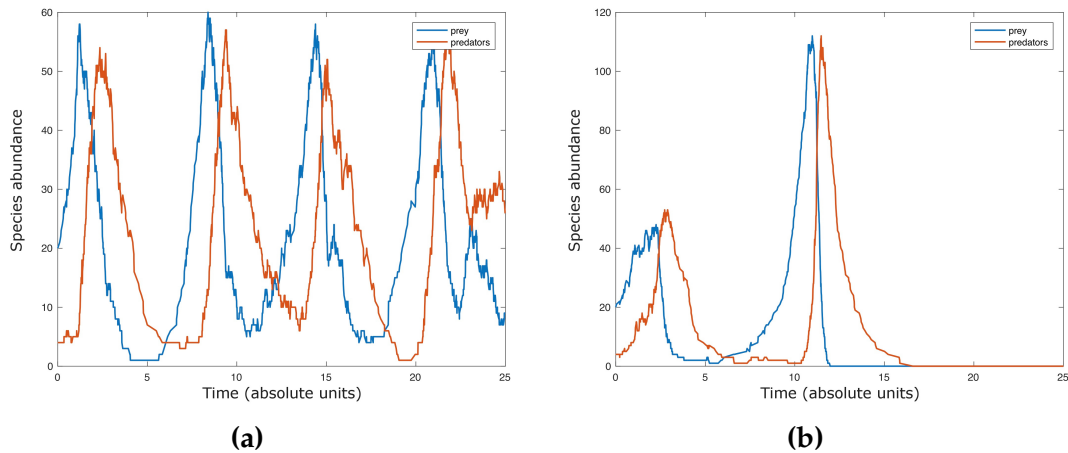
Figure A.3: *Two possible outcomes of the stochastic simulation of the Lotka-Volterra model with the same set of parameter estimates as in Fig. A.1a ($\alpha = 1$, $a = 0.05$, $b = 1$, $\beta = 0.05$). The behavior in Figure A.3a is comparable with the one in Fig. A.1a. The behavior in Figure A.3b shows a dramatically different scenario, with the extinction of the prey and the consequent extinction of the predators.*

process escapes quickly from local solutions. Consequently, the methods are stopped when the stationary distributions seem to be reached by using the so-called *diagnostics* [176] or after a fixed number of iterations. Thanks to the Markov chain properties, if the results are not satisfying the methods can be restarted from the last set of parameters without loss of information. Another consequence of the asymptotic convergence is that the first part of the results should be discarded to avoid starting bias [177]. These first iterations are called *burn-in* or *warm-up*.

We present an implementation of the random walk MCMC method (rw-MCMC) in Algorithm 2. This implementation, as many others, relies on the results of Metropolis et al. [178] and Hastings [179]. Therefore, it is also called the random walk Metropolis-Hastings algorithm. This optimization strategy begins defining a random set of parameters and evaluating its likelihood (Alg. 2, lines 2-3). From this first set of parameters, the covariance matrix is computed (Alg. 2, line 4) and it is used to generate the new candidates. The method can take advantage of some *a priori* knowledge for determining the first set of parameters or the covariance matrix. In fact, certain literature values or distributions for some of the parameters may be known, and these can be used to guide the procedure. Moreover, in some implementations, the covariance matrix may be updated step-wise, gathering information along the procedure [180].

The algorithm continues generating a new set of parameters by perturbing the previous one through random normally distributed coefficients (Alg. 2, line 7). This is why the procedure is called random walk MCMC method. In other cases, such as the independent Metropolis-Hastings algorithm, the new set of parameters is proposed independently from the previous [181]. We refer to [124] for a detailed description of these and other methods.

Input: a likelihood function L that measures the goodness of the fit, for example (A.6); a maximum number of runs N; the number of first iterations to discard *warm-up*.

Output: the *a posteriori* distributions for the parameters stored as a matrix D_θ; the vector of the associated likelihood values V_L.

1   Initialize D_θ, $V_L = \varnothing$;
2   Randomly determine a candidate set of parameters θ_1;
3   Compute $L_1 = L(\theta_1)$;
4   Compute the covariance matrix C from the estimates θ_1;
5   **for** $i = 1, ..., N$ **do**
6   Generate a vector z of random numbers in $N(0, C)$ of the same size of θ_1;
7   Compute $\theta_2 = \theta_1 + z$;
8   Compute $L_2 = L(\theta_2)$;
9   Compute $ratio = L_2/L_1$;
10   Generate a random number $rand \sim U(0,1)$;
11   **if** $rand < ratio$ **then**
12   Update $L_1 = L_2$;
13   Update $\theta_1 = \theta_2$;
14   **end**
15   **if** $i > warm\text{-}up$ **then**
16   append θ_1 to D_θ;
17   append L_1 to V_L;
18   **end**
19 **end**

Algorithm 2: Random walk Markov chain Monte Carlo method for parameter estimation.

When the new set of parameters is generated, its likelihood is computed (Alg. 2, line 8) and compared with the previous. If the new likelihood is bigger then the previous ($L_2/L_1 > 1$), the new set of parameters is always accepted, otherwise with probability L_2/L_1 (Alg. 2, lines 10-13). In order to escape local minima, the latter rule allows the method to randomly accept values that are not better in terms of likelihood. In the long run, the method will return back to the previous value if it was the global solution, otherwise it continues the exploration of the space of parameters. This strategy is in contrast with least squares methods. In those methods, the direction that decreases the objective function is always chosen and, consequently, their results are in general local [131, 182]. Thus, the need to apply a multi-start approach to search for the global solution.

Finally, if the warm-up time is over, the parameters and the likelihood function are stored (Alg. 2, lines 15-18). This set of parameters is needed to build the *a posteriori* distributions of parameter estimates, whereas the likelihood values allow determining the best set in terms of likelihood, if needed. Once these probabilities are estimated, it is possible to infer valuable information from them, such as, the standard deviations and uncertainty measures of the estimates or the correlations between them. Moreover, collecting the output of the model

along with the parameters provides information about the uncertainty of model results.

As mentioned, MCMC methods can be provided with *a priori* knowledge on the parameters, such as bounds, experimental standard deviations or distributions for the parameters. When these values are known, the methods can take advantage of them to determine the candidate sets of parameters. In many cases, this information is processed using Bayesian inference [172]. For particularly complex models, exploiting this information may significantly improve the speed of convergence of the algorithm. For the same end, adaptive implementations have been proposed [180]. These implementations generally use statistics from the results, for example the rate at which new candidates are accepted, to properly update the way in which new candidates are proposed [183]. In addition, *ad hoc* implementations for complex problems have been proposed. In these implementations, multiple independent runs of the algorithm are generated, each of them working on an independent subset of the model or starting from different initial points. The results of these runs are then combined at the end [184,185]. Despite the use of MCMC methods to infer discrete parameter distributions has been for long time overlooked, some implementations have recently extended their realm to address the problem of inferring discrete and mixed-integer parameters [180,186].

An optimization method based on Markov chains has drawbacks and advantages. On the one hand, it allows memory-efficient implementations and this is particularly convenient when very complex models are involved. In fact, the algorithm requires only the information about the previous iteration (Alg. 2, lines 7 and 9), whereas the overall results can be stored at specific sampling rates. On the other hand, the method iterations cannot be computed in parallel, since they depend on the previous. MCMC methods for parameter estimation are usually efficient in the number of objective function evaluations, computing just one evaluation per iteration. However, the lack of termination criteria forces the use of several iterations to ensure the convergence. Nevertheless, they balance this computational cost by returning the *a posteriori* distributions of the parameter estimates, and therefore more information than other methods.

A.5   Genetic Algorithms

Genetic algorithms (GAs), firstly introduced by Holland in 1975 [187] and then improved and varied during the following decades [188–190], are nature inspired heuristic stochastic algorithms. As in nature our genes are encoded in chromosomes as strings of nucleotides, these algorithms encode the space of parameters as strings and they create populations of candidate solutions that evolve according to the principle of survival of the fittest. In analogy with biology, the objective function of GAs is called *fitness function*, and the principle of survival of the fittest selects those candidates that are better in terms of objective function. GAs mimic the processes of natural selection (Fig. A.4a), the genetic exchange between two individuals (Fig. A.4b), known as *crossover* or *recombination*, and the random *mutation* that take place during the process

(Fig. A.4c). One of the key ideas underlying these stochastic algorithms is that the evolution preserves, even under stochastic choices, those strings (or part of them) that guide the process toward the best solution. This concept is formalized in the *building block hypothesis* and it is detailed in [188].

(a)   **(b)**   **(c)**
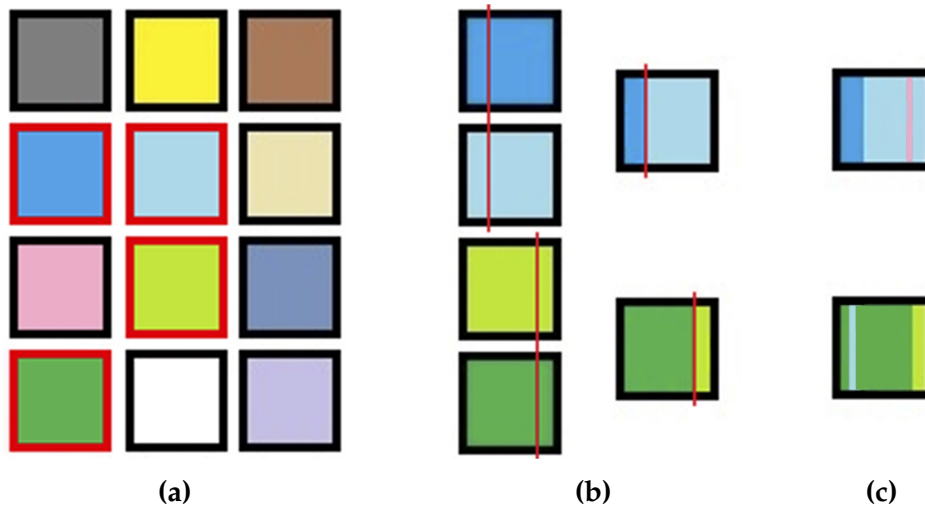
Figure A.4: *A schematic representation of a genetic algorithm. Figure A.4a shows the selection of four parents in a population of twelve individuals, highlighted in red. Figure A.4b shows the crossover for the selected individuals. The crossover points are randomly selected (red lines) for the couple of selected individuals (left) and the recombination of their genetic material produces the new offspring (right). Figure A.4c shows the effect of mutation on the offspring. The mutation randomly changes part of their genetic material.*

GAs have been employed in a variety of fields and for various applications. For example, they have been applied in synthetic and systems biology to determine biomarkers [138, 139], design gene regulatory networks [191], and to estimate parameters [192]. GAs have empirically demonstrated their efficacy and reliability. In addition, some first steps in formally proving their convergence have been done [193, 194]. However, these algorithms lack formal proof for their convergence for the most general case [189]. As a consequence, the convergence of the algorithms is evaluated *a posteriori*, for instance introducing a maximum number of allowed iterations or accounting the changes in the fitness of the population. Nevertheless, in the proximity of the solution, the rate at which the evolution takes place and the fitness increases may slow down, and the maximum number of generations may be encountered before reaching the global solution. In some cases, to get around this limitation and since GAs are very effective in determining the region of the space of parameters where the global solution is located, they have been coupled with other methods. In this way, it is possible to precisely locate the global solution once a GA has selected the proper region of the space of parameters or it has provided promising candidate solutions [195].

We present a basic implementation of a GA, called simple GA algorithm (sGA), as described in [188]. This algorithm effectively describes the three fundamental

steps of selection, recombination and mutation. It is implemented in Algorithm 3. The algorithm begins mapping the vectors of parameters into strings. In this way, the parameters and the strings are in one-to-one correspondence and the algorithm can work with the more convenient representation. A detailed description of these transformations is provided in [188]. An initial population of candidate solutions is then generated. As for the starting points of the multi-start approach, these candidate solutions may be randomly chosen in the space of parameters, or more elaborated sampling techniques may be applied [155–157]. Once the initial population has been produced, the algorithm enters its main loop. Each iteration of the sGA, also referred as *generation*, produces a new population of strings. Among the many possible termination criteria [196], here we considered the maximum number of generations (Alg. 3, line 3).

Input: a fitness function c that measures the goodness of the fit, for example (A.5); the population size N; the rate of mutation σ; the maximum number of generations G.

Output: the best candidate solution $\bar{p}$ after G generations.

1   Map the parameters into strings of length l;

2   Generate an initial population of strings $P = \{p_1, ..., p_N\}$;

3   **for** G *times* **do**

4     $P' = \varnothing$;

5   Compute $f_i = c(p_i), i = 1, ..., N$ and $f_0 = \sum\limits_{i=1}^{N} f_i$;

6   **for** N *times* **do**

7   Generate a random number $j \sim U(0, 1)$;

8   Determine the smallest integer k such that $\sum\limits_{i=1}^{k} f_i > j f_0$;

9   Update $P' = p_k \cup P'$;

10   **end**

11     $P = \varnothing$;

12   **for** N *times* **do**

13   Generate two integer random numbers $m, n \sim U(1, N)$;

14   Select $p_m, p_n \in P'$;

15   Generate an integer random number $t \sim U(1, l)$;

16       $\tilde{p} = \{p_m\{1 : t\}, p_n\{t + 1 : l\}\}$;

17   **for** $i = 1, ..., l$ **do**

18   with probability σ randomly variate $\tilde{p}\{i\}$;

19   **end**

20   Update $P = \tilde{p} \cup P$;

21   **end**

22   **end**

23   Determine the best solution $\bar{p}$ such that $c(\bar{p}) = \min\limits_{p \in P} c(p)$;

Algorithm 3: A simple Genetic Algorithm.

At each iteration, the selection occurs as a weighted random choice among the candidate solutions . Those individuals with higher fitness are more likely to be selected (Alg. 3, lines 7-8). At this stage, these selected individuals are cloned in a new pool of candidates, called *intermediate population* (Alg. 3, line 9). The size of the intermediate population, here assumed for simplicity to be equal to the population size N, may vary. The selection of the candidates may occur in many ways [197]. The here-implemented *roulette* selection [188] divides an interval proportionally to the fitness value of each candidate solution (Alg. 3, line 5), and then individuals are randomly selected in this interval (Alg. 3, lines 7-9). Other popular strategies for the selection of candidate solutions are the *genitor* algorithm [198] and the *tournament* selection [199]. The first, generates each newborn as in the roulette selection. However, it does not use an intermediate population and the newborn replaces the worst string in terms of fitness in the original population. On the other hand, the *tournament* selection randomly picks two or more individuals and only the best in terms of fitness is cloned in the intermediate population.

Once the intermediate population has been determined, its individuals are mated and their genetic material is recombined to determine the next generation of solution candidates. For instance, in the here-described *single point crossover* (Fig. A.4b) , two parents are randomly selected (Alg. 3, lines 13-14) and at a random position in the string, their genetic material is recombined (Alg. 3, lines 15-16). As for the selection, the recombination of candidate solutions may be computed in several ways. Some implementations consider more than two parents at time or more points for the crossover, whereas others produce more than one child from the selected parents [128]. In contrast, some implementations determine part of the intermediate population by cloning the best candidates in terms of fitness in the new population without recombination at all [200].

After the recombination, the *mutation* takes place (Fig. A.4c). With a certain probability σ, usually smaller than 0.01, each element of the string may be randomly replaced (Alg. 3, line 18) [197] and this new string joins the new population (Alg. 3, line 20). Once the termination conditions are met, the algorithm determines the best solution in the latest population and returns the corresponding vector of parameters (Alg. 3, line 23). As for MCMC methods, if the results are not satisfying and the latest population has been saved, the algorithm may be restarted from there in the seek of a better solution.

GAs are powerful approaches to explore high-dimensional spaces of parameters. However, the choice of the population size is crucial: with small populations the algorithms are fast, but they may prematurely converge to local solutions. Larger populations permit the algorithms to better explore the spaces of parameters, but more fitness function evaluations are required. The bigger is the population size, the slower becomes the procedure. In the seek of a balance between the population size and the exploration effectiveness, different implementations of the GAs have been proposed to circumvent the slow down due to large populations. Several of them parallelize the algorithm, or part of it, to speedup

the procedure. For example, the *master slave parallelization* performs the steps of fitness function evaluation, recombination and mutation in parallel, calculating these operations in different cpu cores for different parts of the population [201]. On the other hand, the *island model* considers many small sub-populations that evolve independently, *i.e., islands,* and only after a certain number of generations some of their individuals can migrate in other islands [202]. Analogously, the *cellular* genetic algorithm arranges the candidate strings in a grid of cells and they can mate only with their neighbors [197]. The island and cellular approaches refine many local solutions that are then compared through the migration, which guides the procedure towards the global solution. Moreover, they are suitable for parallel implementation as well, assigning each island or cell to a different cpu core.

GAs are a specific family of algorithms belonging to the class of Evolution Strategy (ES) [203]. This class of optimization techniques shares with the GAs the fundamental steps of selection, recombination, and mutation. In addition, ESs may include steps of self-adaptation, which tune parameters such as the mutation rate [204, 205]. Analogously, ESs may implement more sophisticated selection strategies that increase the selection pressure [203]. For example, the so called *plus strategy* that may lead to better performance [206]. Certain implementation of GAs take advantages of those improvements as well.

Despite the lack of termination criteria or proven convergence for the most general case, genetic algorithms are considered valuable tools to explore the space of parameters thanks to their flexibility [131]. The continuous exchange of genetic material among individuals permits the algorithm to move in the space of parameters evolving towards the best solution, even if there are many local solutions. Moreover, mutation adds variability to the population. This allows the exploration of new areas of the space of parameters that would otherwise remain unexplored [188]. Finally, GAs can be applied to a broad range of problems, from unconstrained to constrained optimization. They allow solving problems involving both continuous and discrete variables, as well as problems with continuous or non-continuous objective functions.

A.6   Conclusions

We presented three powerful methods for global optimization suitable for computational systems biology applications. We highlighted pros and cons of the examined approaches and we provided references for their improvements that may better suit specific tasks.

We presented the multi-start approach for a non-linear least squares method [129], that is suitable for parameter estimation when deterministic simulations are involved, as well as for statistical regression. The least squares methods have many attractive properties like the assured local convergence under specific hypotheses or the valuable termination criteria that assess the convergence of the method. The multi-start approach repeats the least squares procedure from different starting points to explore the space of parameters in the seek of the global solution. However, these methods cannot be applied in case of

non-continuous objective functions or discrete parameters. We also illustrated the random walk Markov chain Monte Carlo method [124] that may be applied for many statistical inferences, including parameter estimation, and it is suitable for the framework of Bayesian inference. Moreover, its asymptotic convergence to the global solution is assured under mild hypotheses and it may be applied in case of non-continuous objective functions, as well as when stochastic simulations are involved. In spite of this, the asymptotic convergence does not provide any termination criteria, and hence the convergence cannot be certified. Finally, we have illustrated a simple Genetic Algorithm [189], a heuristic nature-inspired method that can be applied to a broad range of problems. It is suitable for problems involving continuous and non-continuous objective functions, as well as continuous and discrete parameters. On the other hand, there are no guarantees on its convergence, so it requires cautious result evaluation.

We focused on the general ideas behind each method, without blurring the description with many details. For this reason, we included simple implementations that, in our opinion, could better guide in understanding the algorithms and the approaches. Therefore, our description does not present all the latest improvements and extensions of the considered optimization techniques. These include more accurate versions of least squares procedures [129] and genetic algorithms [190] implementations of MCMC methods that support discrete variables [186] and hybrid methods that merge MCMC and genetic algorithms [207]. These and many other improvements have enlarged the domain of application of these methods and have ameliorated their accuracy and convergence, leading, on the other hand, to more complex procedures.

The presented approaches coexist with a vast literature of exact and heuristics methods. Just to cite some among the countless, there exists the simplex [140] and the gradient [129] methods, evolutionary strategies [203], the branch and bound [208], the particle swarm [209] or the simulated annealing [210]. For the sake of simplicity and shortness, we have not covered the entire spectrum of existing deterministic and stochastic methods. We acknowledge that other reviews have already pointed out the importance of global optimization in computational systems biology [125, 131, 137, 211–213]. However, for most of them, the authors efforts were focused on one particular methodology. On the contrary, this review aims at providing a guide to solve common problems in the field, without focusing on one specific approach.

Author contributions

Under the supervision and the guidance of Luca Marchetti and Corrado Priami, I wrote the manuscript. All the authors edited and reviewed the manuscript.

Declaration

I, Federico Reali, hereby declare that this PhD. thesis was carried out by me for the degree of Doctor of Philosophy in Mathematics under the guidance and supervision of Prof. Corrado Priami and Doctor Ozan Kahramanoğulları, Department of Mathematics, University of Trento, Italy.

I certify that this thesis has not been accepted for the award of any other degree or diploma in my name, in any university or other tertiary institution and, to the best of my knowledge and belief, contains no material previously published or written by another person, except where due reference has been made in the text. In addition, I certify that no part of this work will, in the future, be used in a submission in my name, for any other degree or diploma in any university or other tertiary institution without the prior approval of the University of Trento and where applicable, any partner institution responsible for the joint-award of this degree.

This work is the intellectual property of the author. You may copy up to 5% of this work for private study, or personal, non-commercial research. Any re-use of the information contained within this document should be fully referenced, quoting the author, title, university, degree level and pagination. Queries or requests for any other use, or if a more substantial copy is required, should be directed in the owner(s) of the Intellectual Property Rights.

I give consent to this copy of my thesis, when deposited in the University Library, being made available for loan and photocopying, subject to the provisions of the Copyright Act 1968. I also give permission for the digital version of my thesis to be made available on the web, via the University's digital research repository, the Library Search and also through web search engines, unless permission has been granted by the University to restrict access for a period of time.

Bibliography

[1] Gostner, R., Baldacci, B., Morine, M. J. & Priami, C. Graphical modeling tools for systems biology. *Acm Computing Surveys* **47**, 16 (2015).

[2] Dalla Man, C. *et al.* Measurement of selective effect of insulin on glucose disposal from labeled glucose oral test minimal model. *Am J Physiol Endocrinol Metab* **289**, E909–14 (2005). URL `http://www.ncbi.nlm.nih.gov/pubmed/15972269%7D`.

[3] Gupta, S., Maurya, M. R., Merrill, A. H., Glass, C. K. & Subramaniam, S. Integration of lipidomics and transcriptomics data towards a systems biology model of sphingolipid metabolism. *BMC systems biology* **5**, 26 (2011).

[4] Jamil, M. & Yang, X.-S. A Literature Survey of Benchmark Functions For Global Optimization Problems Citation details: Momin Jamil and Xin-She Yang, A literature survey of benchmark functions for global optimization problems. *Int. Journal of Mathematical Modelling and Numerical Optimisation* **4**, 150–194 (2013). URL `http://www.inderscience.com/link.php?id=55204`. `arXiv:1308.4008v1`.

[5] Priami, C. Algorithmic systems biology. *Communications of the ACM* **52**, 80 (2009).

[6] Priami, C. & Morine, M. J. *Analysis of Biological Systems* (Imperial College Press, 2015).

[7] Diekmann, O., Heesterbeek, H. & Britton, T. *Mathematical Tools for Understanding Infectious Disease Dynamics* (Princeton University Press, 2013).

[8] Formaggia, L., Quarteroni, A. & Veneziani, A. *Cardiovascular Mathematics: Modeling and simulation of the circulatory system* (2009).

[9] Lecca, P. & Priami, C. Biological network inference for drug discovery. *Drug Discovery Today* **18**, 256–264 (2013). URL `http://dx.doi.org/10.1016/j.drudis.2012.11.001`.

[10] Cobelli, C., Pacini, G., Toffolo, G. & Sacca, L. Estimation of insulin sensitivity and glucose clearance from minimal model: new insights from labeled ivgtt. *Am J Physiol* **250**, E591–8 (1986). URL `http://www.ncbi.nlm.nih.gov/pubmed/3518490%7D`.

[11] Bergman, R. N., Ider, Y. Z., Bowden, C. R. & Cobelli, C. Quantitative estimation of insulin sensitivity. *Am J Physiol* **236**, E667–77 (1979). URL `http://www.ncbi.nlm.nih.gov/pubmed/443421%7D`.

[12] Basu, R. *et al.* Use of a novel triple-tracer approach to assess postprandial glucose metabolism. *Am J Physiol Endocrinol Metab* **284**, E55–69 (2003). URL `http://www.ncbi.nlm.nih.gov/pubmed/12485809%7D`.

[13] Steil, G. M. *et al.* Evaluation of insulin sensitivity and beta-cell function indexes obtained from minimal model analysis of a meal tolerance test. *Diabetes* **53**, 1201–7 (2004). URL `http://www.ncbi.nlm.nih.gov/pubmed/15111487%7D`.

[14] Drouin, P. *et al.* Diagnosis and classification of diabetes mellitus. *Diabetes Care* **32**, S62–S67 (2009). `0208024`.

[15] Marchetti, L. *et al.* A Novel Insulin/Glucose Model after a Mixed-Meal Test in Patients with Type 1 Diabetes on Insulin Pump Therapy. *Scientific Reports* **6**, 36029 (2016). URL `http://www.nature.com/articles/srep36029`.

[16] Wilkins, L. *Diabetes Mellitus: A Guide to Patient Care* (Lippincott Williams & Wilkins, 2007).

[17] Holland, W. L. & Summers, S. A. Sphingolipids, Insulin Resistance, and Metabolic Disease: New Insights from in Vivo Manipulation of Sphingolipid Metabolism. *Endocr Rev* **29**, 381–402 (2008). URL `http://edrv.endojournals.org/cgi/content/abstract/29/4/381`.

[18] Merrill, A. H. Sphingolipid and glycosphingolipid metabolic pathways in the era of sphingolipidomics. *Chemical Reviews* **111**, 6387–6422 (2011).

[19] Natali, A., Prato, S. D. & Mari, A. *Normal β-cell function*, vol. 1, book section 8, 108–124 (John Wiley & Sons, Ltd, Chichester, UK, 2015), fourth edn.

[20] Ferrannini, E. & DeFronzo, R. A. *Insulin actions in vivo: glucose metabolism*, vol. 1, book section 14, 211–233 (John Wiley & Sons, Ltd, Chichester, UK, 2015), fourth edn.

[21] Greenbaum, C. J. *et al.* Mixed-meal tolerance test versus glucagon stimulation test for the assessment of beta-cell function in therapeutic trials in type 1 diabetes. *Diabetes Care* **31**, 1966–71 (2008). URL `http://www.ncbi.nlm.nih.gov/pubmed/18628574%7D`.

[22] Cobelli, C., Man, C. D., Pedersen, M. G., Bertoldo, A. & Toffolo, G. Advancing our understanding of the glucose system via modeling: a perspective. *IEEE Trans Biomed Eng* **61**, 1577–92 (2014). URL `http://www.ncbi.nlm.nih.gov/pubmed/24759285%7D`.

[23] Mackenzie, R. & Elliott, B. Akt/PKB activation and insulin signaling: a novel insulin signaling pathway in the treatment of type 2 diabetes. *Diabetes, Metabolic Syndrome and Obesity: Targets and Therapy* 55 (2014). URL `http://www.dovepress.com/aktpkb-activation-and-insulin-signaling-a-novel-insulin-signaling-path-peer-re`

[24] Fayyaz, S., Japtok, L. & Kleuser, B. Divergent role of sphingosine 1-phosphate on insulin resistance. *Cellular Physiology and Biochemistry* **34**, 134–147 (2014).

[25] Yamashita, T. *et al.* ChipperDB: Diabetes Genome Anatomy Project\rEnhanced insulin sensitivity in mice lacking ganglioside GM3. *Pnas* **100**, 3445–3449 (2003). URL `http://www.diabetesgenome.org/chipperdb/expt.cgi?id=65`.

[26] Mayer, J. P., Zhang, F. & DiMarchi, R. D. Insulin structure and function. *Biopolymers* **88**, 687–713 (2007). URL `http://doi.wiley.com/10.1002/bip.20734`. NIHMS150003.

[27] Reali, F. *et al.* Mechanistic interplay between ceramide and insulin resistance. *Scientific Reports* **7**, 41231 (2017). URL `http://www.nature.com/articles/srep41231`.

[28] Pacini, G. & Mari, A. OGTT e IVGTT: Due test a confronto per la valutazione dell'insulino- sensibilità e della funzione beta cellulare. *Giornale Italiano di Diabetologia e Metabolismo* **27**, 220–226 (2007).

[29] Dalla Man, C., Caumo, A. & Cobelli, C. The oral glucose minimal model: estimation of insulin sensitivity from a meal test. *IEEE Trans Biomed Eng* **49**, 419–29 (2002). URL `http://www.ncbi.nlm.nih.gov/pubmed/12002173%7D`.

[30] Breda, E., Cavaghan, M. K., Toffolo, G., Polonsky, K. S. & Cobelli, C. Oral glucose tolerance test minimal model indexes of beta-cell function and insulin sensitivity. *Diabetes* **50**, 150–8 (2001). URL `http://www.ncbi.nlm.nih.gov/pubmed/11147781%7D`.

[31] Dalla Man, C. *et al.* Two-hour seven-sample oral glucose tolerance test and meal protocol: minimal model assessment of beta-cell responsivity and insulin sensitivity in nondiabetic individuals. *Diabetes* **54**, 3265–73 (2005). URL `http://www.ncbi.nlm.nih.gov/pubmed/16249454%7D`.

[32] The DECODE Study Group. Glucose tolerance and cardiovascular mortality: comparison of fasting and 2-hour diagnostic criteria. *Archives of internal medicine* **161**, 397–405 (2001). URL `http://www.ncbi.nlm.nih.gov/pubmed/11176766`.

[33] Morishima, T., Bradshaw, C. & Radziuk, J. Measurement using tracers of steady-state turnover and metabolic clearance of insulin in dogs. *Am J*

Physiol **248**, E203–8 (1985). URL `http://www.ncbi.nlm.nih.gov/pubmed/3881988%7D`.

[34] Caumo, A. & Cobelli, C. Hepatic glucose production during the labeled IVGTT: estimation by deconvolution with a new minimal model. *American Journal of Physiology - Endocrinology and Metabolism* **264**, E829–E841 (1993). URL `http://ajpendo.physiology.org/content/264/5/E829`.

[35] Li, J., Kuang, Y. & Li, B. Analysis of IVGTT glucose-insulin interaction models with time delay. *Discrete Contin. Dyn. Syst. Ser* **1**, 103–124 (2001).

[36] Arino, O., Gaetano, A. & Mukhopadhyay, A. Modeling the intra-venous glucose tolerance test: A global study for a single-distributed-delay model. *Discrete and Continuous Dynamical Systems - Series B* **4**, 407–417 (2004). URL `http://www.aimsciences.org/journals/displayArticles.jsp?paperID=412`.

[37] Pacini, G. & Bergman, R. N. MINMOD: A computer program to calculate insulin sensitivity and pancreatic responsivity from the frequently sampled intravenous glucose tolerance test. *Comput. Methods Programs Biomedicine* **23**, 113–122 (1986).

[38] Sturis, J., Polonsky, K. S., Mosekilde, E. & Cauter, E. V. Computer-model for mechanisms underlying ultradian oscillations of insulin and glucose. *Amer. J. Physiol. Endocrinol. Metab* **260**, E801–E809 (1991).

[39] Panunzi, S., Palumbo, P. & De Gaetano, A. A discrete Single Delay Model for the Intra-Venous Glucose Tolerance Test. *Theoretical Biology and Medical Modelling* **4**, 35 (2007). URL `http://tbiomed.biomedcentral.com/articles/10.1186/1742-4682-4-35`.

[40] De Gaetano, A. & Arino, O. Mathematical modelling of the intravenous glucose tolerance test. *J Math Biol* **40**, 136–68 (2000). URL `http://www.ncbi.nlm.nih.gov/pubmed/10743599%7D`.

[41] DeFronzo, R. A., Tobin, J. D. & Andres, R. Glucose clamp technique: a method for quantifying insulin secretion and resistance. *Am J Physiol* **237**, E214–23 (1979). URL `http://www.ncbi.nlm.nih.gov/pubmed/382871%7D`.

[42] Insel, P. A. *et al.* Insulin control of glucose metabolism in man: a new kinetic analysis. *J Clin Invest* **55**, 1057–66 (1975). URL `http://www.ncbi.nlm.nih.gov/pubmed/15959962%7D`.

[43] Toffolo, G., De Grandi, F. & Cobelli, C. Estimation of beta-cell sensitivity from intravenous glucose tolerance test c-peptide data. knowledge of the kinetics avoids errors in modeling the secretion. *Diabetes* **44**, 845–54 (1995). URL `http://www.ncbi.nlm.nih.gov/pubmed/7789653%7D`.

[44] Cobelli, C. *et al.* Assessment of beta-cell function in humans, simultaneously with insulin sensitivity and hepatic extraction, from intravenous and oral glucose tests. *Am J Physiol Endocrinol Metab* **293**, E1–E15 (2007).

[45] Trombetta, M. *et al.* Type 2 diabetes mellitus: a disease of the governance of the glucose-insulin system: an experimental metabolic control analysis study. *Nutr Metab Cardiovasc Dis* **23**, 23–30 (2013). URL `http://www.ncbi.nlm.nih.gov/pubmed/21937205%7D`.

[46] Cobelli, C. *et al.* The oral minimal model method. *Diabetes* **63**, 1203–13 (2014). URL `http://www.ncbi.nlm.nih.gov/pubmed/24651807%7D`.

[47] Mari, A. *et al.* Meal and oral glucose tests for assessment of beta-cell function: modeling analysis in normal subjects. *Am J Physiol Endocrinol Metab* **283**, E1159–66 (2002). URL `http://www.ncbi.nlm.nih.gov/pubmed/12388151%7D`.

[48] Ferrannini, E. *et al.* Effect of insulin on the distribution and disposition of glucose in man. *J Clin Invest* **76**, 357–364 (1985).

[49] Radziuk, J., McDonald, T., Rubenstein, D. & Dupre, J. Initial splanchnic extraction of ingested glucose in normal man. *Metabolism* **27**, 657–669 (1978). URL `http://linkinghub.elsevier.com/retrieve/pii/0026049578900033`.

[50] Caumo, A., Bergman, R. N. & Cobelli, C. Insulin sensitivity from meal tolerance tests in normal subjects: a minimal model index. *J Clin Endocrinol Metab* **85**, 4396–402 (2000). URL `http://www.ncbi.nlm.nih.gov/pubmed/11095485%7D`.

[51] Salinari, S., Bertuzzi, A. & Mingrone, G. Intestinal transit of a glucose bolus and incretin kinetics: a mathematical model with application to the oral glucose tolerance test. *Am J Physiol Endocrinol Metab* **300**, E955–65 (2011). URL `http://www.ncbi.nlm.nih.gov/pubmed/21364121%7D`.

[52] De Gaetano, A. *et al.* Routine ogtt: a robust model including incretin effect for precise identification of insulin sensitivity and secretion in a single individual. *PLoS One* **8**, e70875 (2013). URL `http://www.ncbi.nlm.nih.gov/pubmed/24009656%7D`.

[53] Mallad, A. *et al.* Exercise effects on postprandial glucose metabolism in type 1 diabetes: a triple-tracer approach. *Am J Physiol Endocrinol Metab* **308**, E1106–15 (2015). URL `http://www.ncbi.nlm.nih.gov/pubmed/25898950%7D`.

[54] Bergman, R. N., Phillips, L. S. & Cobelli, C. Physiologic evaluation of factors controlling glucose tolerance in man: measurement of insulin sensitivity and beta-cell glucose sensitivity from the response to intravenous glucose. *J Clin Invest* **68**, 1456–67 (1981). URL `http://www.ncbi.nlm.nih.gov/pubmed/7033284%7D`.

[55] Dalla Man, C., Raimondo, D. M., Rizza, R. A. & Cobelli, C. Gim, simulation software of meal glucose-insulin model. *J Diabetes Sci Technol* **1**, 323–30 (2007). URL `http://www.ncbi.nlm.nih.gov/pubmed/19885087%7D`.

[56] Dalla Man, C., Rizza, R. A. & Cobelli, C. Meal simulation model of the glucose-insulin system. *IEEE Trans Biomed Eng* **54**, 1740–9 (2007). URL `http://www.ncbi.nlm.nih.gov/pubmed/17926672%7D`.

[57] Manca, V., Marchetti, L. & Pagliarini, R. Mp modelling of glucose-insulin interactions in the intravenous glucose tolerance test. *International Journal of Natural Computing Research (IJNCR)* **2**, 13–24 (2011).

[58] Mari, A. Mathematical modeling in glucose metabolism and insulin secretion. *Curr Opin Clin Nutr Metab Care* **5**, 495–501 (2002). URL `http://www.ncbi.nlm.nih.gov/pubmed/12172472%7D`.

[59] Palumbo, P., Ditlevsen, S., Bertuzzi, A. & De Gaetano, A. Mathematical modeling of the glucose-insulin system: a review. *Math Biosci* **244**, 69–81 (2013). URL `http://www.ncbi.nlm.nih.gov/pubmed/23733079%7D`.

[60] Silber, H. E., Jauslin, P. M., Frey, N. & Karlsson, M. O. An integrated model for the glucose-insulin system. *Basic Clin Pharmacol Toxicol* **106**, 189–94 (2010). URL `http://www.ncbi.nlm.nih.gov/pubmed/20050839%7D`.

[61] Toffolo, G., Bergman, R. N., Finegood, D. T., Bowden, C. R. & Cobelli, C. Quantitative estimation of beta cell sensitivity to glucose in the intact organism: a minimal model of insulin kinetics in the dog. *Diabetes* **29**, 979–90 (1980). URL `http://www.ncbi.nlm.nih.gov/pubmed/7002673%7D`.

[62] Tura, A., Muscelli, E., Gastaldelli, A., Ferrannini, E. & Mari, A. Altered pattern of the incretin effect as assessed by modelling in individuals with glucose tolerance ranging from normal to diabetic. *Diabetologia* **57**, 1199–203 (2014). URL `http://www.ncbi.nlm.nih.gov/pubmed/24658843%7D`.

[63] Man, C. D. *et al.* The uva/padova type 1 diabetes simulator: New features. *J Diabetes Sci Technol* **8**, 26–34 (2014). URL `http://www.ncbi.nlm.nih.gov/pubmed/24876534%7D`.

[64] Mari, A., Pacini, G., Murphy, E., Ludvik, B. & Nolan, J. J. A model-based method for assessing insulin sensitivity from the oral glucose tolerance test. *Diabetes Care* **24**, 539–48 (2001). URL `http://www.ncbi.nlm.nih.gov/pubmed/11289482%7D`.

[65] Vicini, P., Caumo, A. & Cobelli, C. The hot ivgtt two-compartment minimal model: indexes of glucose effectiveness and insulin sensitivity. *Am J Physiol* **273**, E1024–32 (1997). URL `http://www.ncbi.nlm.nih.gov/pubmed/9374690%7D`.

[66] Dalla Man, C. *et al.* Modeling hepatic insulin sensitivity during a meal: validation against the euglycemic hyperinsulinemic clamp. *Am J Physiol Endocrinol Metab* **304**, E819–25 (2013). URL `http://www.ncbi.nlm.nih.gov/pubmed/23443923%7D`.

[67] Visentin, R. *et al.* Hepatic insulin sensitivity in healthy and prediabetic subjects: from a dual- to a single-tracer oral minimal model. *Am J Physiol Endocrinol Metab* **309**, E161–7 (2015). URL `http://www.ncbi.nlm.nih.gov/pubmed/25991649%7D`.

[68] Dalla Man, C. *et al.* Minimal model estimation of glucose absorption and insulin sensitivity from oral test: validation with a tracer method. *Am J Physiol Endocrinol Metab* **287**, E637–43 (2004). URL `http://www.ncbi.nlm.nih.gov/pubmed/15138152%7D`.

[69] Dalla Man, C. *et al.* Insulin sensitivity by oral glucose minimal models: validation against clamp. *Am J Physiol Endocrinol Metab* **289**, E954–9 (2005). URL `http://www.ncbi.nlm.nih.gov/pubmed/16014353%7D`.

[70] Bock, G. *et al.* Effects of nonglucose nutrients on insulin secretion and action in people with pre-diabetes. *Diabetes* **56**, 1113–9 (2007). URL `http://www.ncbi.nlm.nih.gov/pubmed/17395750%7D`.

[71] Mallad, A. *et al.* Nocturnal glucose metabolism in type 1 diabetes: A study comparing single versus dual tracer approaches. *Diabetes Technol Ther* **17**, 587–95 (2015). URL `http://www.ncbi.nlm.nih.gov/pubmed/26121060%7D`.

[72] Steil, G. M. Algorithms for a closed-loop artificial pancreas: the case for proportional-integral-derivative control. *J Diabetes Sci Technol* **7**, 1621–31 (2013). URL `http://www.ncbi.nlm.nih.gov/pubmed/24351189%7D`.

[73] Kropff, J. *et al.* 2 month evening and night closed-loop glucose control in patients with type 1 diabetes under free-living conditions: a randomised crossover trial. *Lancet Diabetes Endocrinol* **3**, 939–47 (2015). URL `http://www.ncbi.nlm.nih.gov/pubmed/26432775%7D`.

[74] Russell, S. J. *et al.* Outpatient glycemic control with a bionic pancreas in type 1 diabetes. *N Engl J Med* **371**, 313–25 (2014). URL `http://www.ncbi.nlm.nih.gov/pubmed/24931572%7D`.

[75] Thabit, H. *et al.* Home use of an artificial beta cell in type 1 diabetes. *N Engl J Med* **373**, 2129–40 (2015). URL `http://www.ncbi.nlm.nih.gov/pubmed/26379095%7D`.

[76] Maffeis, C. *et al.* Ghrelin, insulin sensitivity and postprandial glucose disposal in overweight and obese children. *Eur J Endocrinol* **154**, 61–8 (2006). URL `http://www.ncbi.nlm.nih.gov/pubmed/16381992%7D`.

[77] Bonora, E. *et al.* Hyperinsulinemia and insulin resistance are independently associated with plasma lipids, uric acid and blood pressure in non-diabetic subjects. the gisir database. *Nutr Metab Cardiovasc Dis* **18**, 624–31 (2008). URL `http://www.ncbi.nlm.nih.gov/pubmed/18060751%7D`.

[78] Bonetti, S. *et al.* Variants of gckr affect both beta-cell and kidney function in patients with newly diagnosed type 2 diabetes: the verona newly diagnosed type 2 diabetes study 2. *Diabetes Care* **34**, 1205–10 (2011). URL `http://www.ncbi.nlm.nih.gov/pubmed/21411509%7D`.

[79] Bertuzzi, A., Salinari, S. & Mingrone, G. Insulin granule trafficking in beta-cells: mathematical model of glucose-induced insulin secretion. *Am J Physiol Endocrinol Metab* **293**, E396–409 (2007). URL `http://www.ncbi.nlm.nih.gov/pubmed/17456637%7D`.

[80] Cobelli, C. & Pacini, G. Insulin secretion and hepatic extraction in humans by minimal modeling of c-peptide and insulin kinetics. *Diabetes* **37**, 223–31 (1988). URL `http://www.ncbi.nlm.nih.gov/pubmed/3292317%7D`.

[81] Coleman, L., T.F.; Yuying. On the convergence of interior-reflective newton methods for nonlinear minimization subject to bounds. *Mathematical Programming* **67**, 189–224 (1994).

[82] Coleman, L., T.F.; Yuying. An interior trust region approach for nonlinear minimization subject to bounds. *SIAM Journal on Optimization* **6**, 418–445 (1996).

[83] Polonsky, K. S. *et al.* Quantitative study of insulin secretion and clearance in normal and obese subjects. *J Clin Invest* **81**, 435–41 (1988). URL `http://www.ncbi.nlm.nih.gov/pubmed/3276729%7D`.

[84] Piccinini, F., Dalla Man, C., Vella, A. & Cobelli, C. A model for the estimation of hepatic insulin extraction after a meal. *IEEE Trans Biomed Eng* (2015). URL `http://www.ncbi.nlm.nih.gov/pubmed/26660513%7D`.

[85] Toffolo, G., Campioni, M., Basu, R., Rizza, R. A. & Cobelli, C. A minimal model of insulin secretion and kinetics to assess hepatic insulin extraction. *Am J Physiol Endocrinol Metab* **290**, E169–E176 (2006). URL `http://www.ncbi.nlm.nih.gov/pubmed/16144811%7D`.

[86] Vella, A. *et al.* Type i diabetes mellitus does not alter initial splanchnic glucose extraction or hepatic udp-glucose flux during enteral glucose administration. *Diabetologia* **44**, 729–737 (2001). URL `http://www.ncbi.nlm.nih.gov/pubmed/11440366%7D`.

[87] Straczkowski, M. & Kowalska, I. The Role of Skeletal Muscle Sphingolipids in the Development of Insulin Resistance. *Rev Diabet Stud.* **5**, 13–24 (2008).

[88] Turpin, S. M. *et al.* Obesity-induced CerS6-dependent C16:0 ceramide production promotes weight gain and glucose intolerance. *Cell Metabolism* **20**, 678–686 (2014). URL `http://linkinghub.elsevier.com/retrieve/pii/S1550413114003684`.

[89] Stratford, S., Hoehn, K. L., Liu, F. & Summers, S. A. Regulation of Insulin Action by Ceramide: DUAL MECHANISMS LINKING CERAMIDE ACCUMULATION TO THE INHIBITION OF Akt/PROTEIN KINASE B. *Journal of Biological Chemistry* **279**, 36608–36615 (2004).

[90] Nikolić, D., Priami, C. & Zunino, R. A rule-based and imperative language for biochemical modeling and simulation. In *Lecture Notes in Computer Science (including subseries Lecture Notes in Artificial Intelligence and Lecture Notes in Bioinformatics)*, vol. 7504 LNCS, 16–32 (Springer, 2012).

[91] Dennis, E. A. *et al.* A mouse macrophage lipidome. *Journal of Biological Chemistry* **285**, 39976–39985 (2010). URL `http://www.ncbi.nlm.nih.gov/pubmed/20923771`.

[92] Raetz, C. R. H. *et al.* Kdo2-Lipid A of Escherichia coli, a defined endotoxin that activates macrophages via TLR-4. *Journal of lipid research* **47**, 1097–1111 (2006). URL `http://www.ncbi.nlm.nih.gov/pubmed/16479018`.

[93] Prieur, X. *et al.* Differential lipid partitioning between adipocytes and tissue macrophages modulates macrophage lipotoxicity and M2/M1 polarization in obese mice. *Diabetes* **60**, 797–809 (2011).

[94] Camell, C. D. *et al.* Macrophage-specific de Novo synthesis of ceramide is dispensable for inflammasome-driven inflammation and insulin resistance in obesity. *Journal of Biological Chemistry* **290**, 29402–29413 (2015). URL `http://www.ncbi.nlm.nih.gov/pubmed/26438821`.

[95] Aburasayn, H., Al Batran, R. & Ussher, J. R. Targeting ceramide metabolism in obesity. *American Journal of Physiology - Endocrinology And Metabolism* **311**, E423–E435 (2016). URL `http://www.ncbi.nlm.nih.gov/pubmed/27382035`.

[96] Shahrezaei, V. & Swain, P. S. The stochastic nature of biochemical networks. *Current Opinion in Biotechnology* **19**, 369–374 (2008).

[97] Kitatani, K., Idkowiak-Baldys, J. & Hannun, Y. A. The sphingolipid salvage pathway in ceramide metabolism and signaling. *Cellular Signalling* **20**, 1010–1018 (2008). `NIHMS150003`.

[98] Gómez-Muñoz, A. Ceramide 1-phosphate/ceramide, a switch between life and death. *Biochimica et Biophysica Acta (BBA) - Biomembranes* **1758**, 2049–2056 (2006). URL `http://linkinghub.elsevier.com/retrieve/pii/S0005273606001866`.

[99] Mullen, T. D. *et al.* Selective knockdown of ceramide synthases reveals complex interregulation of sphingolipid metabolism. *Journal of lipid research* **52**, 68–77 (2011).

[100] Barth, B. M., Cabot, M. C. & Kester, M. Ceramide-based therapeutics for the treatment of cancer. *Anti-cancer agents in medicinal chemistry* **11**, 911–919 (2011). URL `http://www.ncbi.nlm.nih.gov/pubmed/21707481`.

[101] Hartmann, D. *et al.* The equilibrium between long and very long chain ceramides is important for the fate of the cell and can be influenced by co-expression of CerS. *The International Journal of Biochemistry & Cell Biology* **45**, 1195–1203 (2013). URL `http://www.ncbi.nlm.nih.gov/pubmed/23538298`.

[102] Morad, S. a. F. & Cabot, M. C. Ceramide-orchestrated signalling in cancer cells. *Nature reviews. Cancer* **13**, 51–65 (2013). URL `http://www.ncbi.nlm.nih.gov/pubmed/23235911`.

[103] Batheja, A. D., Uhlinger, D. J., Carton, J. M., Ho, G. & D'Andrea, M. R. Characterization of serine palmitoyltransferase in normal human tissues. *The journal of histochemistry and cytochemistry : official journal of the Histochemistry Society* **51**, 687–96 (2003). URL `http://www.ncbi.nlm.nih.gov/pubmed/12704216`.

[104] Saxena, R. *et al.* Genetic variation in GIPR influences the glucose and insulin responses to an oral glucose challenge. *Nature genetics* **42**, 142–148 (2010). URL `http://www.ncbi.nlm.nih.gov/pubmed/20081857`.

[105] Dupuis, J. *et al.* New genetic loci implicated in fasting glucose homeostasis and their impact on type 2 diabetes risk. *Nature genetics* **42**, 105–16 (2010). 270.

[106] Florez, J. C., Manning, A. K., Mcateer, J. & Irenze, K. A 100K Genome-Wide Association Scan for Diabetes and Related Traits in the Framingham Heart Study. *Diabetes* **56**, 3063–3074 (2007).

[107] Hayes, M. *et al.* Identification of type 2 diabetes genes in Mexican Americans through genome-wide association studies. *Diabetes* **56**, 3033 (2007). URL `http://diabetes.diabetesjournals.org/content/56/12/3033.short`.

[108] WTCCC. Genome-wide association study of 14,000 cases of seven common diseases and 3,000 shared controls. *Nature* **447**, 661–78 (2007). URL `http://www.ncbi.nlm.nih.gov/pubmed/17554300`. t8jd4qr3m.

[109] Irvin, M. R. *et al.* Genome-wide detection of allele specific copy number variation associated with insulin resistance in african americans from the hyperGEN study. *PLoS ONE* **6**, 9–11 (2011).

[110] Ruangsiriluk, W. *et al.* Silencing of enzymes involved in ceramide biosynthesis causes distinct global alterations of lipid homeostasis and gene expression. *Journal of lipid research* **53**, 1459–71 (2012). URL `http://www.jlr.org/cgi/doi/10.1194/jlr.M020941`.

[111] Holland, W. L. *et al.* Inhibition of Ceramide Synthesis Ameliorates Glucocorticoid-, Saturated-Fat-, and Obesity-Induced Insulin Resistance. *Cell Metabolism* **5**, 167–179 (2007). URL `http://www.ncbi.nlm.nih.gov/pubmed/17339025`.

[112] Ussher, J. R. *et al.* Inhibition of de novo ceramide synthesis reverses diet-induced insulin resistance and enhances whole-body oxygen consumption. *Diabetes* **59**, 2453–2464 (2010).

[113] Hu, W., Ross, J. S., Geng, T., Brice, S. E. & Cowart, L. A. Differential regulation of Dihydroceramide desaturase by palmitate vs. monounsaturated fatty acids:Implications to insulin resistance. *The Journal of biological chemistry* **286**, 16596 –16605 (2011). URL `http://www.ncbi.nlm.nih.gov/pubmed/21454530`.

[114] Gillespie, D. T. General Method for Numerically Simulating Stochastic Time Evolution of Couple Chemical Reactions. *Journal of Computational Physics* **22**, 1–32 (1976). URL `http://linkinghub.elsevier.com/retrieve/pii/0021999176900413`.

[115] Benjamini, Y. & Hochberg, Y. Controlling the False Discovery Rate: a Practical and Powerful Approach to Multiple Testing. *Journal of the Royal Statistical Society. Series B (Methodological)* **57**, 289–300 (1995). URL `http://www.jstor.org/stable/2346101`.

[116] Barth, B. M. *et al.* Gaucher's disease and cancer: a sphingolipid perspective. *Critical reviews in oncogenesis* **18**, 221–34 (2013). URL `http://www.ncbi.nlm.nih.gov/pubmed/23510065`.

[117] Wronowska, W., Charzyńska, A., Nienałtowski, K. & Gambin, A. Computational modeling of sphingolipid metabolism. *BMC systems biology* **9**, 47 (2015). URL `http://www.biomedcentral.com/1752-0509/9/47`.

[118] Csardi, G. N. T. The igraph software package for complex network research. *Inter J Complex Syst* **1695**, 1695 (2006). URL `http://igraph.org`.

[119] Muoio, D. M. & Newgard, C. B. Mechanisms of disease: Molecular and metabolic mechanisms of insulin resistance and β-cell failure in type 2 diabetes. *Nature Reviews Molecular Cell Biology* **9**, 193–205 (2008). URL `http://dx.doi.org/10.1038/nrm2327`.

[120] Kahramanoğulları, O., Fantaccini, G., Lecca, P., Morpurgo, D. & Priami, C. Algorithmic Modeling Quantifies the Complementary Contribution of Metabolic Inhibitions to Gemcitabine Efficacy. *PLoS ONE* **7**, e50176 (2012). URL `http://dx.plos.org/10.1371/journal.pone.0050176`.

[121] Marchetti, L., Priami, C. & Thanh, V. H. HRSSA – Efficient hybrid stochastic simulation for spatially homogeneous biochemical reaction networks. *Journal of Computational Physics* **317**, 301–317 (2016). URL `http://linkinghub.elsevier.com/retrieve/pii/S0021999116301115`.

[122] Senkal, C. E. *et al.* Alteration of ceramide Synthase 6/C16-ceramide induces activating transcription factor 6-mediated ER-stress and apoptosis via perturbation of cellular Ca+2 and ER/Golgi membrane network. *The Journal of biological chemistry* **286**, 42446–58 (2011).

[123] Altman, N. & Krzywinski, M. Points of Significance: Simple linear regression. *Nature Methods* **12**, 999–1000 (2015). URL `http://www.nature.com/doifinder/10.1038/nmeth.3627`.

[124] Brooks, S., Gelman, A., Jones, G. & Meng, X.-L. (eds.) *Handbook of Markov Chain Monte Carlo*. Chapman & Hall/CRC Handbooks of Modern Statistical Methods (Chapman and Hall/CRC).

[125] Balsa-Canto, E., Banga, J. R., Egea, J. A., Fernandez-Villaverde, A. & De Hijas-Liste, G. M. Global optimization in systems biology: Stochastic methods and their applications. In *Advances in Experimental Medicine and Biology*, vol. 736, 409–424 (2012). URL `http://www.ncbi.nlm.nih.gov/pubmed/22161343`.

[126] Romeijn, H. E. & Schoen, F. *Handbook of Global Optimization*, vol. 62 (2002). `arXiv:1011.1669v3`.

[127] Weise, T. *Global Optimization Algorithms - Theory and Application*, vol. 1 (2009).

[128] Davis, L. *Handbook of Genetic Algorithms* (Van Nostrand Reinhold, 1991).

[129] Nocedal, J. & Wright, S. *Numerical Optimization*. Springer Series in Operations Research and Financial Engineering (Springer-Verlag New York, 2006).

[130] Levenberg, K. A method for the solution of certain non-linear problems in least squares. *Quarterly Journal of Applied Mathematics* **2**, 164–168 (1944).

[131] Moles, C. G., Mendes, P. & Banga, J. R. Parameter estimation in biochemical pathways: a comparison of global optimization methods. *Genome research* **13**, 2467–74 (2003). URL `http://www.ncbi.nlm.nih.gov/pubmed/14559783`.

[132] Jones, E., Oliphant, T., Peterson, P. *et al.* SciPy: Open source scientific tools for Python (2001–). URL `http://www.scipy.org/`. [Online; accessed 2017-03-10].

[133] Baty, F. *et al.* A toolbox for nonlinear regression in R: The package nlstools. *Journal of Statistical Software* **66**, 1–21 (2015). URL `http://www.jstatsoft.org/v66/i05/`.

[134] Agarwal, S., Mierle, K. & Others. Ceres solver. `http://ceres-solver.org`.

[135] Saltelli, A., Chan, K., Scott, E. M. & Wiley, J. Sensitivity Analysis 504 (2000).

[136] Goryanin, I. Computational optimization and biological evolution. *Biochemical Society transactions* **38**, 1206–9 (2010). URL `http://www.ncbi.nlm.nih.gov/pubmed/20863285`.

[137] Banga, J. R. Optimization in computational systems biology. *BMC systems biology* **2**, 47 (2008). URL `http://www.biomedcentral.com/1752-0509/2/47`.

[138] Lacroix, S. *et al.* Systems biology approaches to study the molecular effects of caloric restriction and polyphenols on aging processes. *Genes & nutrition* **10**, 58 (2015).

[139] Caberlotto, L., Marchetti, L., Lauria, M., Scotti, M. & Parolo, S. Integration of transcriptomic and genomic data suggests candidate mechanisms for APOE4-mediated pathogenic action in Alzheimer's disease. *Scientific reports* **6**, 32583 (2016). URL `http://www.nature.com/articles/srep32583`.

[140] Papadimitriou, C. & Steiglitz, K. *Combinatorial optimization: algorithms and complexity* (Dover Publications; Unabridged edition, 1998).

[141] Boyd, S. & Vandenberghe, L. *Convex Optimization* (Cambridge University Press, New York, NY, USA, 2004).

[142] Wolpert, D. H. & Macready, W. G. No Free Lunch Theorems for Optimization. *IEEE Transactions on Evolutionary Computation* **1** (1997).

[143] Riz, M. & Pedersen, M. G. Mathematical Modeling of Interacting Glucose-Sensing Mechanisms and Electrical Activity Underlying Glucagon-Like Peptide 1 Secretion. *PLOS Computational Biology* **11**, e1004600 (2015). URL `http://dx.plos.org/10.1371/journal.pcbi.1004600`.

[144] Capuani, F. *et al.* Quantitative analysis reveals how EGFR activation and downregulation are coupled in normal but not in cancer cells. *Nature communications* **6**, 7999 (2015). URL `http://www.nature.com/doifinder/10.1038/ncomms8999{%}5C`.

[145] Bollig-Fischer, A. *et al.* Modeling time-dependent transcription effects of HER2 oncogene and discovery of a role for E2F2 in breast cancer cell-matrix adhesion. *Bioinformatics* **30**, 3036–3043 (2014). URL `https://academic.oup.com/bioinformatics/article-lookup/doi/10.1093/bioinformatics/btu400`.

[146] Herman, G. A. *et al.* Effect of single oral doses of sitagliptin, a dipeptidyl peptidase-4 inhibitor, on incretin and plasma glucose levels after an oral glucose tolerance test in patients with type 2 diabetes. *Journal of Clinical Endocrinology and Metabolism* **91**, 4612–4619 (2006).

[147] Ge, L. *et al.* The Model of PK/PD for Danhong Injection Analyzed by Least Square Method. In *2015 7th International Conference on Information Technology in Medicine and Education (ITME)*, 292–296 (IEEE, 2015). URL `http://ieeexplore.ieee.org/document/7429150/`.

[148] Manca, V. & Marchetti, L. Log-Gain Stoichiometric Stepwise Regression for Mp Systems. *International Journal of Foundations of Computer Science* **22**, 97–106 (2011). URL `http://www.worldscientific.com/doi/abs/10.1142/S0129054111007861`.

[149] Manca, V. & Marchetti, L. Solving dynamical inverse problems by means of Metabolic P systems. *Biosystems* **109**, 78–86 (2012). URL `http://linkinghub.elsevier.com/retrieve/pii/S0303264712000032`.

[150] Manca, V. & Marchetti, L. An algebraic formulation of inverse problems in MP dynamics. *International Journal of Computer Mathematics* **90**, 845–856 (2013). URL `http://www.tandfonline.com/doi/abs/10.1080/00207160.2012.735362`.

[151] Marchetti, L. & Manca, V. Recurrent Solutions to Dynamics Inverse Problems: A Validation of MP Regression. *Journal of Applied & Computational Mathematics* **03**, 1–8 (2014).

[152] Marchetti, L. & Manca, V. MpTheory Java library: a multi-platform Java library for systems biology based on the Metabolic P theory. *Bioinformatics* **31**, 1328–1330 (2015). URL `http://bioinformatics.oxfordjournals.org/cgi/doi/10.1093/bioinformatics/btu814`.

[153] Björck, Å. *Numerical Methods for Least Squares Problems* (Society for Industrial and Applied Mathematics, 1996). URL `http://epubs.siam.org/doi/book/10.1137/1.9781611971484`.

[154] Dennis, J. E. & Schnabel, R. B. *Numerical methods for unconstrained optimization and nonlinear equations*, vol. 16 (Society for Industrial and Applied Mathematics, 1996). URL `http://epubs.siam.org/doi/book/10.1137/1.9781611971200`.

[155] Morris, M. D. & Mitchell, T. J. Exploratory designs for computational experiments. *Journal of Statistical Planning and Inference* **43**, 381–402 (1995).

[156] Pronzato, L. & Müller, W. G. Design of computer experiments: Space filling and beyond. *Statistics and Computing* **22**, 681–701 (2012).

[157] Viana, F. A. C. Things You Wanted to Know About the Latin Hypercube Design and Were Afraid to Ask. *10th World Congress on Structural and Multidisciplinary Optimization* 1–9 (2013).

[158] Kelley, C. T. *Iterative Methods for Optimization* (Society for Industrial and Applied Mathematics, 1999).

[159] Gill, P. E. & Murray, W. Algorithms for the Solution of the Nonlinear Least-Squares Problem. *SIAM Journal on Numerical Analysis* **15**, 977–992 (1978). URL http://epubs.siam.org/doi/abs/10.1137/0715063.

[160] Marquardt, D. W. An Algorithm for Least-Squares Estimation of Nonlinear Parameters. *Journal of the Society for Industrial and Applied Mathematics* **11**, 431–441 (1963). URL http://epubs.siam.org/doi/abs/10.1137/0111030.

[161] Byrd, R. H., Schnabel, R. B. & Shultz, G. A. A Trust Region Algorithm for Nonlinearly Constrained Optimization. *SIAM Journal on Numerical Analysis* **24**, 1152–1170 (1987). URL http://epubs.siam.org/doi/abs/10.1137/0724076.

[162] Yuan, Y.-x. A Review of Trust Region Algorithms for Optimization. *Iciam* **99**, 271–282 (2000).

[163] Geyer, C. Practical Markov Chain Monte Carlo. *Statistical Science* **7**, 473–483 (1992).

[164] Gamerman, D. & Lopes, H. F. *Markov Chain Monte Carlo: Stochastic Simulation for Bayesian Inference, Second Edition.* Chapman & Hall/CRC Texts in Statistical Science (Taylor & Francis, 2006).

[165] Kahramanoğulları, O. & Lynch, J. F. Stochastic flux analysis of chemical reaction networks. *BMC Systems Biology* **7**, 1–21 (2013). URL http://www.biomedcentral.com/1752-0509/7/133.

[166] Thanh, V. H., Priami, C. & Zunino, R. Efficient rejection-based simulation of biochemical reactions with stochastic noise and delays. *The Journal of Chemical Physics* **141**, 134116 (2014). URL http://scitation.aip.org/content/aip/journal/jcp/141/13/10.1063/1.4896985.

[167] Pahle, J. Biochemical simulations: stochastic, approximate stochastic and hybrid approaches. *Briefings in Bioinformatics* 53–64.

[168] Golightly, A. & Wilkinson, D. J. Bayesian parameter inference for stochastic biochemical network models using particle Markov chain Monte Carlo. *Interface Focus* **1**, 807–820 (2011). URL http://www.ncbi.nlm.nih.gov/pubmed/23226583.

[169] Wilkinson, D. J. *Stochastic modelling for systems biology* (CRC Press/Taylor & Francis, 2012).

[170] Newman, K. *et al. Modelling population dynamics. Model formulation, fitting and assessment using state-space methods*. Methods in Statistical Ecology (Springer New York, New York, NY, 2014). URL `http://link.springer.com/10.1007/978-1-4939-0977-3`.

[171] Marini, G. *et al.* The role of climatic and density dependent factors in shaping mosquito population dynamics: The case of culex pipiens in north-western Italy. *PLoS ONE* **11**, e0154018 (2016). URL `http://journals.plos.org/plosone/article/asset?id=10.1371/journal.pone.0154018.PDF`.

[172] Cauchemez, S., Carrat, F., Viboud, C., Valleron, A. J. & Boëlle, P. Y. A Bayesian MCMC approach to study transmission of influenza: Application to household longitudinal data. *Statistics in Medicine* **23**, 3469–3487 (2004). URL `http://doi.wiley.com/10.1002/sim.1912`.

[173] Marziano, V. *et al.* The impact of demographic changes on the epidemiology of herpes zoster: Spain as a case study. *Proceedings. Biological sciences / The Royal Society* **282**, 20142509 (2015). URL `http://rspb.royalsocietypublishing.org/cgi/doi/10.1098/rspb.2014.2509`.

[174] Merler, S. *et al.* Spatiotemporal spread of the 2014 outbreak of Ebola virus disease in Liberia and the effectiveness of non-pharmaceutical interventions: a computational modelling analysis. *The Lancet Infectious Diseases* **15**, 204–211 (2015). URL `http://linkinghub.elsevier.com/retrieve/pii/S1473309914710746`.

[175] Geyer, C. J. Markov Chain Monte Carlo Maximum Likelihood. *Computing Science and Statistics: Proceedings of the 23rd Symposium on the Interface* 156–163 (1991).

[176] Cowles, M. K. & Carlin, B. P. Markov Chain Monte Carlo Convergence Diagnostics: A Comparative Review. *Journal of the American Statistical Association* **91**, 883–904 (1996).

[177] Andrieu, C., De Freitas, N., Doucet, A. & Jordan, M. I. An introduction to MCMC for machine learning. *Machine Learning* **50**, 5–43 (2003). URL `http://link.springer.com/10.1023/A:1020281327116`. 1109.4435v1.

[178] Metropolis, N., Rosenbluth, A. W., Rosenbluth, M. N., Teller, A. H. & Teller, E. Equation of State Calculations by Fast Computing Machines. *The Journal of Chemical Physics* **21**, 1087 (1953).

[179] Hastings, W. K. Monte Carlo sampling methods using Markov chains and their applications. *Biometrika Vol* **57**, 97–109 (1970).

[180] Andrieu, C. & Thoms, J. A tutorial on adaptive MCMC. *Statistics and Computing* **18**, 343–373 (2008). URL `http://link.springer.com/10.1007/s11222-008-9110-y`.

[181] Corcoran, J. & Tweedie, R.   Perfect sampling from independent Metropolis-Hastings chains. *Journal of Statistical Planning and Inference* **104**, 297–314 (2002). URL `http://linkinghub.elsevier.com/retrieve/pii/S0378375801002439`.

[182] Mendes, P. & Kell, D. B. Non-linear optimization of biochemical pathways: Applications to metabolic engineering and parameter estimation. *Bioinformatics* **14**, 869–883 (1998). URL `http://bioinformatics.oxfordjournals.org/cgi/doi/10.1093/bioinformatics/14.10.869`.

[183] Atchade, Y. F. & Rosenthal, J. S. On adaptive Markov chain Monte Carlo algorithms. *Bernoulli* **11**, 815–828 (2005).

[184] Neiswanger, W., Wang, C. & Xing, E. Asymptotically Exact, Embarrassingly Parallel MCMC. *CoRR* **abs/1510.0** (2015). URL `http://arxiv.org/abs/1311.4780`. `arXiv:1311.4780v2`.

[185] Andrieu, C., Doucet, A. & Holenstein, R. Particle Markov chain Monte Carlo methods. *Journal of the Royal Statistical Society Series B-Statistical Methodology* **72**, 269–342 (2010).

[186] Vrugt, J. A. & Ter Braak, C. J. F.   DREAM(D): An adaptive Markov Chain Monte Carlo simulation algorithm to solve discrete, noncontinuous, and combinatorial posterior parameter estimation problems. *Hydrology and Earth System Sciences* **15**, 3701–3713 (2011).   URL `www.hydrol-earth-syst-sci.net/15/3701/2011/`.

[187] Holland, J. H. *Adaptation in Natural and Artificial Systems: An Introductory Analysis with Applications to Biology, Control and Artificial Intelligence* (MIT Press, Cambridge, MA, USA, 1992).

[188] Goldberg, D. E. *Genetic Algorithms in Search, Optimization, and Machine Learning* (Addison-Wesley Longman Publishing Co., Inc., Boston, MA, USA, 1989), 1st edn.

[189] Mitchell, M. *An introduction to genetic algorithms* (MIT press, 1998).

[190] Sivanandam, S. N. & Deepa, S. N. *Introduction to Genetic Algorithms* (Springer Publishing Company, Incorporated, 2007), 1st edn.

[191] Chu, D. Evolving genetic regulatory networks for systems biology. In *2007 IEEE Congress on Evolutionary Computation*, 875–882 (IEEE, 2007). URL `http://ieeexplore.ieee.org/document/4424562/`.

[192] Carta, A., Chaves, M. & Gouzé, J.-L. A Simple Model to Control Growth Rate of Synthetic E. coli during the Exponential Phase: Model Analysis and Parameter Estimation. In *Computational Methods in Systems Biology*, 107–126 (Springer Berlin Heidelberg, 2012).

[193] Oliveto, P. S. & Witt, C. On the analysis of the simple genetic algorithm. In *Proceedings of the fourteenth international conference on Genetic and evolutionary computation conference - GECCO '12*, 1341 (ACM Press, New York, New York, USA, 2012). URL `http://dl.acm.org/citation.cfm?doid=2330163.2330349`.

[194] Oliveto, P. S. & Witt, C. Improved time complexity analysis of the Simple Genetic Algorithm. *Theoretical Computer Science* **605**, 21–41 (2015). URL `http://linkinghub.elsevier.com/retrieve/pii/S0304397515000298`.

[195] Goldberg, D. E. & Voessner, S. Optimizing Global-Local Search Hybrids. *Proceedings of the Genetic and Evolutionary Computation Conference* **1**, 220–228 (1999). URL `http://www.cs.bham.ac.uk/~wbl/biblio/gecco1999/GA-882.pdf`.

[196] Safe, M., Carballido, J., Ponzoni, I. & Brignole, N. On Stopping Criteria for Genetic Algorithms. In *Advances in Artificial Intelligence - SBIA 2004*, 405–413 (Springer Berlin Heidelberg, 2004). URL `http://www.springerlink.com/content/cgt7635e3lhu3pdn`.

[197] Whitley, D. A genetic algorithm tutorial. *Statistics and Computing* **4**, 65–85 (1994). `arXiv:1011.1669v3`.

[198] Whitley, L. D. The GENITOR Algorithm and Selection Pressure: Why Rank-Based Allocation of Reproductive Trials is Best. *Icga* **89**, 116–123 (1989).

[199] Miller, B. L. & Goldberg, D. E. Genetic Algorithms, Tournament Selection, and the Effects of Noise. *Complex Systems* **9**, 193–212 (1995).

[200] Baluja, S. & Caruana, R. Removing the genetics from the standard genetic algorithm. *Icml* 1–11 (1995).

[201] Cantú-Paz, E. A Survey of Parallel Genetic Algorithms. *Calcul. Paralleles Reseaux Syst. Repart.* **10**, 141–171 (1998).

[202] Whitley, D., Rana, S. & Heckendorn, R. B. The island model genetic algorithm: On separability, population size and convergence. *Journal of Computing and Information Technology* **7**, 33–47 (1999).

[203] Beyer, H.-G. & Schwefel, H.-P. Evolution strategies - A comprehensive introduction. *Natural Computing* 3 – 52.

[204] Ostermeier, a., Gawelczyk, a. & Hansen, N. Step-size adaptation based on non-local use of selection information. *Lecture Notes in Computer Science, Vol. 866* 282–291 (1994).

[205] Hansen, N. The CMA Evolution Strategy: A Tutorial (2016). URL `http://arxiv.org/abs/1604.00772`. `1604.00772`.

[206] Jagerskupper, J. & Storch, T. When the Plus Strategy Outperforms the Comma Strategyand When Not. In *2007 IEEE Symposium on Foundations of Computational Intelligence*, 25–32 (IEEE, 2007). URL `http://ieeexplore.ieee.org/document/4233881/`.

[207] Braak, C. J. F. T. A Markov Chain Monte Carlo version of the genetic algorithm Differential Evolution: easy Bayesian computing for real parameter spaces. *Statistics and Computing* **16**, 239–249 (2006). URL `http://link.springer.com/10.1007/s11222-006-8769-1`.

[208] Derhy, M.-F. *Integer Programming : The Branch and Bound Method* (2010), linear pro edn. URL `http://www.pearsoned.co.uk/bookshop/detail.asp?item=100000000289101`.

[209] Kennedy, J. & Eberhart, R. Particle swarm optimization. In *Proceedings of ICNN'95 - International Conference on Neural Networks*, vol. 4, 1942–1948 (IEEE, 1995). URL `http://ieeexplore.ieee.org/document/488968/`.

[210] Kirpatrick, S., Gelatt, C. D. & Vecchi, M. P. Optimization by simulated annealing. *Science 200(2548)* **220**, 671–680 (1983). URL `http://www.jstor.org/stable/1690046`.

[211] Wilkinson, D. J. Bayesian methods in bioinformatics and computational systems biology. *Briefings in Bioinformatics* **8**, 109–116 (2007). URL `http://bib.oxfordjournals.org/cgi/doi/10.1093/bib/bbm007`.

[212] Lillacci, G. & Khammash, M. Parameter estimation and model selection in computational biology. *PLoS Computational Biology* **6**, e1000696 (2010). URL `http://dx.plos.org/10.1371/journal.pcbi.1000696`.

[213] Wang, Y., Zhang, X.-S. & Chen, L. Optimization meets systems biology. *BMC Systems Biology* **4**, S1 (2010). URL `http://www.ncbi.nlm.nih.gov/pubmed/20840723`.